VILNIUS UNIVERSITY

CENTER FOR PHYSICAL SCIENCE AND TECHNOLOGY

Jonas Jurkevičius

Photoluminescence efficiency in wide-band-gap III-nitride semiconductors and their heterostructures

Doctoral dissertation

Physical Science, Physics (02 P)

Vilnius 2016

The doctoral dissertation was prepared in 2012 – 2016 at the Semiconductor Physics Department, Vilnius University.

Scientific advisor:

Prof. habil. dr. Gintautas Tamulaitis (Vilnius University, Semiconductor Physics Department, Physics - 02P)

VILNIAUS UNIVERSITETAS

FIZINIŲ IR TECHNOLOGIJOS MOKSLŲ CENTRAS

Jonas Jurkevičius

Fotoliuminescencijos našumas plačiatarpiuose III grupės nitridiniuose puslaidininkiuose ir jų heterodariniuose

Daktaro disertacija

Fiziniai mokslai, fizika (02 P)

Vilnius 2016

Disertacija rengta 2012-2016 metais Vilniaus universiteto Fizikos fakultete ir Taikomųjų mokslų institute.

Mokslinis vadovas – prof. habil. dr. Gintautas Tamulaitis (Vilniaus universitetas, fiziniai mokslai, fizika – 02P)

Acknowledgements

I would like thank my scientific advisor, Prof. Gintautas Tamulaitis, for invaluable and patient mentorship, imparted scientific knowledge, and the opportunity to work in the field of semiconductor physics.

I would also like to thank my colleagues. First of all, dr. Jūras Mickevičius, whom I'd like to thank for patience in developing my experimental skills, tenacity in discussions, and advisory during my research. Among others whom I would like to thank for direct involvement with my thesis are Dr. Darius Dobrovolskas, Dr. Karolis Kazlauskas, Dr. Ramūnas Aleksiejūnas, Dr. Arūnas Kadys, Dr. Tadas Malinauskas, Dr. Mindaugas Karaliūnas, and Žydrūnas Podlipskas. This work would not have been possible without your efforts, suggestions and discussions. The excellent working conditions in my research group at the Semiconductor Physics Department and the Institute of Applied Research were contributed by the friendly community of colleagues, many of whom I consider true friends, and who deserve a separate mention.

I am grateful to many of my teachers I had the privilege to be educated by. Though the list is vast, I would like to mention Edita Dijokienė, who inspired me to study physics, and Prof. Artūras Žukauskas, whose excellent course of introduction into semiconductor physics pointed me into this field of research. A special mention is reserved to Prof. Vytautas Karpus, whose lectures and professionalism left a profound imprint in my view towards the academy.

I acknowledge the Lithuanian Research Council and the Physics Faculty at Vilnius University for the financial support during my doctoral studies.

To my dear friends outside of the field of physics, I would like to thank you all for your much needed support in problematic moments and tolerance for my occasional eccentricities.

Most importantly, I am grateful to and for my loving family – my Mother Ramunė, Father Paulius and Sister Dalia. Nothing compares to you.

Contents

List of Abbreviations:

AFM	Atomic force microscopy
CW	Continuous wave
FWHM	Full width at half-maximum
ICCD	Intensified charge-coupled device
IQE	Internal quantum efficiency
LD	Laser diode
LED	Light emitting diode
LITG	Light-induced transient grating
MBE	Molecular beam epitaxy
MEMOCVD	Migration-enhanced metal-organic chemical vapor deposition
MOCVD	Metal-organic chemical vapor deposition
MQW	Multiple quantum well
NRC	Non-radiative recombination center
n-type	Negative type
p-type	Positive type
PL	Photoluminescence
QW	Quantum well
SE	Stimulated emission
UV	Ultraviolet
XRD	X-Ray diffraction

Introduction

III-nitrides are arguably already a classic semiconductor material group. The period of intensive research of III-nitride semiconductors started by Nobel Prize winners Shuji Nakamura, A. Akasaki and H. Amano in 1994 after the breakthrough in the development of high-brightness blue light emitting diodes (LEDs). In short time, the blue InGaN-based LEDs paved the way for the introduction of efficient white LEDs, blue laser diodes and UV LEDs. Today, the InGaN-based nitride semiconductor technology has reached a high level of commercial and technological success.

Simultaneously to the InGaN, a wide band-gap alloy of AlGaN was studied and AlGaN-based optoelectronic devices were developed. Alloying $Al_xGa_{1-x}N$ with different aluminum content tunes the emission wavelength from 365 nm to almost 200 nm. It is this potential of producing solid state emitters operating at desired wavelengths that attracts, to this day, the attention and efforts of the scientific community.

Commercially available AlGaN LEDs are already applied in medicine (dermatological treatment), surface and water sterilization, material processing (polymerization). Further and wider applications would become feasible if the issues hampering the AlGaN emitter development were solved. The sought-for deep UV emission requires the incorporation of larger aluminum content. However, this results in increasingly poor material quality, primarily because of large densities of dislocations and point defects. This results in low power, low efficiency and lower service time of AlGaN-based emitters in comparison to those based on InGaN.

In addition to overall lower efficiency, AlGaN based LEDs suffer from the decrease of PL efficiency at high carrier density – the efficiency droop. This issue is even more severe in LDs, which operate at even greater current densities. The luminescence efficiency droop is observed in InGaN also and the causes,

both intrinsic and extrinsic, of the effect are largely agreed upon. While the device-related causes such as carrier escape from QWs and decreased capture of the injected carriers are inherent for both InGaN and AlGaN, there is no consensus on the issue of intrinsic causes of the droop in AlGaN. Therefore, the related problems of low internal quantum efficiency and the droop effect are still the key topics in further development of AlGaN-based UV LEDs.

The aforementioned decline of material quality with increasing aluminum content in AlGaN is largely related to the lattice mismatch between layers with different composition. Poor lattice matching ultimately affects the overall efficiency and performance of the device. One of possible ways to address this problem is to introduce BGaN. Properties of the III-nitride ternary compounds containing boron are expected to be similar to those of InGaN or AlGaN with the additional advantage of better lattice matching to AlN and SiC substrates. However, incorporation of boron at levels sufficient to ensure the lattice matching is problematic and attracted little scientific attention up to now.

Main goal

This work is aimed at investigating the processes limiting luminescence efficiency, and its droop in wide band-gap III-nitrides, especially in BGaN-based epitaxial layers, where boron is introduced to mitigate the lattice mismatch.

Objectives:

1. To study the links between the stimulated emission and the PL efficiency droop in GaN, AlGaN, and AlGaN MQWs.

2. To investigate the interplay between carrier localization conditions and PL efficiency in AlGaN epilayers and MQWs.

3. To reveal the mechanisms of the PL efficiency droop in AlGaN epilayers and MQWs

4. To study the applicability of BGaN epilayers grown on different substrates and templates to solve lattice matching problems in III-nitride-based UV LED structures.

Novelty and importance

The inherent issue of low luminescence efficiency and the detrimental efficiency droop effect in AlGaN is one of the main topics addressed in current III-nitride research. Investigation of these issues by the means of photoluminescence spectroscopy enables the study of exclusively the droop mechanisms, which are intrinsic to the material and are not related to device design.

By simultaneously studying the PL efficiency dynamics, carrier localization conditions and carrier dynamics we were able to perform an in-depth analysis of the interrelated origins and the competing mechanisms of the PL efficiency droop in AlGaN. The results of this study provide new insight into the complicated and obscure issue of the PL efficiency droop in AlGaN.

The influence of stimulated emission is pointed out, for the first time, as one of the origins of the droop in efficiency of spontaneous emission observed in luminescence experiments and in real LEDs. It is revealed that the carrier delocalization plays a dual role in the emission efficiency: the efficiency is decreased due to enhanced nonradiative recombination and increased due to a larger contribution of bimolecular recombination. The ratio of thermal energy and carrier localization strength parameter is demonstrated to be a reliable figure of merit, indicating the prevailing mechanism of droop in different AlGaN

epitaxial layers and MQWs with aluminum content ranging from several to more than 70 %.

A record-high boron content of 5.5% in BGaN, which is the least researched ternary compound in III-nitride family, is demonstrated after a thorough study of novel BGaN epilayers grown by MOCVD on sapphire/GaN, sapphire/AlN, and SiC templates. A partial phase separation is shown to occur in BGaN with the resulting high boron content regions enhancing the nonradiative recombination. This results in the PL efficiency dropping substantially with growing boron content and being lower by orders of magnitude than that in pure GaN even at 8 K temperature. Additionally, the band-gap bowing parameter is evidenced to be ~4 eV, i.e. substantially smaller than reported previously.

Points to be maintained

1. The onset of stimulated recombination, stabilizing the carrier density at higher excitation power density, is the dominant mechanism of the efficiency droop observed in photoluminescence of GaN epilayers and is feasible as one of the droop origins in other III-nitride compounds and structures.

2. The main factor determining the stimulated emission threshold in AlGaN MQWs is not the localization conditions but rather the density of nonradiative recombination centers.

3. The ratio of the thermal energy and the dispersion parameter of potential fluctuations $k_B T/\sigma$ might be used as the parameter indicating the predominant origin of PL droop in AlGaN-based MQWs and epilayers: occupation-enhanced redistribution of nonthermalized carriers at $k_B T/\sigma < 0.35$, enhancement of nonradiative recombination as

the localized states are filled-in and an increasing fraction of carriers becomes delocalized at $0.35 < k_B T/\sigma < 1$, stimulated emission in AlGaN MQWs and excitation-enhanced carrier transport to extended defects in AlGaN epilayers at $k_B T/\sigma > 1$.

4. Partial phase separation occurs in BGaN epilayers with boron content above 2%. Nonradiative recombination in the boron-rich regions is the dominant factor decreasing the PL efficiency in high-boron-content BGaN.

5. The bowing parameter in BGaN is shown to be ~4 eV, substantially lower than that reported before (9.2 eV).

Layout of the thesis

The thesis consists of an introduction, a review of III-nitride materials and related works, a brief description of experimental techniques and samples under study, four chapters presenting experimental results, and a summarizing chapter. The first part is dedicated to an overview of GaN, AlGaN and BGaN material properties. Also, the luminescence efficiency issues in AlGaN are discussed in more detail. ,

Further on in the second part, experimental techniques used and the samples under study are presented. The main experimental setups of steady-state and quasi-steady-state PL spectroscopy are presented in detail and information about different measurement configurations is provided. The samples under this study include GaN, AlGaN, and BGaN epitaxial layers, and AlGaN multiple quantum wells.

Chapter 1 describes different approaches used to determine the carrier localization conditions, which have been exploited in this study. The carrier localization strength is evaluated by the analysis of the data obtained by steady-

state PL measurements at different temperatures. Several different approaches of analyzing the temperature dependences of the PL band peak position are described. The obtained value of the energy dispersion parameter σ, which reflects the potential profile fluctuations, is used in the following chapters as a measure of localization strength.

In chapter 2, experimental results of the stimulated emission spectroscopy are presented and discussed. Different mechanisms of stimulated emission in AlGaN are revealed and linked with different carrier localization conditions. At the same time, the stimulated emission threshold is shown to depend not on the localization conditions, but on the density of the nonradiative recombination centers. Stimulated emission is shown to cause the efficiency droop observed in photoluminescence of GaN.

Chapter 3 is dedicated to an in-depth analysis of the PL efficiency and its droop in AlGaN, and is divided into three sections. The competition between the efficiency-increasing and the efficiency-decreasing effects of carrier delocalization is analyzed and leads to the introduction of parameter $k_B T/\sigma$. Together with localization strength σ, this parameter is shown to act as a figure of merit to determine the prevailing mechanism of the PL efficiency droop in AlGaN MQWs and epilayers. As a result, at least three different origins of the PL droop in AlGaN are distinguished.

Chapter 4 reports on the properties of novel BGaN epilayers with boron content of up to 5 %, grown on three different types of sapphire and SiC templates. A partial BGaN phase separation, evidenced by second PL band, is shown to occur in all samples regardless of growth conditions. Higher nonradiative recombination rate in regions with larger boron content is demonstrated to be responsible for the catastrophic PL efficiency decrease in BGaN epilayers with increasing boron content. The value of the band-gap bowing parameter in BGaN layers is reliably determined to be substantially lower than that previously reported.

A short summarizing chapter concludes the main results.

Approbation of the research results

The majority of the results presented in this thesis are published in several peer-reviewed scientific journals. The results were presented in a number of international and national scientific conferences. The scientific papers (12) and conference presentations related to this study (23) are listed below. 4 conference presentations were presented by the author of this thesis. They are highlighted in bold. A separate list is given for scientific papers which are not directly related to this study.

List of publications directly related to this thesis (numbering later used in text for references):

P1. J. Mickevičius, <u>J. Jurkevičius</u>, A. Kadys, G. Tamulaitis, M. Shur, M. Shatalov, J. Yang, R. Gaska, „Temperature-dependent efficiency droop in AlGaN epitaxial layers and quantum wells", *AIP Advances*, **6**, 045212 (2016).

P2. <u>J. Jurkevičius</u>, J. Mickevičius, A. Kadys, M. Kolenda, and G.Tamulaitis, „Photoluminescence efficiency of BGaN epitaxial layers with high boron content", *Physica B: Condensed Matter*, **492**, p. 23 (2016)

P3. J. Mickevičius, G. Tamulaitis, <u>J. Jurkevičius,</u> M.S. Shur, M. Shatalov, J. Yang, R. Gaska, „Efficiency droop and carrier transport in AlGaN epilayers and heterostructures", *Physica Status Solidi B* **252** (5), p. 961 (2015).

P4. T. Malinauskas, A. Kadys, S. Stanionytė, K. Badokas, J. Mickevičius, <u>J. Jurkevičius,</u> D. Dobrovolskas, G. Tamulaitis, „Growth of BGaN epitaxial layers using close coupled showerhead MOCVD", *Physica Status Solidi B*, **252** (5), p. 1138 (2015).

P5. A. Kadys, J. Mickevičius, T. Malinauskas, J. Jurkevičius, M. Kolenda, S. Stanionytė, D. Dobrovolskas, G. Tamulaitis, „Photoluminescence of BGaN layers grown on different substrates", *Journal of Physics D*, **48**, 465307 (2015).

P6. J. Mickevičius, J. Jurkevičius, A. Kadys, G. Tamulaitis, M. Shur, M. Shatalov, J. Yan, R. Gaska, „Low-temperature redistribution of non-thermalized carriers and its effect on efficiency droop in AlGaN epilayers", *Journal of Physics D*, **48**, 275105 (2015).

P7. J. Mickevičius, Ž. Podlipskas, R. Aleksiejūnas, A. Kadys, J. Jurkevičius, G. Tamulaitis, M. S. Shur, M. Shatalov, J. Yang, and R. Gaska, „Nonradiative recombination, carrier localization, and emission efficiency of AlGaN epilayers with different Al content", *Journal of Electronic Materials*, **44** (12), p. 4706 (2015).

P8. J. Mickevičius, J. Jurkevičius, G. Tamulaitis, M. S. Shur, M. Shatalov, J. W. Yang, R. Gaska, „Influence of carrier localization on high-carrier-density effects in AlGaN quantum wells", *Optics Express* **22** (S2), p. A491 (2014).

P9. G. Tamulaitis, J. Mickevičius, J. Jurkevičius, M. S. Shur, M. Shatalov, J. Yang, R. Gaska, „Photoluminescence Efficiency in AlGaN Quantum Wells", *Physica B Condensed Matter* **453**, p. 453 (2014).

P10. J. Mickevičius, J. Jurkevičius, M. S. Shur, J. W. Yang, R. Gaska, G. Tamulaitis, "Photoluminescence efficiency droop and stimulated recombination in GaN epilayers", *Optics Express* **20** (23), 25195 (2012).

P11. J. Mickevičius, J. Jurkevičius, K. Kazlauskas, A. Žukauskas, G. Tamulaitis, M. S. Shur, M. Shatalov, J. Yang, R. Gaska, "Stimulated emission in AlGaN/AlGaN quantum wells with different Al content", *Applied Physics Letters*, **100**, 081902 (2012).

P12. J. Mickevičius, J. Jurkevičius, K. Kazlauskas, A. Žukauskas, G. Tamulaitis, M. S. Shur, M. Shatalov, J. Yang, R. Gaska, "Stimulated

emission due to localized and delocalized carriers in $Al_{0.35}Ga_{0.65}N/Al_{0.49}Ga_{0.51}N$ quantum wells", *Applied Physics Letters*, **101**, 041912 (2012).

List of the presentations in conferences:

1. **J. Jurkevičius**, A. Kadys, J. Mickevičius, T. Malinauskas, A. Vaitkevičius, S. Stanionytė, G. Tamulaitis, "Photoluminescence of BGaN epitaxial layers grown on sapphire and SiC substrates with GaN and AlN buffer layers", Lietuvos nacionalinė fizikos konferencija, Vilnius, 2015.

2. **J. Jurkevičius,** , J. Mickevičius , A. Kadys, G. Tamulaitis, M. Shur, M. Shatalov, J. Yang, R. Gaska, „Efficiency droop in AlGaN epitaxial layers and multiple quantum wells", The 4th International Conference on the Physics of Optical Materials and Devices, Budva, 2015.

3. G. Tamulaitis, J. Mickevičius, J. Jurkevičius, S. Nargelas, M. Shur, M. Shatalov, J. Yang and R. Gaska, Radiative and nonradiative exciton recombination in quantum dots unintentionally formed in AlGaN, International Conference on Optics of Excitons in Confined Systems (OECS), Jerusalem, 2015.

4. J. Mickevičius, J. Jurkevičius, A .Kadys, G. Tamulaitis, M. Shur, M. Shatalov, J. Yang, and R. Gaska, Influence of Temperature and Carrier Localization on Efficiency Droop in AlGaN Epitaxial Layers and Multiple Quantum Wells, The 11th International Conference on Nitride Semiconductors (ICNS-11), Beijing, 2015.

5. G. Tamulaitis, S. Nargelas, Ž. Podlipskas, R. Aleksiejūnas, J. Mickevičius, J. Jurkevičius, T. Saxena, M. Shur, M. Shatalov, J. Yang, and R. Gaska, Temperature dependence of carrier dynamics in AlGaN epitaxial

layers, The 11th International Conference on Nitride Semiconductors (ICNS-11), Beijing, 2015.

6. G. Tamulaitis, A. Kadys, J. Jurkevičius, J. Mickevičius T. Malinauskas, A. Vaitkevičius, S. Stanionytė, Photoluminescence of BGaN epitaxial layers grown on sapphire and SiC substrates with GaN and AlN buffer layers, The 11th International Conference on Nitride Semiconductors (ICNS-11), Beijing, 2015.

7. J. Mickevičius, J. Jurkevičius, G. Tamulaitis, M. S. Shur, M. Shatalov, J. Yang, and R. Gaska, Carrier localization, efficiency droop and stimulated emission in AlGaN quantum wells, E-MRS 2015 Spring Meeting, Lille, 2015.

8. G. Tamulaitis, T. Malinauskas, A. Kadys, K. Badokas, J. Mickevičius, J. Jurkevičius, and D. Dobrovolskas, MOCVD growth and investigation of epitaxial BGaN layers, ISSLED 2014 10th International Symposium on Semiconductor Light Emitting Devices, Kaohsiung, 2014.

9. **J. Jurkevičius**, J. Mickevičius, G. Tamulaitis, M. S. Shur, M. Shatalov, J. W. Yang, R. Gaska, „Photoluminescence Efficiency Dependence on Carrier Localization Conditions in AlGaN Epilayers and Quantum Wells", Advanced Materials and Technologies, Palanga, 2014.

10. J. Mickevičius, J. Jurkevičius, G. Tamulaitis, M. S. Shur, M. Shatalov, J. Yang, and R. Gaska, Efficiency droop and carrier transport in AlGaN epilayers and heterostructures, International Workshop on Nitride Semiconductors, Wroclaw, 2014.

11. R. Aleksiejūnas, Ž. Podlipskas, A. Kadys, J. Mickevičius, J. Jurkevičius, G. Tamulaitis, M. S. Shur, M. Shatalov, J. Yang, and R. Gaska, Radiative and non-radiative recombination of nonequilibrium carriers in AlGaN

epilayers with various Al content, International Workshop on Nitride Semiconductors, Wroclaw, Poland, 2014.

12. G. Tamulaitis, J. Mickevičius, <u>J. Jurkevičius</u>, M. S. Shur, M. Shatalov, J. Yang, and R. Gaska, The link between carrier localization and high-carrier-density effects in AlGaN quantum wells, International Workshop on Nitride Semiconductors, Wroclaw, 2014.

13. T. Malinauskas, A. Kadys, S. Stanionytė, K. Badokas, J. Mickevičius, <u>J. Jurkevičius</u>, D. Dobrovolskas, and G. Tamulaitis, Growth of BGaN epitaxial layers using closed coupled showerhead MOCVD, International Workshop on Nitride Semiconductors, Wroclaw, 2014.

14. G. Tamulaitis, J. Mickevičius<u>, J. Jurkevičius</u> , M. S. Shur, M. Shatalov , J. Yang, and R. Gaska, Influence of carrier localization on efficiency droop and stimulated emission in AlGaN quantum wells, ISSLED 2014 10th International Symposium on Semiconductor Light Emitting Devices, Kaohsiung, 2014.

15. G. Tamulaitis, J. Mickevičius, <u>J. Jurkevičius</u>, M. S. Shur, M. Shatalov, J. Yang, and R. Gaska, "Photoluminescence efficiency in AlGaN quantum wells", the XXII International Materials Research Congress, Cancun, 2013.

16. G. Tamulaitis, J. Mickevicius, **<u>J. Jurkevičius</u>**, M. S. Shur, M. Shatalov, J. Yang, and R. Gaska, "Temperature and carrier density dependence of photoluminescence efficiency in AlGaN epilayers and quantum wells", the International Conference on Nitride Semiconductors (ICNS-10), Washington D.C., 2013.

17. J. Mickevičius, <u>J. Jurkevičius</u>, G. Tamulaitis, M. S. Shur, M. Shatalov, J. Yang, and R. Gaska, "Stimulated emission and carrier localization in AlGaN/AlGaN quantum wells", the E-MRS Spring Meeting, Strasbourg, 2012.

18. G. Tamulaitis, J. Mickevicius, <u>J. Jurkevicius</u>, M. S. Shur, J. Yang and R. Gaska, "Efficiency droop and stimulated emission in GaN epilayers", the 31st International Conference on the Physics of Semiconductors, Zurich, 2012.

19. J. Mickevicius, <u>J. Jurkevicius</u>, G. Tamulaitis, M. Shur, J. Yang, M. Shatalov, and R. Gaska, "Influence of potential fluctuations on stimulated emission in AlGaN quantum wells", the 31st International Conference on the Physics of Semiconductors, Zurich, 2012.

20. J.Mickevičius, **<u>J.Jurkevičius</u>**, M.Shur, R.Gaska, G.Tamulaitis, „Photoluminescence Efficiency Decrease and Stimulated Emission in GaN epilayers", the 14th International Conference-School Advanced Materials and Technologies, Palanga, 2012.

21. G.Tamulaitis, J.Mickevičius, <u>J.Jurkevičius</u>, M.S.Shur, J.Yang, and R.Gaska, "Droop in GaN epilayers: the role of stimulated emission", the International Workshop on Nitride Semiconductors (IWN2012), Sapporo, 2012.

22. **<u>J. Jurkevičius</u>**, J. Mickevičius, G. Tamulaitis, M. S. Shur, J. Yang, R. Gaska, „Stimulated emission in high-aluminum content AlGaN/AlGaN multiple quantum wells", the 13-th International Summer School-Conference Advanced Materials and Technologies, Palanga, 2011.

23. <u>G. Tamulaitis</u>, J. Mickevičius, J. Jurkevičius, M. S. Shur, M. Shatalov, J.Yang, and R. Gaska, "Stimulated emission threshold in AlGaN/AlGaN quantum wells with different Al content", Program and Abstracts of the 9th International Conference on Nitride Semiconductors, Glasgow, 2011.

List of the publications directly unrelated to this thesis:

1. Ž. Podlipskas,   R. Aleksiejūnas,   S. Nargelas,   J. Jurkevičius, J. Mickevičius, A. Kadys, G. Tamulaitis, M. S. Shur, M. Shatalov, J. Yang, and R. Gaska, "Photomodification of carrier lifetime and diffusivity in AlGaN epitaxial layers", *Semiconductor Science and Technology*, **16** (6), p. 633 (2016).

2. Ž. Podlipskas, R. Aleksiejūnas, A. Kadys, J. Mickevičius, J. Jurkevičius, G. Tamulaitis, M. S. Shur, M. Shatalov, J. Yang, R. Gaska, "Dependence of radiative and nonradiative recombination on carrier density and Al content in thick AlGaN epilayers", *Journal of Physics D: Applied Physics*, **49** (14), 145110 (2016.)

3. P. Ščajev,   J. Jurkevičius,   J. Mickevičius,   K. Jarašiūnas,   H. Kato, "Features of free carrier and exciton recombination, diffusion, and photoluminescence in undoped and phosphorus-doped diamond layers", *Diamond and Related Materials*, **57**, p. 9 (2015).

III-nitride materials

Blue/UV emitters based on metal-insulator-semiconductor GaN structure were produced as early as in 1971[1] and even briefly commercialized[2]. However, for almost two decades from then on the potential of III-nitride optoelectronics laid dormant. In 1989, the successful development of p-type doping of the extrinsically n-type GaN by I. Akasaki and H. Amano[3] and the development of suitable growth techniques (such as MOCVD and MBE) opened the way for the revolutionary development of the blue InGaN-based LED in Nichia lab by S. Nakamura. These achievements were closely followed by development of green, amber, white, near-UV LEDs. Continuous wave blue and near-UV operating LDs were demonstrated in 1997[4]. These ground-braking technological advancements that paved way for a whole field of III-nitride research were acknowledged by the scientific community by awarding the 2014 Nobel Prize in physics to I. Akasaki, H. Amano, and S. Nakamura.

The successes of III-nitride development is based on the unique properties of the nitride material family. The possible band gaps of ternary alloys of GaN, InN, AlN and BN span an extremely wide range from 0.8 eV to 6.2 eV, enabling development of light emitters operating at the wavelengths from infrared (1600 nm) to deep UV (200 nm)[5]. As this work focuses on the wide-band-gap nitrides, InN and its alloys are largely left aside. In this chapter, the structural and optical properties of GaN, AlN, BN, their alloys and structures are reviewed. The main challenges and progress in the development of these materials are also summarized.

III-nitride structure and material properties; growth issues

Gallium nitride is a direct wide-band-gap (3.44 eV at 300 K) crystalline semiconductor with three possible crystal structures: wurtzite, zincblende, and rock salt. Though at ambient conditions the thermodynamically stable structure for bulk GaN is wurtzitic[6], the cubic zincblende structure can be stabilized by growing thin epitaxial layers on the (001) planes of cubic substrate (Si, MgO, GaAs). The rock salt structure can be forced by at high pressures[7].

AlN structurally is very similar to GaN: a direct band-gap (6.2 eV at 300 K) semiconductor, crystallizing in the wurtzite lattice at ambient conditions. Inside the wurtzite lattice (see Fig. 1a) each atom is tetrahedrally coordinated (bonded to four atoms of other type, which are situated in the vertices of a symmetrical tetrahedron). The wurtzite lattice can be seen as comprised of the layers of hexagonally arranged atoms, which are shifted in respect to one another in such a way that every second layer is in the same position (ABAB). The layers are stacked in the {0001} crystallographic plane and the hexagonal wurtzite structural axis *c* is perpendicular to these planes.

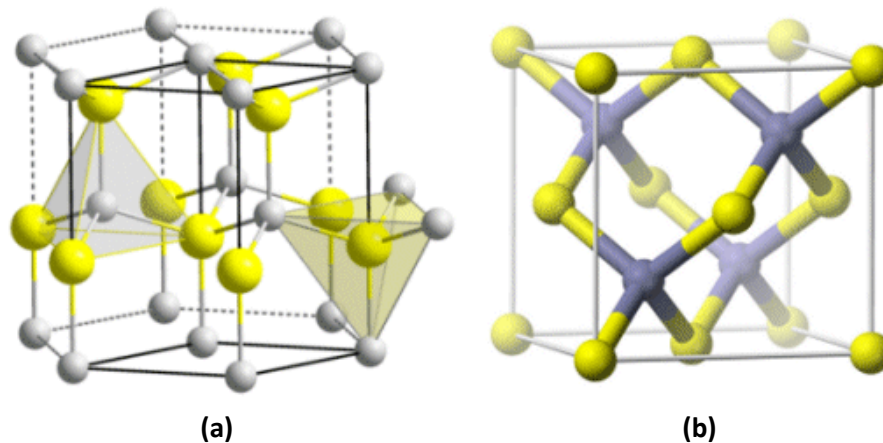(a)   (b)

Fig. 1. GaN in the wurtzite (a) and zincblende (b) lattice structures. Pictures taken from: https://en.wikipedia.org/wiki/File:Wurtzite_polyhedra.png (a); https://commons.wikimedia.org/w/index.php?curid=2068452 (b).

If the stacking of layers is slightly shifted and every third layer ends up in the same position (ABCABC), a zincblende structure is obtained (Fig. 1b). However, in this case the layers are stacked in plane {111}.

Inside the layer of both wurtzite and zincblende structures, the atoms of different group form two sublayers: the atoms of one group are shifted in respect to the other group perpendicularly to the layer plane. As a result, III-nitride materials do not have inversion symmetry along the *c* axis. Depending on the growth conditions, the topmost sublayer can be engineered to have either the nitrogen ions, or the group III ions facing out[8]. The chemical and mechanical properties of a crystalline layer depend on the type of face.

Another result of the shifting of atoms along the *c* axis in the layers is the spontaneous polarization of the lattice, present in both wurtzite and zincblende lattices. The strong ionic bond between a nitrogen atom and a group III atom results in each layer being a polarized plane. In a perfect lattice of a bulk crystal, the neighboring planes compensate each other's polarization, but in heterostructures such as MQW the interfaces experience internal electric field due to uncompensated charges.

The structural properties of BN, meanwhile, are considered as a special case, because of the four stable polytypes: wurtzite structure, cubic zinc blende structure, hexagonal, and rhombohedral. All of these BN structures are indirect band-gap semiconductors with significantly different band gap values (see Table. 1). The only polytype stable under ambient conditions is the hexagonal structure[9]. However, the study of PL in a single h-BN crystal has presented evidence that hexagonal BN might have a direct band-gap close to 6 eV[10].

The hexagonal, wurtzite and zincblende lattices are anisotropic – the lattice constant differs at crystallographic axes *c* and *a*. The lattice constants for different materials are given in Table 1.

Table 1. Lattice constant and band gap in III-nitride materials[11]

	GaN Wurtzite	AlN Wurtzite	BN	
			Hexagonal	Cubic
Lattice constant a (Å)	3.16 - 3.19	3.11	6.661	3.616
Lattice constant c (Å)	5.125 - 5.190	4.98	2.504	-
Band-gap (eV), 300 K	3.39-3.44 eV	6.2	5.2	6.4

Up to now, there is no ideal substrate for the growth of III-nitrides. Some high-quality GaN films were grown on GaN platelets, grown from liquid phase under high pressure, as high quality substrates.[12–14]. However, such a substrate is unfit for device manufacturing. The complete majority of III-nitride growth is performed on foreign substrates. Among the most popular are sapphire (Al_2O_3), SiC, and Si.

Silicon carbide (polytype 6h-SiC) has one of the smallest possible lattice mismatches with GaN and AlN ($a = 3.073$ Å) and hexagonal symmetry. Moreover, SiC has excellent thermal conductivity. However, SiC wafers are small, brittle, and the cost of SiC per area exceeds that of the common substrates of sapphire by orders of magnitude. The application of SiC substrates is mainly limited to the fabrication of deep UV-emitting devices, as the relatively low band gap of 3.0 eV (6h-SiC) causes undesirable absorption[11].

Most widely used are sapphire substrates. Despite the lattice mismatch of ~15 %, sapphire is cheap, available in high quality, the wafers are of larger area, have good thermal conductivity and are transparent to UV in the range important for III-nitrides (the sapphire band gap is 9.9 eV). The significant lattice mismatch is commonly dealt with by growing a thick buffer layer, as the quality of a heteroepitaxial film increases with layers thicknes[7].

While growing pure nitrides is challenging because of lack of suitable substrates, growing ternary alloys, such as AlGaN, raises additional issues. The

optimal growth temperature of GaN (~800 C) and AlN (1000-1200 C) differ significantly[7]. Therefore, when growing AlGaN ternary alloy, optimal conditions for different III-group elements to be deposited on the crystals surface cannot be achieved.

Boron incorporation into BGaN alloy is even more problematic. The ion radii of boron and gallium are substantially different[15], which is in turn expected to result in a wide miscibility gap and phase separation already at several percent of boron[16,17]. Growing BGaN layers by using different substrates have been attempted[15,17–26], and BGaN layers with the boron content of up to ~1.5% and ~1.8% have been reported in BGaN deposited on SiC substrates[15,17,20,27] and AlN/sapphire templates[21,22], respectively.

Considerably more attempts to incorporate boron into GaN were based on deposition on GaN/sapphire templates, and the contents of incorporated ranging from 0.7% to 7% are reported in these layers[18,24,28,29]. The highest reported boron content of 7% in BGaN film was obtained using ion implantation into GaN film grown on sapphire[24]. In all cases, the phase separation in the solid phase and the surface saturation caused by the boron precursor were considered to be the main factors limiting the boron incorporation. Unfortunately, the published studies of boron incorporation were based on a single substrate/template and no comparison of BGaN growth on different substrates and under different deposition conditions using the same reactor was reported.

The reports on optical properties of BGaN layers are still quite scarce and usually present the comparison of BGaN photoluminescence (PL) spectrum with that of the reference GaN layer[15,20,21,27,29]. While several early publications reported the broadening of the band gap with increasing boron content[20,27,30], the later studies showed a decrease of the band gap for BGaN with small boron content[21,29], which was in consistence with the results of theoretical studies[31,32]. However, the extremely large bowing parameter value of 9.2 eV

reported in Ref. 21 is unreliable, since its estimation is based on the study of BGaN layers with boron content of only up to ~1.8%.

Efficiency issues in AlGaN based devices

The performance of the AlGaN-based deep-UV LEDs is rapidly improving, and the external efficiency of the LEDs emitting in the 270-280 nm spectral range already exceeds 10%[33]. The main technological challenges include material quality, achieving high *p*-type doping[34,35], and increasing light extraction[36]. A large scientific effort remains focused on the device efficiency issues.

The LEDs based on III-nitride materials highly benefit from the carrier localization, which results in a high internal quantum efficiency (IQE)[37,38]. S-shaped and W-shaped temperature dependences of PL band peak position and width, respectively, are usually considered to be a fingerprint of carrier (exciton) localization and were observed in ternary AlGaN[39,40] and quaternary AlInGaN[41,42]. The data reported in literature[43,44] show that carrier localization in AlGaN, especially at high Al content, does play an important role in carrier dynamics even at room temperature.

Coexistence of localized and free carriers in AlGaN obscures the carrier dynamics, which is much better understood in two limiting cases. In III-nitrides with only free carriers, the rate equation with constant coefficients for linear, bimolecular, and Auger recombination can be applied (usually referred to as the ABC model), though with considerable caution[45–47]. In the case of strong carrier localization (e.g., at low temperatures), the carriers are localized predominantly at the same potential minimum building an exciton-like electron-hole pair, which moves through the crystal by hopping via localized states[48,49]. The description and understanding of the processes in a dense

carrier system containing significant fractions of both localized and free carriers is considerably more difficult and needs further investigation.

The efforts in this direction are encouraged by the notorious problem of efficiency droop deteriorating performance of LEDs based both on InGaN and AlGaN. In addition to external mechanisms (the decreased capture of the injected carriers into the QWs or their enhanced escape out of the wells[50–54]), there are several internal mechanisms suggested to be responsible for the droop.

The nonradiative Auger recombination[45,55], especially after direct observation of Auger electrons[56], is the most popular explanation of the droop origin in InGaN-based LEDs. However, Auger recombination has been studied theoretically[57] and was observed experimentally[56,58] only in InGaN structures. It is expected to be less pronounced in AlGaN due to anticipated reduction of Auger coefficient, both direct and phonon (or impurity) assisted, with increasing band gap[59,60].

At the same time, the role of delocalization-activated nonradiative recombination[61–63], phase-space filling and saturated radiative recombination rate[63–65], stimulated emission[66], junction heating[67] and incomplete carrier localization[48], thermally-activated carrier delocalization and current transport along dislocations, and screening of the localization potential fluctuations[68], might be important, especially in LEDs based on wide-band-gap AlGaN, where the Auger recombination still has not been unambiguously evidenced.

Though the internal origin or origins of the efficiency droop are still not clear, several peculiarities on the topic may be pointed out. First of all, the efficiency droop has mostly been studied at room temperature, which is relevant to the operation conditions of light emitting devices, while relatively little attention has been paid to the droop at lower temperatures. At lower temperatures, the droop is even more pronounced and the internal quantum efficiency (IQE) reaches its peak value at lower excitations[46,69,70] and at

23

considerably lower carrier densities than those corresponding to the droop occurring at room temperature[70]. The excitation power densities corresponding to the droop onset at low and room temperatures differ considerably more than the carrier lifetimes determining the carrier densities[71]. Such temperature dependence cannot be explained by the Auger mechanism, both direct and indirect, since the Auger coefficient strongly depends on carrier density and is not expected to increase at low temperatures[59,60]. On the other hand, carrier delocalization and/or redistribution within localized states have been shown to correlate well with the droop onset[62,72].

Secondly, two types of the efficiency dependence on the excitation intensity are usually observed: a slow rise and a slow decay for type I, and a fast rise and a fast decay for type II[73,74]. The desirable efficiency droop curve, type III, should exhibit a fast rise and a slow decay. Spatially resolved electroluminescence studies revealed that weak and strong carrier localization lead to the type I and type II droop curves, respectively[73]. The efficiency dependence on excitation was attributed to the competition of the following three effects: i) nonradiative recombination via point defects, ii) nonradiative recombination at the extended defects, and iii) carrier localization. For the type I behavior observed in the samples with small potential profile fluctuations, the initial rise rate in efficiency depends on the density of microscopic defects that need to be saturated. For the type II behavior in the samples with significant potential fluctuations, the local energy minima provide sites for carrier trapping and inhibit carrier diffusion to nonradiative recombination centers[74]. To achieve the Type III scenario, the material has to contain low densities of point and extended defects and have optimal potential fluctuations for the carrier localization[73]. However, the role of the carrier localization is not completely clear, as most of the previous studies were focused on the role of defects.

Experimental

The optical characterization of the samples under study was performed by photoluminescence (PL) spectroscopy. PL spectroscopy is a versatile and widely used technique for investigation of optical properties of semiconductors and their structures. We have performed PL measurements under continuous wave (CW) and pulsed laser excitation, under steady-state and quasi-steady-state excitation conditions.

The steady-state excitation conditions are achieved when the carrier generation and recombination rates are constant and equal. As a result, a constant carrier density is obtained. As the PL signal is time-independent, it can be registered for the exposure time as long as needed, and even very weak PL signals can be measured. However, the limited power of CW laser source also limits the maximum carrier density that can be excited in the sample.

To perform PL spectroscopy at higher excitation levels, quasi-steady-state excitation was employed. A high-power laser pulse excitation allows for a higher carrier density. However, the excitation conditions are considered quasi steady state only if the duration of the excitation pulse is larger than the duration of lifetime of nonequilibrium carriers.

The quasi-steady-state PL measurement setup is presented in Fig. 2. The samples were excited at 266 nm (4.66 eV) or 213 nm (5.82 eV) using the 4th and 5th harmonics of the Q-switched YAG:Nd laser (1) radiation with pulse duration of 4 ns and repetition rate of 10 Hz (*Ekspla NL301*). In some cases, radiation of tunable-wavelength nanosecond laser (*Ekspla NT342B*) was used. An iris diaphragm was used as an aperture (2) to adjust the excitation beam width.

The excitation intensity was varied in a wide range by using an attenuator (3). Usually, the attenuator was comprised of a polarizing half-wave plate and an analyzing Glan prism. To achieve extremely low intensities, a quartz cuvette filled with water/ink solution was used as an additional intensity damper. The

excitation intensity was gauged by a photodiode-based power meter (*OPHIR PD-10*), which was placed in the sample position. During the measurement process, a fraction of the excitation beam was reflected by a quartz plate (4),
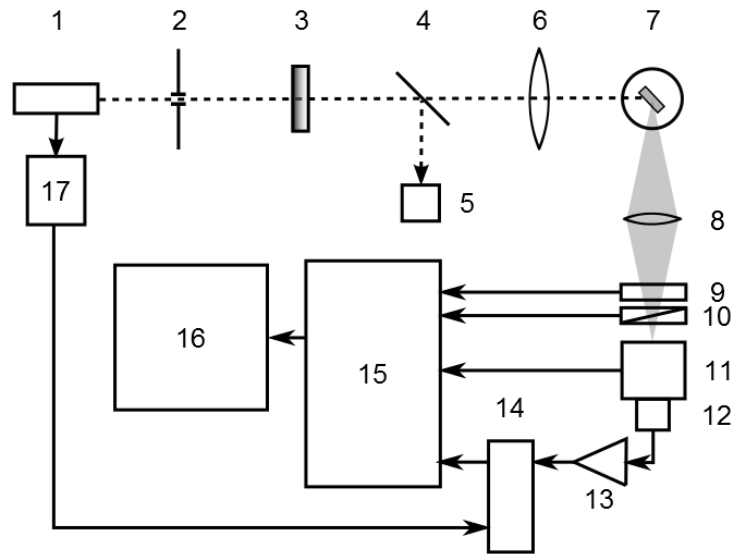

Fig. 2. Setup for quasi-steady-state PL measurements at front face excitation: excitation source (1), aperture (2), attenuator (3), beam-splitter (4), intensity gauge (5), excitation beam focusing lens (6), sample in the chamber of the cryostat (7), PL signal focusing lens (8), shutter (9), polarizer (10), monochromator (11), photomultiplier (12), amplifier (13), box-car integrator (14), control unit (15), computer (16), signal generator (17).

and the intensity was monitored by the same power meter (5).

Quartz lenses were used for focusing the excitation beam (6) and collecting the PL signal (8). The focusing lens (6) was mounted on a rail aligned parallelly to the beam path. This enabled us to change the size of the excited area without changing the location of the excitation spot.

Samples were investigated in a wide range of temperatures (from 8 K to 300 K) by placing the sample in a cryostat (7). The temperature variation and stabilization in the closed-cycle helium cryostat (*CTI-Cryogenics 22*) was ensured by its temperature controller (*Lake Shore Cryotronics 331*).

The PL signal was collected into the slit of a double monochromator (*Jobin Yvon HRD-1*) (11) with holographic gratings. An UV - enhanced photomultiplier tube (*Hamamatsu R1463P*) detected the dispersed PL signal (12). The resulting electric signal was amplified (13) and sent into a box-car integrator (14), which

is synchronized by a pulse generator (17), which was triggered by the laser pulse.

The electromechanical shutter (9), the monochromator (11) and signal registration system (the voltage for the photomultiplier, the box-car parameters) is controlled electronically via computer (16) by a control unit (15).

Several modifications of the above described setup of quasi-steady-state PL measurement were employed. To facilitate the measurements of stimulated emission, sample excitation geometry was changed. The conventional front-face excitation (also known as back-scattering) configuration and the edge emission configuration are presented in Fig. 3. In front-face excitation (Fig. 3a), a spherical lens (1) focuses the excitation beam into a spot (from 100 μ to 1 mm in diameter) on the sample surface. The PL radiation is emitted almost uniformly at all directions, and a fraction of it is collected with another lens into the monochromator slit.

Fig. 3. Front-face (a) and edge-emission (b) measurement configurations.

In the case of edge-emission configuration (Fig. 3b), the excitation beam is focused with a cylindrical lens into a narrow stripe (25 to 50 μm wide and 1 to 2 mm long). If carrier density above the stimulated emission threshold is achieved, the narrow stripe is favorable for the propagation of stimulated emission along the axis of the stripe. The stimulated emission exiting the edge of the sample is collected by a lens for detection.
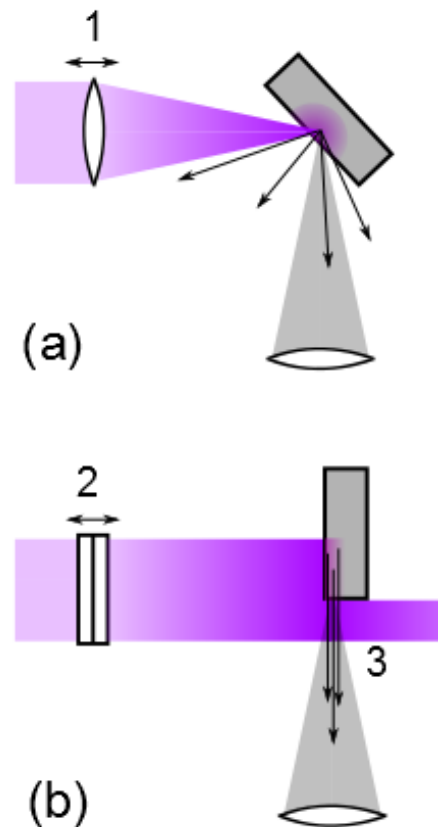
The steady-state setup was similar to the quasi-steady-state setup shown in Fig. 2. In this case, a He-Cd CW laser (*Plasma HCCL-4UM*) emitting at 325 nm was used as the excitation source (1). Instead of amplifier (13) and box-car integrator (14), a single photon counter was used to register the signal. The steady-state PL measurements were used mainly to achieve low carrier density, which was necessary to investigate carrier localization conditions.

In some PL measurements of BGaN samples, an ICCD detector (*Andor DH320T*) was used with a spectrometer (*Andor Shamrock 500i*) as the signal registration device. During these measurements, the spectrometer and the camera were controlled via computer without any additional control unit.

Although the vast majority of the experimental results were acquired by using PL spectroscopy, the results obtained by other experimental techniques were also used in this study. The carrier lifetime and its decay in the samples under study were measured by using the light-induced transient grating technique (measurements performed by Dr. R. Aleksiejūnas and Ž. Podlipskas). The sample structural quality and composition were evaluated by XRD spectroscopy (measurements performed by Dr. T. Malinauskas, and S. Stanionytė). The sample surface was investigated by atomic force microscopy (measurements performed by Dr. D. Dobrovolskas).

Samples under study

In this study, selected sets of GaN, AlGaN and BGaN samples were investigated.

GaN. Eight GaN epitaxial layers grown on c-plane sapphire using a combination of Metal-Organic Chemical Vapor Deposition (MOCVD) and Migration Enhanced MOCVD (MEMOCVD®) techniques. Samples with different carrier lifetimes ranging from 41 ps to 3630 ps were selected. The difference in carrier lifetimes was caused by different growth conditions and layer thicknesses.

AlGaN. The samples for this work were selected to cover a wide range of carrier localization conditions. In total, 30 samples of AlGaN epilayers and MQWs were selected for investigation. All the AlGaN epilayers and MQWs were grown on c-plane sapphire substrates by using MOCVD and MEMOCVD® techniques. To cover a wider range in localization conditions, samples with aluminum content ranging from 17% to 78% were selected. The thicknesses of the layers varied between 1 and 2 μm. All the MQW samples contained ten QWs. The Al molar fraction in the MQW samples ranged from 8% to 35%. The well thickness in the MQW samples was from 2.5 to 5.0 nm. The dislocation densities in the AlGaN samples under study were estimated using the pits detected by AFM and ranged between $5×10^8$ and $1×10^{10}$ cm^{-3}.

BGaN. The BGaN epitaxial layers were grown by MOCVD. Three different substrates were used for the growth of BGaN layers: GaN/sapphire, AlN/sapphire templates, and 6H-SiC substrates.

The 3 μm-thick GaN templates were grown using a standard low-temperature GaN buffer and growing the subsequent high-temperature GaN

29

layer. The AlN/sapphire templates were grown at 1135 °C temperature after substrate annealing in hydrogen ambient and growth of a thin nucleation layer. The SiC substrates were used without any special nucleation or buffer layers, except for substrate annealing at 1050 °C temperature before growth.

A total of 22 BGaN epitaxial layers were successfully grown with different boron contents of up to 5 %. Three of them were grown on sapphire/GaN template, 9 on sapphire/AlN template, and 10 on SiC.

1. Determining carrier localization conditions

Typically the peak of the photoluminescence (PL) spectrum of a semiconductor material exhibits red-shifting with increasing temperature[75]. This monotonous peak position movement towards lower energies is caused by band gap shrinkage with growing temperature and can be described by an empirical equation:

$$E_{peak}\left(T\right) = E_g\left(0\right) - \frac{\alpha T^2}{\beta + T}. \tag{1.1}$$

Here $E_g(0)$ is band gap energy at 0 K temperature, α and β are empirical parameters. However, PL spectra of the studied aluminum gallium nitride (AlGaN) epitaxial layers and multiple quantum wells (MQWs) exhibit a non-monotonous shift of PL band peak position (Fig. 1.1). This S–shape peak position dependence is characteristic of InGaN and AlGaN epilayers and MQWs and is usually attributed to carrier hopping through localized states in potential profile[76,77].

At low temperatures, carriers are completely localized at different states. Their distribution is not thermalized. Increasing thermal energy allows for
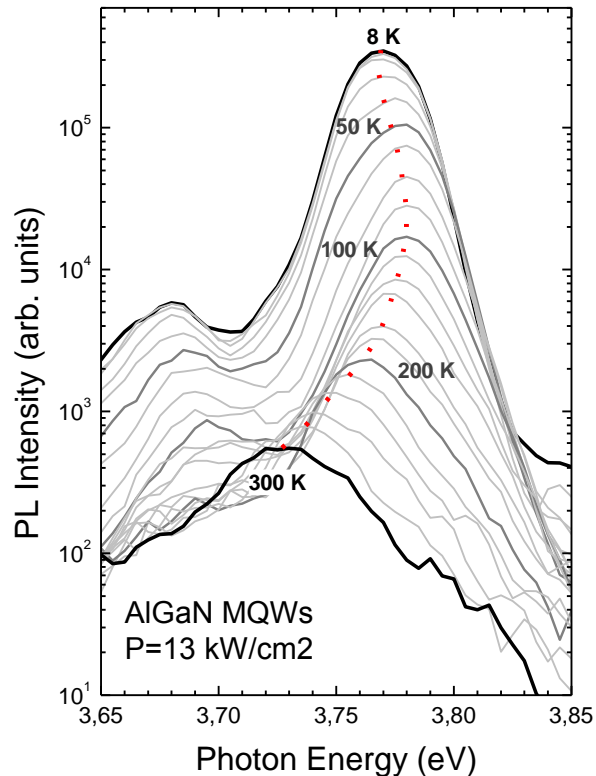
Fig. 1.1 PL spectra of AlGaN MQWs at different temperatures. Dotted line indicates the S–shaped temperature dependence of the band peak position

31

some carriers to leave the shallower localized states and get trapped in the deeper localized states. As a result, the initial red shift of PL band peak position occurs. Further increase of thermal energy initiates the thermalization of carriers. The PL peak position shifts towards higher energies. As most of the carriers become free at elevated temperatures, the temperature-induced band gap shrinkage causes the PL peak position to redshift once again, following the empirical relation given in Eq. (1.1).

As the carrier localization in the potential profile is responsible for the temperature dependence of the position and shape of the PL band, the localization strength can be quantitatively evaluated by analyzing these dependences.

The localization strength can be estimated by measuring the temperature dependence of PL band width. The points in Fig. 1.2 present the extracted full width at half maximum (FWHM) dependences on temperature for AlGaN MQWs. The dependence observed in MQWs with 8% Al (sample A) content can be well approximated by phonon-assisted band broadening (see the solid line drawn according to the equation in the figure). In MQWs with 35% Al content (sample C), the temperature dependence of FWHM has an abnormal W-shape that is typical of compounds with strong localization. We fitted the low-temperature part of the dependence with the curve obtained by the Monte Carlo simulations of the exciton hopping through localized states. Previously, we applied this approach to AlInGaN[42], AlGaN[78], and InGaN[79] epilayers and heterostructures. All Monte Carlo simulations were conducted by Dr. K. Kazlauskas.

The fitting result is plotted by a solid line in Fig. 1.2. A simple model of potential fluctuations with a single dispersion could not fit experimental data, while the model of double-scaled potential fluctuations ensured a reasonable fit. According to this model (see Ref. 42 for more details), the carriers (excitons) accumulate in the areas, where the average exciton energy is lower than that

in surrounding regions. The average exciton energy fluctuates from area to area with a dispersion parameterΓ, which determines inhomogeneous broadening. Furthermore, while moving in the low-potential area, an exciton experiences potential fluctuations on a smaller spatial scale with an energy dispersion parameter σ, which directly governs hopping. The best fit is achieved at σ = 36 meV and Γ = 27 meV. The obtained σ value of 36 meV shows that the carriers in sample C are strongly affected by localization even at room temperature (with the average thermal energy of 25 meV).
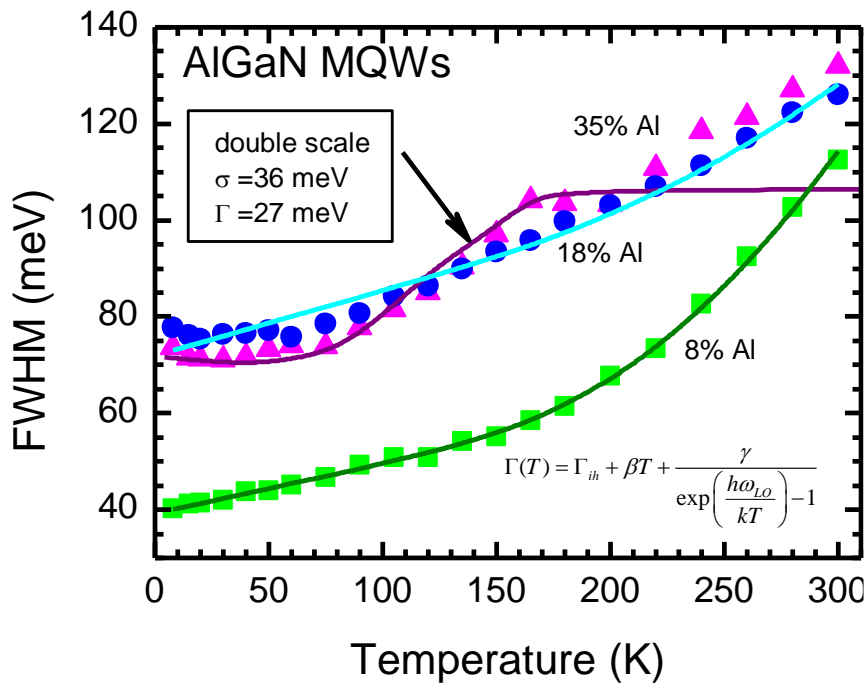
Fig. 1.2. Temperature dependences of spontaneous emission band FWHM for three AlGaN epilayers with different Al content (points). Solid lines show the best fit using the double-scaled potential profile model or phonon-assisted band broadening model.[P11]

Fitting the peak position dependencies for MQWs with 18 % and 8 % Al (samples B and A, respectively) with results of double-scale potential profile Monte Carlo simulations did not produce a good fit. In MQWs with 8 % aluminum, a clear fit was obtained by using phonon-assisted band broadening

model (Fig. 1.2, green line). This might be explained by lower Al content, which causes a relatively low level of inhomogeneity and, subsequently, weak localization.

The larger FWHM values at low temperatures indicate stronger localization in sample B compared to sample A. The shape of the dependence of FWHM of the spontaneous emission band on temperature in sample B (18% of Al) is intermediate between those obtained in samples A and C and can be properly described neither by phonon – assisted band broadening nor by the double-scaled potential fluctuations. The characteristic W – shape of the temperature dependence of FWHM points to even stronger carrier localization in sample C.

The increasing localization strength with growing Al content in AlGaN epilayers and quantum wells might be attributed to larger composition fluctuations, which in turn lead to larger fluctuations of potential profile. Therefore, increasing Al content leads to stronger carrier localization.

The localization strength depends not only on composition of ternary AlGaN epilayers or structures, but also, in the case of MQWs, on the quantum well width. Figure 1.3 presents the best fit values for σ and Γ in AlGaN MQWs samples with different quantum well width (all MQWs had a 35 % Al content in the quantum well). The dispersion parameter Γ is similar for the two widest QWs (27 meV and 29 meV) and is slightly higher for the narrowest QWs (36 meV). Meanwhile, the dispersion parameter σ strongly depends on the well width and equals 36 meV, 46 meV, and 52 meV in 5.0 nm-, 4.1 nm-, and 2.5 nm-wide QWs, respectively. Thus, the exciton localization, which is basically caused by the compositional disorder in the alloy, is enhanced in narrower QWs, probably, owing to the well-width fluctuations, which modulate the quantum confinement energy. This is consistent with the carrier lifetimes measured in these structures at low carrier densities (58 ps, 90 ps, and 125 ps at room temperature in the 5.0 nm-, 4.1 nm-, and 2.5 nm-wide QWs,

respectively)[80]. Thus, the small-spatial-scale potential profile, which is responsible for carrier localization, becomes deeper with decreasing well width.
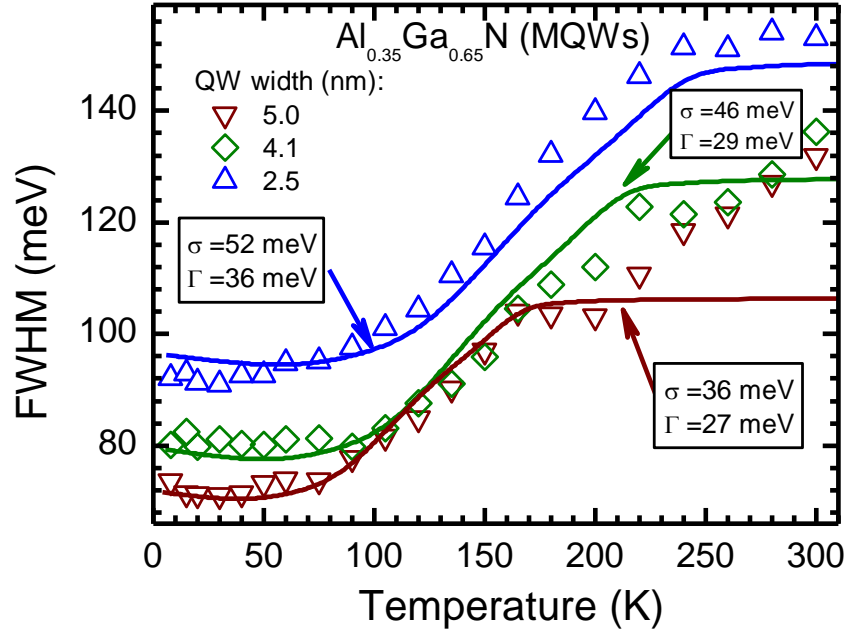

Fig. 1.3 Temperature dependences of spontaneous emission band FWHM for three AlGaN MQWs samples (points) with different QW width. Solid lines show the best fit using the double-scaled potential profile model. The dispersion parameters are indicated.[P12]

The determination of carrier localization strength through FWHM temperature dependences is complicated and requires carrying out Monte Carlo simulations. However, in many cases, determination of localization parameter σ alone is possible by application of a simpler method. The S – shaped dependence at elevated temperatures can be described using a simple quantitative model linking the band shift to the fluctuations of the local potential. At nondegenerate occupation, the temperature dependence of PL peak position can be expressed by adding an addition term to the empirical *Varshni* equation[76]:

$$E_{peak}(T) = E_g(0) - \frac{\alpha T^2}{\beta + T} - \frac{\sigma^2}{k_B T}. \qquad (1.2)$$

Here, $E_g(0)$ is the effective band gap at $T = 0$, α and β are the Varshni coefficients for band gap reduction with increasing temperature, and σ is the standard deviation of the Gaussian distribution of the band gap fluctuations due to the random fluctuations in Al content and/or QW width.

The points in Fig. 1.4 show the dependences of the shift in the PL peak position relative to its value at 8 K. The dependences shown by solid lines were calculated according to Eq. (1.2) with α and β values from Ref. 81, and $E_g(0)$ as an adjustable parameter to fit the maximum value of the calculated shift for each curve.
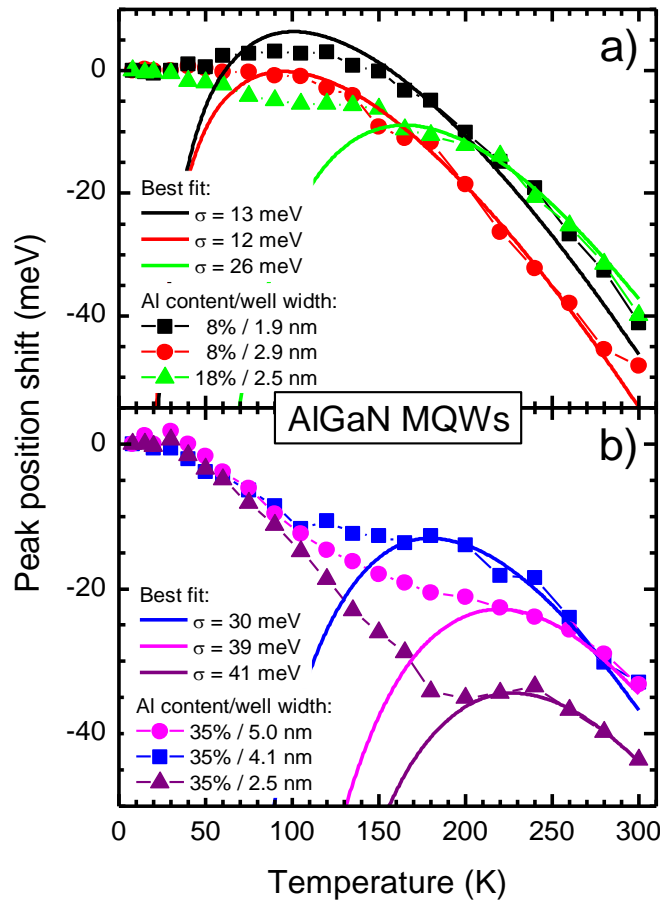
Fig. 1.4. Temperature dependences of PL band peak position shift relative to the position at 8 K in AlGaN MQWs (points) with different Al content (a) and different well width (b), resulting in different localization strength (indicated). Solid lines show the best fit using the model of carrier (exciton) hopping through localized states.[P8]

Adequate fits of experimental data and curves calculated by Eq. (1.2) were produced by matching the elevated temperature region to experimental

data, where carriers are close to thermalization or completely thermalized. At low temperatures, the freeze-out of carriers (excitons) takes place and the experimental data deviate from the dependence described by Eq. (1.2).

The determined values of the localization parameter σ clearly indicate several trends. First of all, increasing aluminum content in MQWs has the greatest impact on localization strength. This is evident from the carrier thermalization temperature in different samples. Quantum wells with very similar well width (2 – 2.5 nm) and increasing Al content (8, 18, and 35 % for black, green and purple data points and curves, respectively in Fig. 1.4) exhibit growing thermalization temperature (approximately 100, 160, and 230 K). The determined σ values complies to this trend and are 13, 26, and 41 meV, respectively.

The previously described Eliseev model does not enable fitting the experimental data points in the low temperature region. A slightly modified model, with an additional equation for temperatures below the start of carrier thermalization, was proposed[82]. Denoting the temperature at which the carrier (exciton) thermalization starts as T_0, the temperature dependence of the PL peak position can be expressed as:

$$E_{peak}\left(T\right)=\begin{cases} E_g\left(0\right)-\dfrac{\alpha T^2}{\beta+T}-\dfrac{\sigma^2}{k_B T}, & \left(T>T_0\right), \\[3mm] E_g\left(0\right)-\dfrac{\alpha T^2}{\beta+T}-\dfrac{\sigma^2}{k_B T_0}, & \left(T\leq T_0\right). \end{cases} \tag{1.3}$$

Here, $E_g(0)$ is the band gap at $T = 0$, α and β are the Varshni coefficients for the band gap reduction with temperature, and σ is the standard deviation of the Gaussian distribution of the band gap fluctuations.
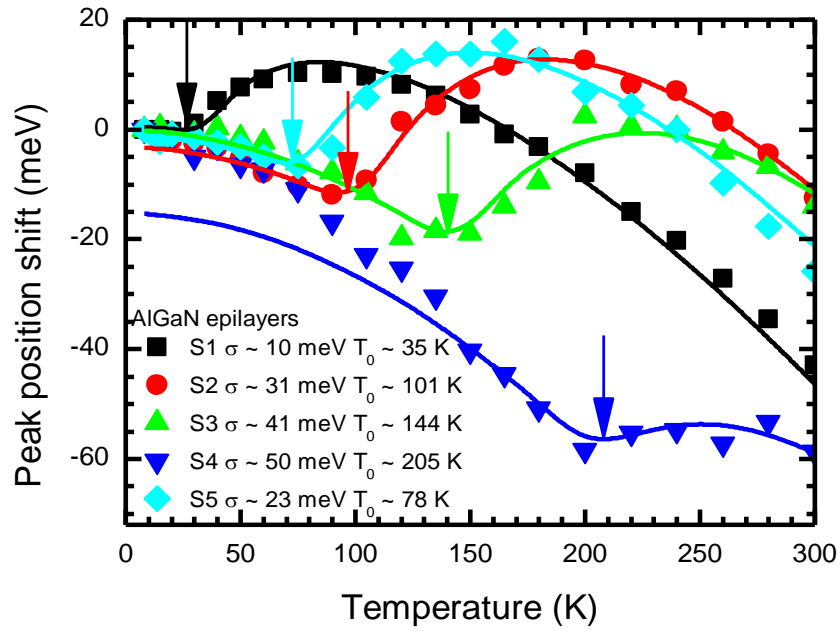
Fig. 1.5. Temperature dependences of PL band peak position shift in AlGaN epilaye (points). Solid lines show the best fit using the model of carrier (exciton) hoppir through the localized states given by Eq. (1.3).[P6]

The solid lines in Fig. 1.5 show the best-fit dependences of the PL peak position calculated according to Eq. (1.3) for AlGaN epilayers with different Al content. In addition to fitting experimental data with Eq. (1.2), the two – equation model allows for fitting the data in the entire temperature range, including the carrier freeze – out at low temperatures.

Just as with MQWs, the general trend is that localization strength increases with growing Al content: from $\sigma = 10$ meV in epilayer with 17 %, to $\sigma = 50$ meV in epilayer with 65 % Al. In relation to localization parameter σ values in AlGaN MQWs, these values are lower for the same Al content. It should be noted, however, that in this case the samples under study are AlGaN epilayers and not MQWs, so the influence of quantum confinement is eliminated.

In addition to determining the localization strength via localization parameter σ, the characteristic temperature of carrier thermalization was

determined (marked with arrows in FIg. 1.5). The carrier thermalization temperature T_0 is defined as the temperature at which the carrier thermalization induced peak position blue shift starts. This thermalization temperature steadily increases with increasing Al content, from 35 K at 17 %, to 205 K at 65 % aluminum content.

Applying the methods described above, the localization strength was investigated in a number of AlGaN samples, both MQWs and epilayers. Though the main trend of growing localization strength with increasing Al content is evident in the band width and PL peak position temperature dependencies previously shown in figures 1.2, 1.3, 1.4, and 1.5, plotting the localization parameter σ as a function of aluminum content permits a closer analysis of this dependence (see Fig. 1.6).
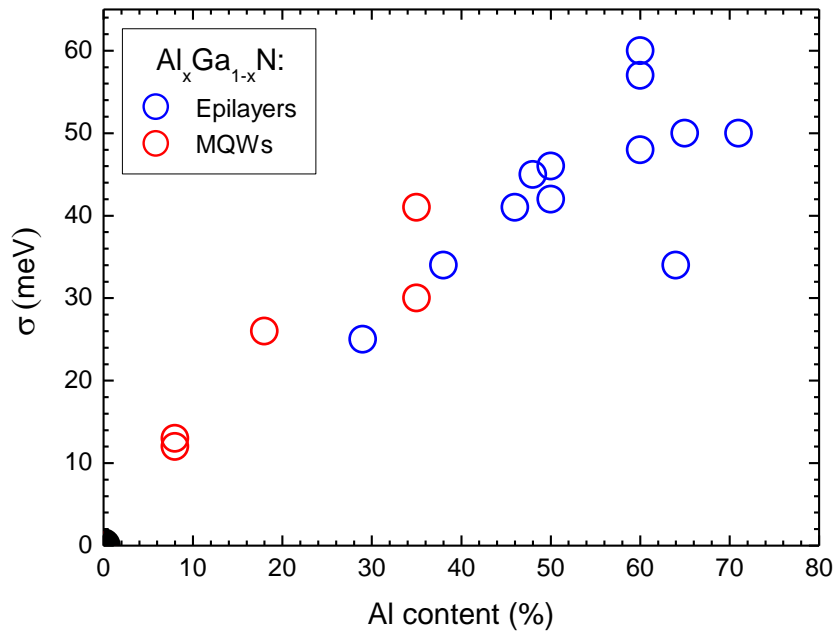
Fig. 1.6. Localization parameter σ dependence on aluminum content in AlGa MQWs (red circles) and epitaxial layers (blue circles)

Aside from some expected scattering of points, there is no substantial discrepancy between the dependencies for AlGaN MQWs (red circles) and

epilayers (blue circles). As expected, MQWs exhibit slightly larger values of σ for the same Al content than that in epitaxial layers (additionally caused by variations of the quantum well width), however, this difference is probably too small to make deeper conclusions based on the existing number of data points and their scattering.

The increase in localization strength caused by increasing potential profile fluctuations will inevitably cease at 100 % aluminum content as AlN is not a ternary material and has no content fluctuations. Thus, it is reasonable to assume that the value of σ should decrease as aluminum content approaches 100 %. In our study, the localization strength was determined in samples with aluminum content as high as 70 %. Though the expected decrease of σ is not distinctly observed, the dependence exhibits signs of saturation with increasing Al content.

2. Stimulated emission and PL efficiency

2.1 SE and PL droop in GaN

Elevated photoexcitation of III-nitride epilayers or multiple quantum wells (MQWs) might cause stimulated emission (SE). The SE spectrum has a narrow band, rapidly growing with increasing excitation intensity. The stimulated emission threshold and intensity might be influenced by multiple factors, such as the localization strength, the density of nonradiative recombination centers, and the overall structural quality. The high carrier density required for the SE to occur might also result in photoluminescence (PL) droop effect, which is inherent for III-nitride materials.

To perform a controlled study of SE and investigate possible interplay between its emergence and the PL droop, we studied photoluminescence in GaN epilayers. The absence of the composition fluctuations, which is typical for ternary III-nitrides, and the fluctuations of quantum well width, which are important in QW structures eliminates the influence of carrier localization in binary GaN epilayers, which were selected for reference study in order to better understand the SE and efficiency droop in ternary AlGaN. Moreover, GaN has significantly higher structural quality, thus reducing the influence of nonradiative recombination.

The luminescence spectra of GaN epilayers have been measured in two configurations. In the front-face configuration, the laser beam was focused on the layer surface into a spot of ~350 µm in diameter. The luminescence collected from the spot contained mainly the contribution from spontaneous emission. The absorption (or carrier diffusion) depth of $0.1 - 1$ µm was too small for the single-pass amplification of the light propagating perpendicular to the sample surface even when the population inversion was high enough for a strong optical gain. The contribution of stimulated emission might be detected

in this configuration only due to scattering of the light amplified in a single pass by propagating parallel to the sample surface along the spot of ~350 μm in diameter. The edge emission configuration was used to extract the stimulated emission. The excitation light was focused into a narrow stripe (~30 μm in width and 2 mm in length) on the sample edge, and the light propagating along the stripe was detected.
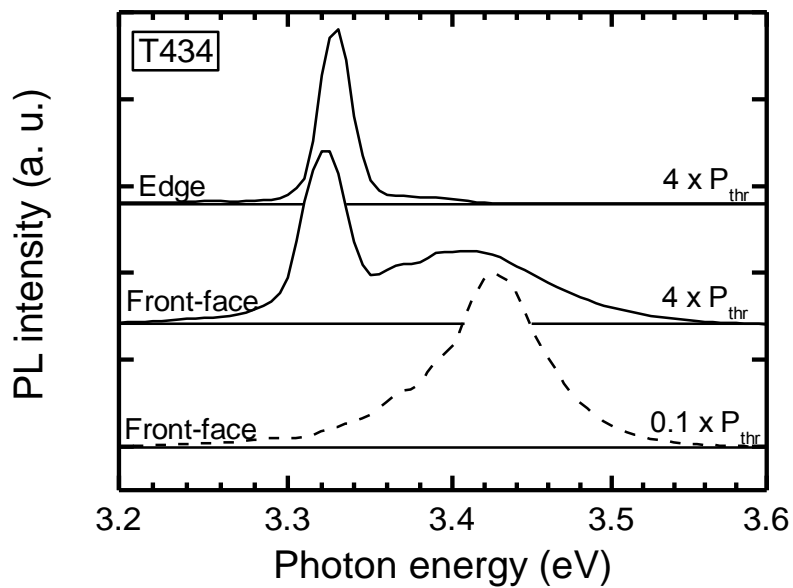

Fig. 2.1. PL spectra of GaN epitaxial layer measured above (solid lines) and below (dashed line) the threshold of stimulated recombination in edge and front-face configurations (indicated). Spectra are vertically shifted for clarity.[P10]

Figure 2.1 shows typical spectra recorded in both configurations below and above the threshold for the stimulated optical transitions. A broad (40-50 meV) spontaneous emission band (peaked at ~3.42 eV with minor position shift from sample to sample) dominates the spectrum recorded in the front-face configuration at low excitations. A narrower (~20 meV) stimulated emission band at the low-energy side of the spontaneous band was observed at high

excitations in both configurations but, as expected, was considerably more pronounced in the edge configuration.
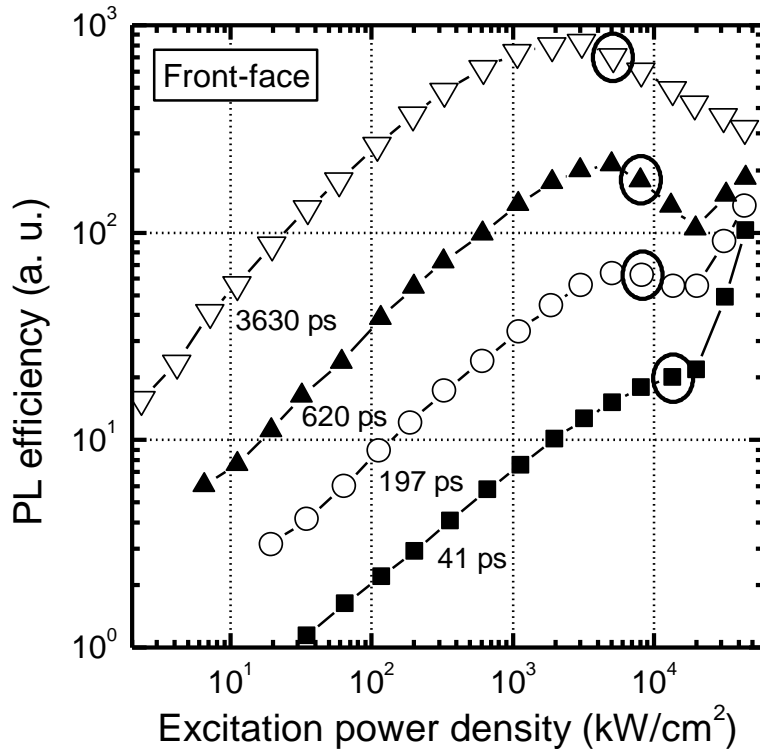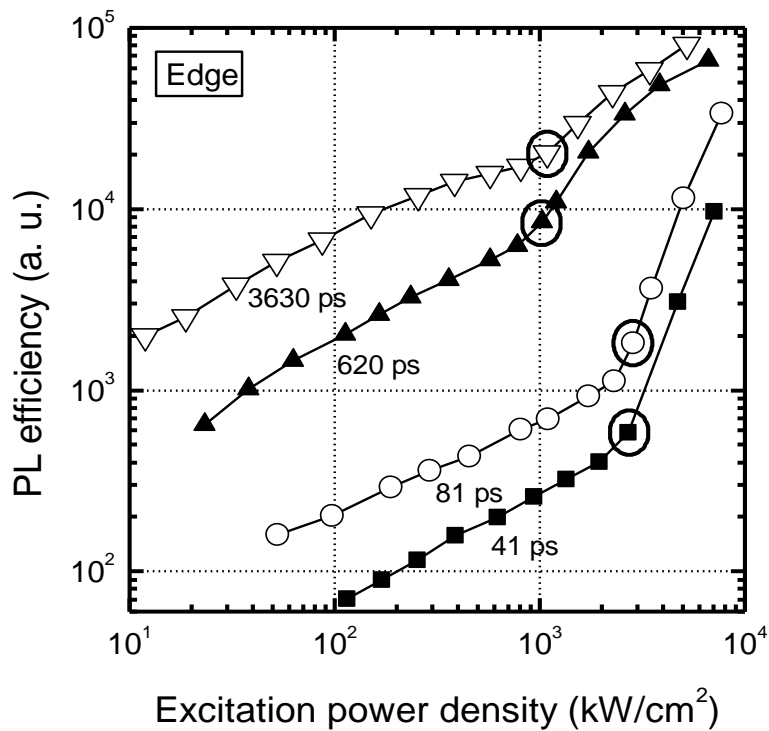

Fig. 2.2. PL efficiency dependence on excitation power density of epitaxial GaN samples measured in front-face configuration. The carrier lifetimes in the samples are indicated. The points corresponding to the threshold for stimulated emission are encircled.[P10]

Figures 2.2 and 2.3 present the PL efficiency, i.e., the spectrally-integrated PL intensity divided by the excitation intensity, as a function of the excitation power density for the front-face and edge configurations, respectively. The efficiency of different samples at a fixed excitation power density was approximately proportional to the carrier lifetime. This proportionality was slightly distorted due to the different surface morphology of the samples resulting in different light collection conditions during the PL measurements. The efficiency increased with increasing the excitation power density. This increase might be primarily explained by two concurrent effects: i) the saturation of nonradiative recombination centers; and ii) an increasing fraction

of the carriers recombining via bimolecular band-to-band recombination in respect to the linear, mostly nonradiative, recombination. As expected, the efficiency increase was more pronounced in the samples with longer carrier lifetimes corresponding to higher carrier densities at the same excitation intensities (see Fig. 2.2). The samples with higher carrier lifetimes reached the onset of the droop effect at lower excitation intensities. A similar tendency was observed for the threshold for stimulated optical transitions.

Fig. 2.3. PL efficiency dependence on excitation power density of epitaxial GaN samples measured in edge emission configuration. The carrier lifetimes in the samples are indicated. The point corresponding to stimulated emission threshold are encircled.[P10]

The SE threshold was investigated in the samples under study using the edge configuration. The emission efficiency as a function of excitation power density is plotted in Fig. 2.3. The threshold corresponding to the onset of a stronger increase of emission intensity (see encircled points in Fig. 2.3) is plotted as a function of carrier lifetimes in different samples in Fig. 2.4(a). The stimulated emission band was also observed in front-face configuration. The

44

points when the stimulated emission band becomes distinguishable are encircled in Fig. 2.2. The carrier lifetime dependence of the onset of stimulated emission band in front-face configuration is presented in Fig. 2.4(b) and shows the same trend as the threshold of stimulated emission depicted in Fig. 2.4(a).
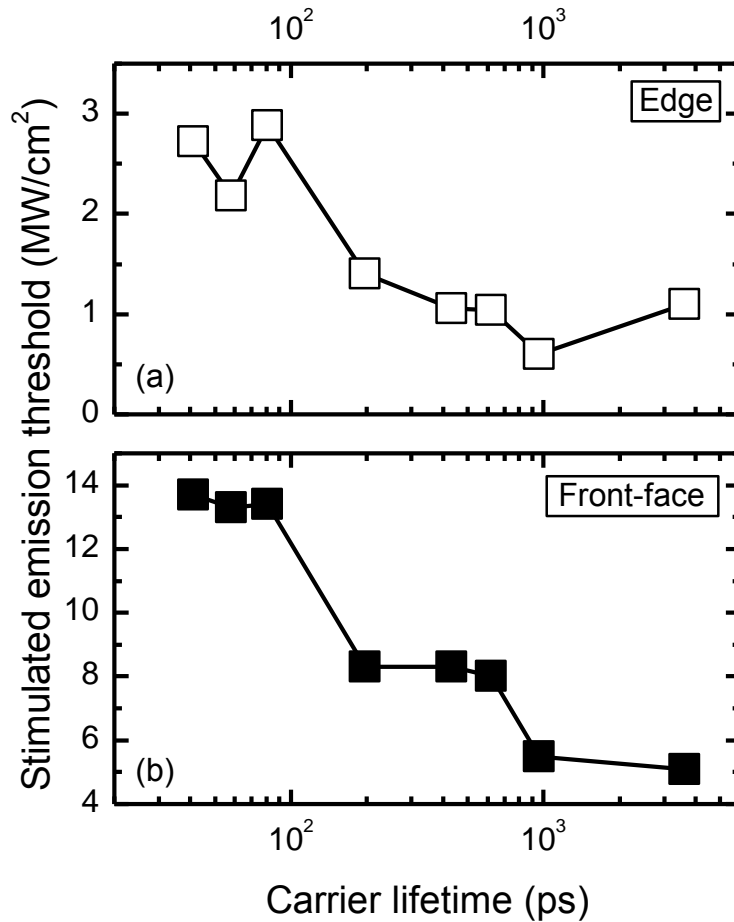

Fig. 2.4. Stimulated emission threshold dependence on carrier lifetime in epitaxial GaN samples measured at edge (a) and front face (b) emission configurations.[P10]

Since the front-face configuration is not favorable to observe stimulated emission, the stimulated recombination might become important in the dependences presented in Fig. 2.2 earlier than the encircled points, which represent an obvious emergence of the stimulated emission band. Despite large uncertainties in comparison of excitation power densities in front-face and edge configurations (mainly due to uncertainties in spot size determination and, especially, edge quality at the selected position), it is clear that the

stimulated optical transitions became important in the carrier recombination earlier than they appear as a separate emission peak in the front-face configuration. Thus, the threshold for stimulated emission was close to the onset of the efficiency droop. Consequently, the stimulated recombination, being a faster recombination channel than the spontaneous recombination, might be the mechanism limiting the increase of carrier density at elevated excitation intensities and result in the droop in efficiency of spontaneous emission in GaN epilayers observed in the front-face configuration. Above the threshold, the dependence of the recombination rate due to stimulated transitions on carrier density is considerably stronger than that of the spontaneous bimolecular recombination. Thus, the stimulated emission tends to stabilize the carrier density just above the stimulated emission threshold due to a negative feedback: an increase in carrier density increases the gain coefficient and results, in turn, in reduction of the carrier density due to the enhanced stimulated recombination rate. This stabilization of carrier density at increasing excitation intensity results in the efficiency droop for the "useful" emission detected in front-surface recombination. Meanwhile, the efficiency of the total (spontaneous and stimulated) emission spatially-integrated in all directions does not suffer any droop. Note that at very high excitation power densities, when the signal detected in front-surface configuration is dominated by contribution of stimulated emission, the emission efficiency in this configuration increases again (see Fig. 2.2). The increase in the total emission intensity is very obvious in edge configuration (see Fig. 2.3), where the share of the stimulated emission is considerably larger than that in front-face configuration. It is worth noting that we could not expect such an increase in efficiency of the total emission in case of considerable influence of nonradiative Auger recombination, which is often considered as the main origin of the droop effect.

In conclusion, the droop of photoluminescence efficiency in GaN epilayers observed in the front-face configuration coincided with the onset of stimulated optical transitions. The droop onset and threshold of stimulated emission occurred at higher excitation power densities in the samples with shorter carrier lifetimes. These results imply that the onset of stimulated recombination, stabilizing the carrier density at higher excitation power density, might be sufficient to explain the droop effect in GaN epilayers. Stimulated optical transitions might also be an important contributor to the droop in other III-nitride epilayers, heterostructures, and LEDs. In the latter case, stimulated recombination initiated by the light propagating parallel to the well plane might inhibit the increase of carrier density at increased injection rate (driving current) and cause the droop in the efficiency of LED emission extracted mainly in the direction perpendicular to the well plane.

2.2 Stimulated emission in AlGaN

After observing the relation of stimulated emission and efficiency droop in GaN, further investigations were directed into stimulated emission (SE) in AlGaN multiple quantum wells (MQWs) and epilayers. In the case of AlGaN, carrier localization comes into play due to aluminum content fluctuations or, additionally, due to quantum well width variation. Therefore, we focused our efforts towards investigating SE in AlGaN MQW samples with different aluminum content (from 8 % to 35 %) and with different QW widths (2.5 nm to 5 nm at 35 % aluminum content).

The edge emission spectra of the samples were measured under excitation power density varied from 40 kW/cm^2 to 7 MW/cm^2 at temperatures ranging from 20 to 300 K. Figure 2.5 presents the spectra measured under different excitation power densities at 20 K for the AlGaN MQWs sample with 5.0 nm thick quantum well. At low excitations, the spectrum consisted of one

broad band. When the excitation power density exceeded a certain threshold, a new band emerged on the high-energy slope of the initial band. The abrupt emergence of a rapid intensity increase with increasing excitation as well as a comparatively narrow width of the new band is an indication of stimulated emission[83–87].
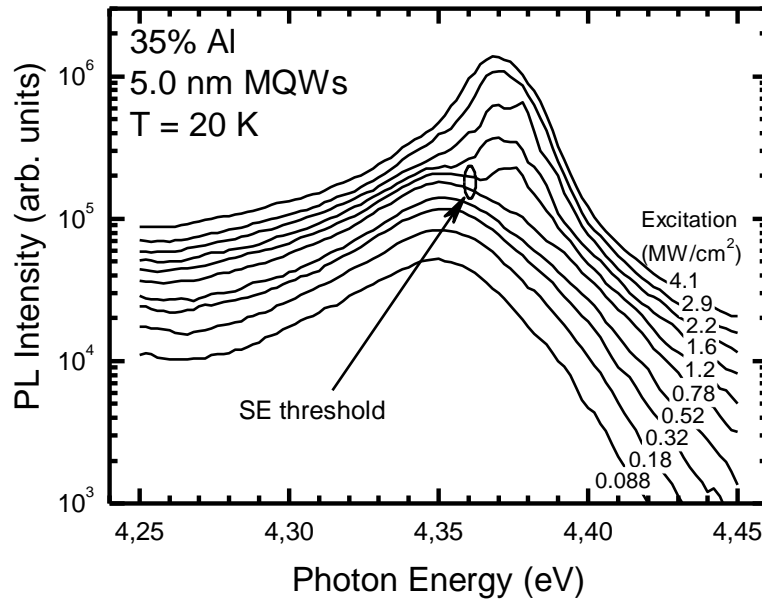

Fig. 2.5. Edge PL spectra of AlGaN MQWs with well width of 5.0 nm measured at 20 K temperature under several excitation power densities (indicated). Two subsequent spectra below and above the SE threshold are indicated.[P12]

Similar behavior of the edge emission spectra with increasing excitation was observed for all of AlGaN MQWs under study. The value of SE threshold was determined as the excitation power density value between the excitation corresponding to the last spectrum with no SE band and that corresponding to the first spectrum with an evident SE band. The absolute value of the threshold is determined with a high degree of uncertainty due to the variations in the edge cleavage quality. However, the threshold temperature dependence shows the same trends at any location of the excited stripe on the sample edge.
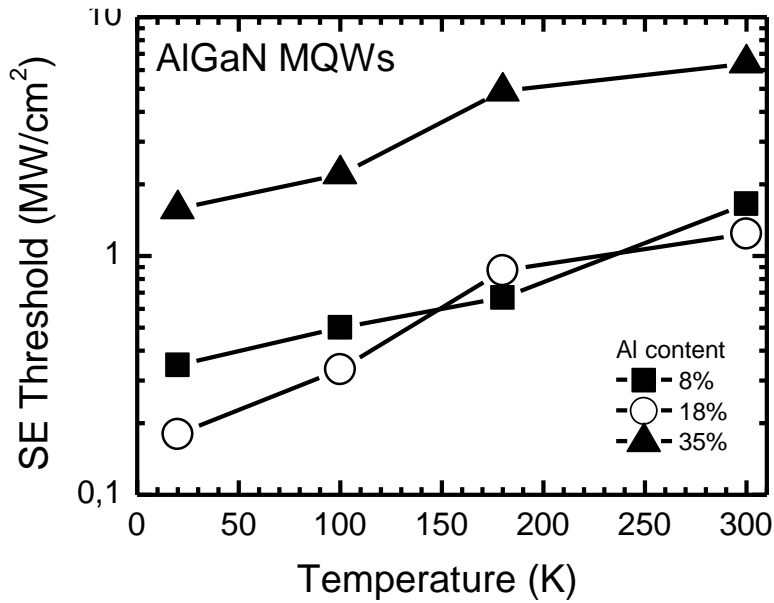
Fig. 2.6. Temperature dependence of the SE threshold for three AlGaN
MQW samples with different Al content (indicated).[P11]

Figure 2.6 presents the temperature evolution of the SE threshold for
three AlGaN MQWs with different Al content. The threshold measured at
different places along the sample edge varied by a factor of up to ~1.6. The
threshold power density was different in different MQWs. At 20 K, it was equal
to ~175 kW/cm² in MQWs with the lowest Al content (8 %), ~350 kW/cm² in
MQWs with a higher Al content (18 %), and ~1 MW/cm² in MQWs with the
highest aluminum content (35 %). The threshold for samples with high Al
content is significantly higher than that for samples with 8 % and 18 % of
aluminum in quantum wells. All the thresholds steadily increase with
temperature. The difference between the SE thresholds in the samples with
8 % and 18 % of aluminum gradually decreases with increasing temperature,
and the respective SE thresholds remain similar at elevated temperatures.
Meanwhile, the SE threshold in sample with 35 % Al is higher by a factor varying
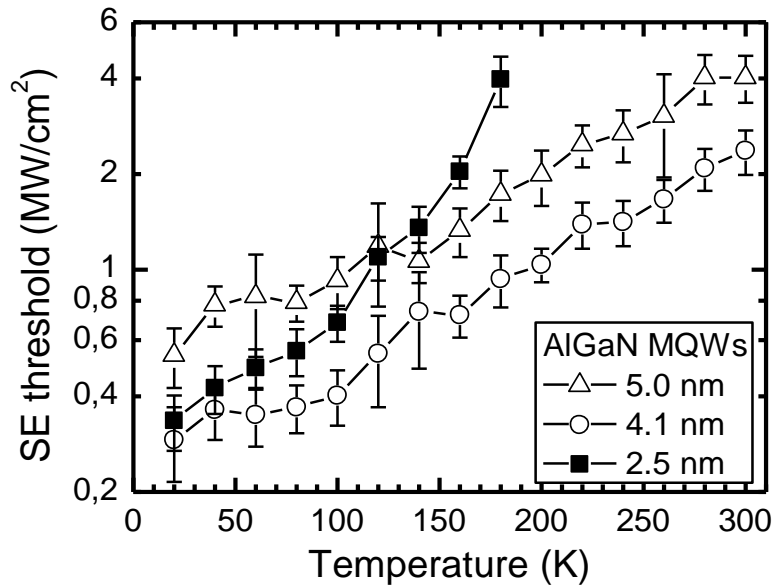from 10 to 5 throughout the entire temperature range.

Fig. 2.7. Temperature dependence of SE threshold for three AlGaN MQW samples with different QW widths (indicated). The error bars indicate the range between two subsequent spectra measured to determine the threshold.[P12]

The rate of the threshold increase due to increasing temperature depends on the QW width (see Fig. 2.7). In MQW structures with 5.0 nm and 4.1 nm-wide wells, the SE threshold increases at similar rates, while in the structures with 2.5-nm-wide QWs, the SE threshold growth rate is significantly higher. Increase in temperature above 200 K results in SE threshold above the threshold for permanent optical damage to the MQWs. Therefore, the exact SE threshold at higher temperatures in these samples cannot be obtained.

An interesting feature is the shifting of the position of the stimulated emission band in respect to that of the spontaneous emission band. The SE band is located on the low-energy slope of the spontaneous band in MQWs with low Al content (Fig. 2.8(a)). This position is typical of bulk semiconductors and heterostructures, i.e., the structures with weak or no carrier localization[88]. Meanwhile, in MQWs with a higher Al content (35 % in our experiments), the SE band is located on the high-energy slope (see Fig 2.8(b)). Such a position of

the SE band has been previously observed in InGaN[89–92] and AlGaN[84,85,92], and has been attributed to the SE originating from localized states[85,89,91,92]. Screening of the built-in electric field has also been suggested as an additional mechanism of the blue shift of the SE band[92]. The different influence of localization in the samples with different indium content has been previously observed in InGaN LEDs[93].
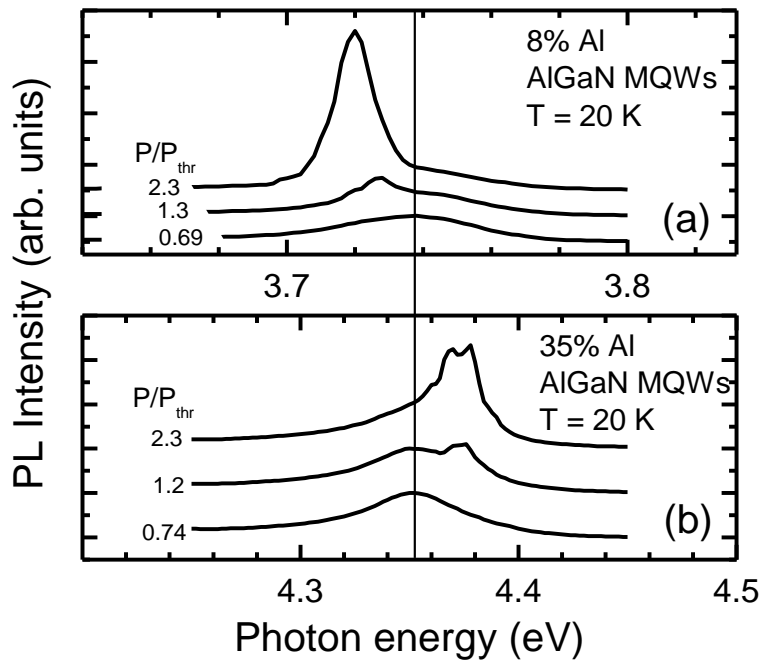

Fig 2.8. Edge PL spectra of AlGaN MQWs with 8 % (a) and 35 % (b) aluminum measured at 20 K temperature under several excitation power densities below and above the threshold for stimulated emission. The threshold was equal to 170 kW/cm2 and 970 kW/cm2 for samples with 8 % and 35 % aluminum, respectively. The spectra were normalized and vertically shifted for clarity. The vertical line indicates the peak position of spontaneous luminescence band. [P8]

Relations between the localization parameter σ and the characteristics of SE band can be observed. The SE band appears on the low - energy slope in the samples with weak localization (σ ≤ 26 meV). As localization becomes stronger (σ ≥ 30 meV), the SE peak shifts to high - energy slope of the spontaneous emission band. This observation implied the conclusion that the carrier localization is important in high-Al-content AlGaN MQWs up to the carrier

densities high enough for stimulated emission to occur. Using the carrier lifetime of 58 ps determined for sample with 35 % Al and 5 nm wide QWs in Ref. [80], the carrier density corresponding to the SE threshold at room temperature is estimated at ~3×10^{19} cm^{-3}.

The temperature dependence of the edge emission spectra supports the assumption that the carrier dynamics in the samples under study are strongly affected by localization. Figure 2.9 shows the temperature dependences of the peak positions of the spontaneous and SE bands for the MQWs with different aluminum content. The excitation power densities used in measuring the edge emission spectra above the threshold were increased with temperature (the change is indicated by different type of points used in Fig. 2.9), since the SE threshold increased with temperature. (The excitation power density for measuring the spectra below the threshold was maintained constant.)

The solid lines in Fig. 2.9 correspond to the Varshni equation (Eq. 1.1) with parameters taken from Ref. [81] and depict the band gap shrinkage with increasing temperature without accounting for localization effects. The deviation of the measured position of the spontaneous emission band from the Varshni dependence shows an increasing influence of localization with the increase in Al content.

The peak position of the stimulated emission band in the samples with lower Al content follows the Varshni dependence with the redshift of ~50 meV, which is approximately constant throughout the entire measurement temperature range. This behavior is consistent with the SE being caused by free carrier recombination.
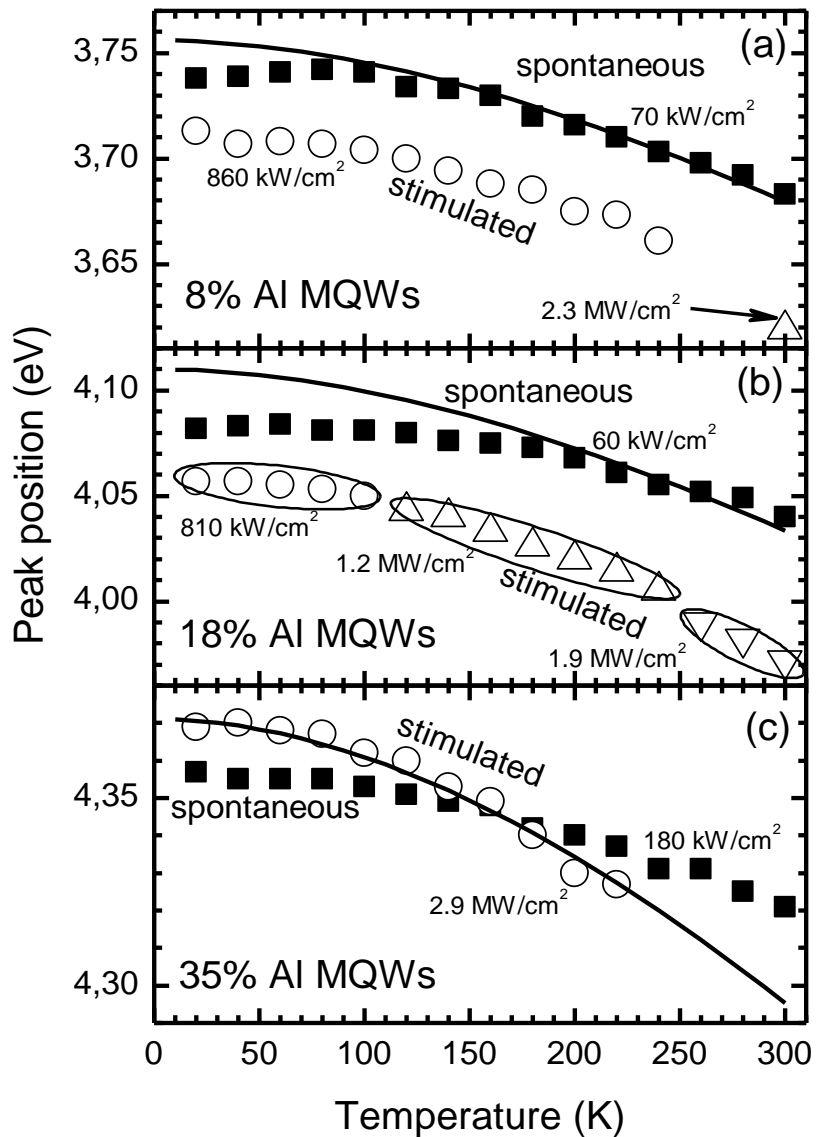
Fig. 2.9. Temperature dependences of the peak positions of the spontaneous emission band (filled squares) and stimulated emission band (open circles and triangles) in samples with different aluminum content (denoted). Excitation power densities used in measurements are indicated.[P11]

Meanwhile, the temperature dependence of the SE band peak position in MQWs containing 35% of Al follows the Varshni dependence and shifts from the high-energy side of the spontaneous band to the low-energy side at temperatures above ~160 K. This is consistent with the stimulated emission

occurring approximately at the mobility edge due to a high density of localized states in this sample. The obtained σ value of 36 meV shows that the carriers in sample with 35% of Al (Fig. 1.2) are strongly affected by localization even at room temperature (with the average thermal energy of 25 meV) and supports the assumption that stimulated emission in this sample occurs via optical transitions between localized states.

The majority of carriers at low temperature occupy states below the mobility edge and their spontaneous recombination results in the emission band below the mobility edge. At elevated temperatures, the higher energy states are increasingly occupied, and the spontaneous emission band shifts up in energy toward the mobility edge.

Strong effect of carrier localization on carrier was also observed in AlGaN MQWs with different quantum well width (quantum wells with 35 % of aluminum). Figure 2.10 shows the temperature dependences of the peak positions of the spontaneous band (measured at excitation intensities below the SE threshold) and SE band for three MQWs under study: with 5 nm, 4.1 nm, and 2.5 nm wide quantum wells. Since the temperature increase also causes the SE threshold increase, the excitation power density used in measuring these edge emission spectra was consistently increased with temperature relatively to the SE threshold (~0.5 and ~1.5 of the SE threshold for excitation below and above the SE threshold, respectively).
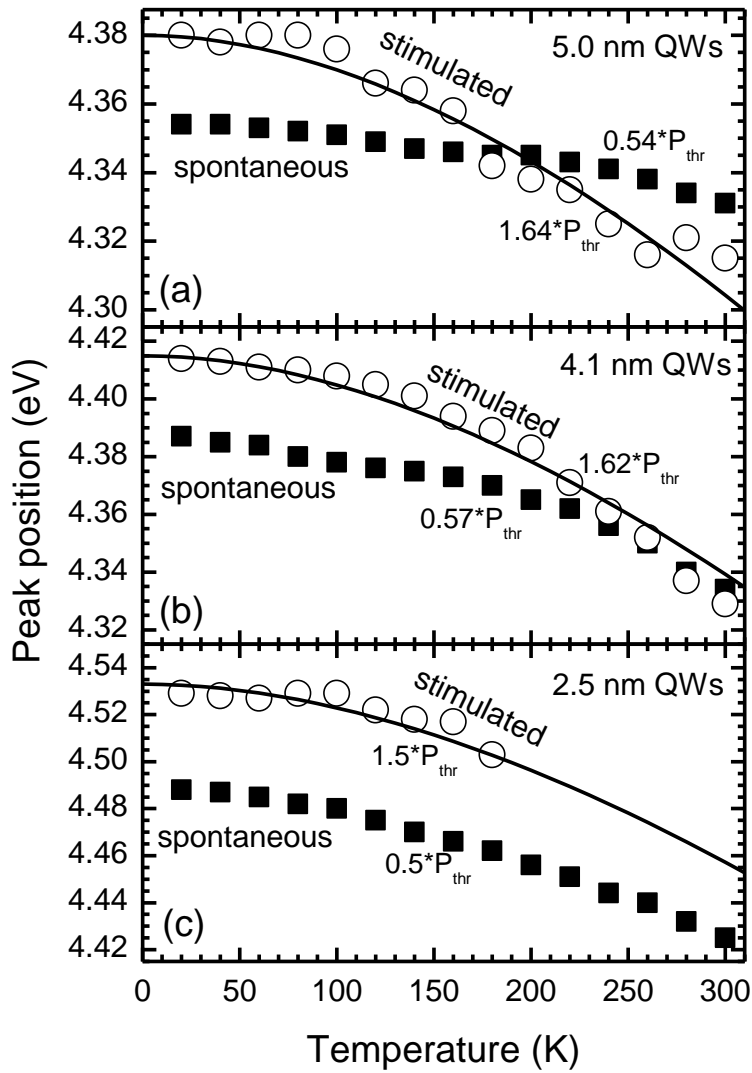
Fig. 2.10. Temperature dependences of the peak positions of the spontaneous emission band (filled squares) and stimulated emission band (open circles) in AlGaN MQWs with well width of 5.0 nm (a), 4.1 nm (b), and 2.5 nm (c). The average ratios of excitation power densities used in the measurements with the SE thresholds are indicated.[P12]

At 20 K temperature, the SE band peak position was on the high-energy side of the spontaneous band in all three samples. With the temperature increase, the SE band redshifted faster than the spontaneous emission band did. This effect exhibited a remarkable dependence on QW width. In the widest (5.0 nm) QWs, a clear crossover of the SE band from the high-energy side to the low-energy side of the spontaneous band was observed at about 180 K (Fig. 2.10(a)). With the reduction of QW width to 4.1 nm, the temperature of

55

the crossover increased to ~280 K (Fig. 2.10(b)). In the thinnest (2.5 nm) QWs, where SE was observed only below ~180 K (Fig. 2.10(c)), an extrapolated value for the crossover temperature of ~430 K can be deduced.

The solid lines in Fig. 2.10 are calculated according to the empirical Varshni formula (Eq. 1.1), just as in Fig. 2.9. The temperature dependence of the SE band peak position (empty points) follows the Varshni dependence in all three MQWs with different QW widths. This behavior is consistent with the SE occurring at the mobility edge and the spontaneous emission band being mainly determined by the localized energy states below the mobility edge.

The red shift of the spontaneous band with increasing temperature is partially compensated due to the thermal redistribution of carriers through the localized states that shifts the band to higher energies toward the mobility edge. As the temperature exceeds a certain crossover temperature, the spontaneous band peak becomes located at higher energies compared to the SE band peak, i.e. above the mobility edge. This implies that above the crossover temperature, the spontaneous emission band is dominated by recombination from the delocalized (extended) states, rather than recombination from localized states. The observed increase of the crossover temperature with decreasing QW width (~180 K and ~280 K for 5.0 nm and 4.1 nm wide QWs, respectively, and extrapolated value of ~430 K for 2.5 nm-wide QWs) indicates weaker delocalization effect in narrower QWs.

As discussed above, stimulated emission might be caused by two different mechanisms: recombination from the extended states (free carrier recombination) and recombination of carriers localized at mobility edge. The first mechanism was observed in MQW samples with low aluminum content (8 – 18 %) which results in weaker localization. The latter mechanism was observed in MQWS with larger aluminum content and the resulting strong localization. Therefore, it is evident that the degree of carrier localization in AlGaN MQWs is responsible for different SE mechanisms.

The band potential fluctuations determines the efficiency of optical amplification and the SE threshold in InGaN materials[91,93]. However, in the AlGaN MQWs under study, the degree of localization seems to have weak effect on the SE threshold in the structures where SE involves the extended states (MQWs with 8 % and 18 % of aluminum) – the respective temperature dependences in Figure 2.11 are almost coinciding. Though SE thresholds in MQWs with higher Al content are higher at given temperature (see Fig. 2.6), the normalized dependences are qualitatively very similar, with the exception of MQWs with high aluminum content and the smallest QW width (Fig. 2.11, points joined with line).
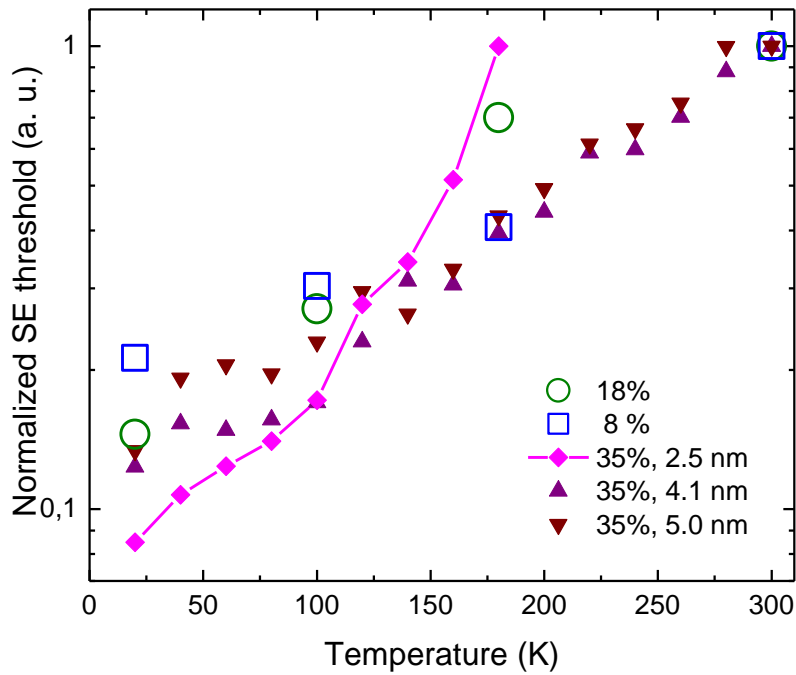

Fig. 2.11. Temperature dependences of normalized SE threshold for AlGaN MQWs with different Al content and QW width.

Such behavior evidences that the degree of localization is not the main factor responsible for the SE threshold. If that was the case, the SE threshold would exhibit a consistent and monotonous dependence (at given temperature) with increasing localization strength. Instead, the SE threshold dependences presented in Fig. 2.6 and Fig. 2.7 exhibit contradictory trends. The

stimulated emission threshold increases with growing aluminum content and localization strength (see Fig. 2.6), but does not increase with the decrease of quantum well width, which also causes an increase in localization strength (see Fig. 2.7). More likely, the SE threshold in AlGaN is governed mainly by the density of nonradiative recombination centers. Increase in Al content deteriorates material quality in the sample with a higher Al molar fraction and results in a higher density of nonradiative recombination centers. At the same time, decreasing quantum well width in samples with the same aluminum content does not affect the material quality noticeably. Therefore, the SE threshold does not exhibit a significant dependence.

In case of MQWs with the greatest localization strength (35 % Al and 2.5 nm wide quantum wells), the faster increase in SE threshold can be explained by several effects. First of all, the gain spectrum broadens and the peak value of the gain coefficient decreases with the increasing influence of carrier localization. This was demonstrated experimentally in InGaN-based laser diode structures (linked to increasing inhomogeneous broadening of the emission band[94]) and in InGaN-based MQWs (linked to increasing In content[95,96]) and was also predicted for AlGaN/AlGaN MQWs[97]. The second and probably even more important effect is that the deeper localization results in depopulation of the states at the mobility edge, where SE occurs. In general, the shift of the quasi-Fermi levels towards the band edge or mobility edge with increasing carrier density is slower in semiconductor with localized states compared to that without localization.

In conclusion, we investigated AlGaN multiple quantum well samples with different aluminum content and quantum well width resulting in different profile and amplitude of band potential fluctuations. The carrier localization is stronger in quantum wells with larger aluminum content and narrower quantum wells. However, strong localization in 2.5 nm wide quantum wells results in a faster increase of the SE threshold as the temperature increases

(see Fig. 2.11). The profile of potential fluctuations is of crucial importance to achieve efficient SE.

Stimulated emission occurs via extended states in the samples with lower Al content (up to approximately 20%) and via localized states in the samples with elevated aluminum content. However, the temperature dependence of the threshold for the stimulated emission is similar in all three samples. Thus, the main factor determining the threshold is not the localization conditions but rather the density of nonradiative recombination centers. Increase in aluminum content is favorable for the formation of dislocations and point defects in AlGaN epilayers and MQWs on sapphire substrate and, consequently, reduces carrier density and increases the threshold for stimulated emission.

3. Photoluminescence efficiency droop in AlGaN

The successful development and application of AlGaN based UV emitters require improvements of the device efficiency. At high injection current density, the AlGaN-based LEDs exhibit a characteristic decrease of luminescence efficiency. The device efficiency decrease at high carrier density might be caused by several different mechanisms (see section *Efficiency issues in AlGaN based devices*, p. 25). This effect (also known as the efficiency droop) is also present in photoexcited AlGaN multiple quantum wells (MQWs) and epitaxial layers.

It is generally accepted that carrier localization facilitates high internal quantum efficiency (IQE) in III-nitride semiconductors[38,98]. However, as the carrier density is increased, carriers populate higher energy states than those predominantly occupied at low carrier density, thus, becoming more mobile and having a larger probability to recombine at nonradiative recombination centers. Thus, the effective localization strength decreases[48,62]. Such carrier delocalization due to increasing carrier density plays an important role in the efficiency droop in InGaN quantum well (QW) structures[46,62,73] and AlGaN epilayers[99].

The stronger localizing potential fluctuations might be expected to increase the IQE. However, it also has an impact on high carrier density effects influencing the stimulated emission threshold[88,91,92,100] and also results in the efficiency droop at lower excitation levels[99]. The interrelation between localization conditions, efficiency droop, and stimulated emission threshold is quite complex. Moreover, temperature strongly affects the redistribution of carriers through the localized states, which makes the recombination processes even more complicated.

Our investigations[88,99,101–104] and the data reported in literature[43,44] show that carrier localization in AlGaN, especially at high Al content, does play an

important role in carrier dynamics even at room temperature. In this work, we report on a study of the efficiency droop in AlGaN MQWs and epilayers. We investigated the interplay between PL efficiency droop and numerous related processes. The influence of carrier localization conditions on radiative and nonradiative recombination, also thermally activated carrier transport were linked to the PL efficiency droop. The PL efficiency in the samples under study was investigated simultaneously with stimulated emission (SE), which was already observed as a possible droop mechanism in GaN (see chapter 2). This kind of simultaneous investigation into various processes and conditions related to the PL efficiency droop enabled us to draw generalized conclusions about different mechanisms causing the efficiency droop in AlGaN epilayers and MQWs.

3.1 Carrier localization and the efficiency droop

We analyze the interplay between nonradiative recombination and carrier localization and the impact of this interplay on the efficiency droop curves in numerous AlGaN epilayers and multiple quantum wells (MQWs) with considerably different defect densities and carrier localization conditions. We also show correlation between carrier localization conditions, thermally activated transport processes and PL efficiency droop.

A large number of AlGaN samples were studied. The samples were selected to cover a wide range the carrier localization parameters. Since localization is caused by both Al content fluctuations and QW width fluctuations, the AlGaN epilayers and MQWs, even with similar Al content, might exhibit very different localization conditions. The AlGaN epilayers under study had the aluminum content in the range from 17 % to 71 %. The AlGaN MQWs contained ten QWs with the Al molar fraction in the range from 8 % to 35 %.
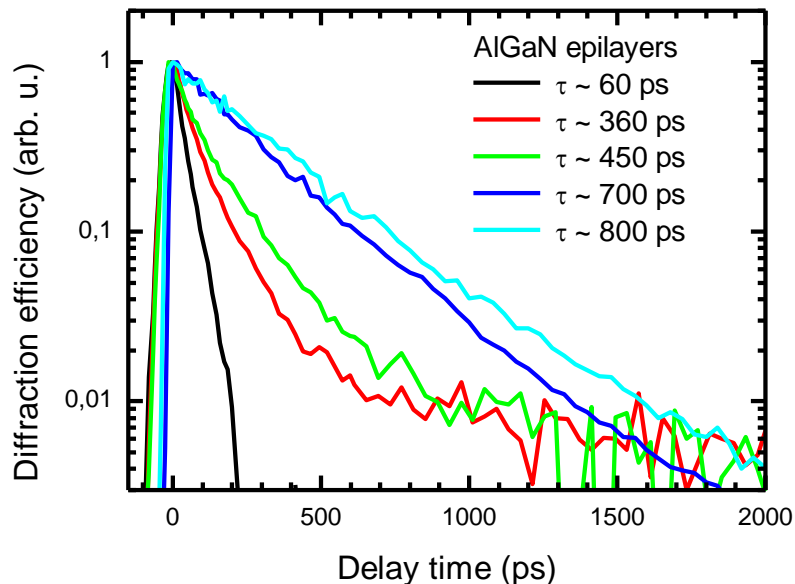

Fig. 3.1.1 Normalized LITG transients for several AlGaN epilayers measured at 300 K temperature. Estimated carrier recombination times τ_R indicated.[P7]

The carrier localization conditions were measured as previously described in Chapter 2. The carrier recombination time values were obtained by light induced transient grating (LITG) measurements (all LITG measurements were carried out by out by Ž. Podlipskas and Dr. R. Aleksiejūnas). Figure 3.1.1 shows typical LITG (Light induced transient grating) transients for several AlGaN epilayer samples, measured at room temperature.

Initially, the diffraction efficiency decays exponentially. In addition, a slow decay component with the decay time exceeding 5 ns is observed and might be attributed to the recombination of carriers trapped at deep defect or localized states. The values of carrier lifetimes τ_R extracted from the initial decay are different for different samples and vary from 30 ps to 800 ps at photoexcited carrier density of ~1×10^{19} cm^{-3}. At room temperature, the dominant recombination process is nonradiative recombination, thus, the observed large variation of carrier lifetimes can be mainly caused either by different densities of the nonradiative recombination centers (NRC) or by the amplitude of the potential fluctuations, which prevent carriers from reaching those recombination centers.

To distinguish between these two effects, we plotted the room temperature carrier lifetime τ_R as a function of the localization parameter σ for the AlGaN samples under study (see Fig. 3.1.2). Several peculiarities can be pointed out. For σ
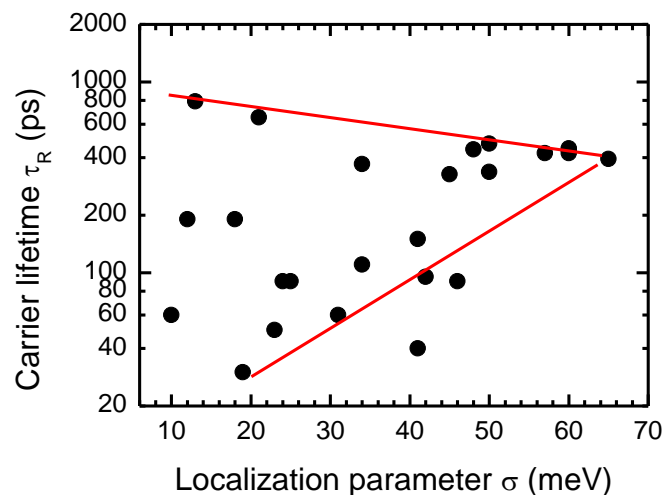

Fig. 3.1.2 Normalized PL efficiency dependences on excitation power density in AlGaN epilayers with different Al content (indicated), measured at room temperature.[P7]

values above ~26 meV, i.e., at $\sigma \geq k_B T$, since $k_B T \approx 26$ meV at room temperature, the lowest limit of carrier lifetime τ_R increases with localization parameter σ. Thus, the carrier localization prevents the carriers from reaching the NRCs in this region of τ_R versus σ plot. The top limit for the points in the plot is caused by the nonradiative recombination. The slight downward slope of the line indicating this limit as σ becomes larger can be explained by the increasing density of NRCs as the Al content increases, which, on the other hand, results also in larger potential fluctuations leading to stronger carrier localization. The higher Al content in AlGaN compound is typically accompanied by stronger structural imperfections[105,106].

The decrease of carrier lifetime with Al content might also be caused by the increase of the radiative recombination rate. However, the typical radiative lifetimes at room temperature are of the order of several nanoseconds or even larger[107,108] and should not affect the carrier lifetime significantly.

Both the localization parameter σ and the density of NRC determine the internal quantum efficiency (IQE), which can be estimated using the temperature dependence of PL intensity, provided that the nonradiative recombination is negligible at low temperatures and the excitation intensity is low enough[100]. Higher IQE is generally associated either with better material quality (lower density of NRC) or stronger localization. The IQE also increases with increasing excitation. However, once certain excitation level is
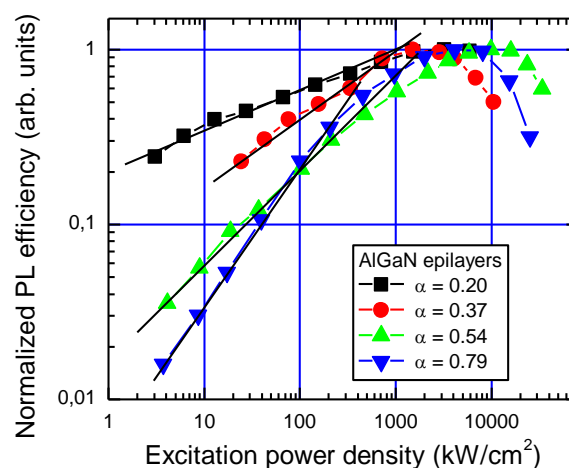

Fig. 3.1.3 Normalized photoluminescence efficiency dependences on excitation power density in AlGaN epilayers measured at 300 K temperature. The efficiency increase rates are indicated.[P7]

reached, the efficiency droop emerges. The rate of the efficiency increase with excitation can be described by the power α in the expression $IQE \propto G^{\alpha}$, where G is the generation rate directly proportional to the excitation power density (see Fig. 3.1.3).

In GaN epilayers, the typical experimental dependences can be described using α values in the range $0.5 < \alpha < 1$. The efficiency increase rate α in AlGaN epilayers under study varies in a wider range (from 0.17 to 0.8, see Fig. 3.1.3). Compared to the binary GaN material, an additional factor of the carrier localization is important in the ternary AlGaN materials. The localized states could affect the carrier dynamics due to carrier trapping-detrapping processes. In addition, the localized carriers can also recombine radiatively, since an electron and a hole have a higher probability to be localized at the same place in real space forming an exciton-like pair[49]. It might be expected that the efficiency increase rate and, thus, parameter α should be determined by the localization conditions (described by σ) and by the density of NRC (described by τ_R). However, no specific correlation between these parameters was observed.
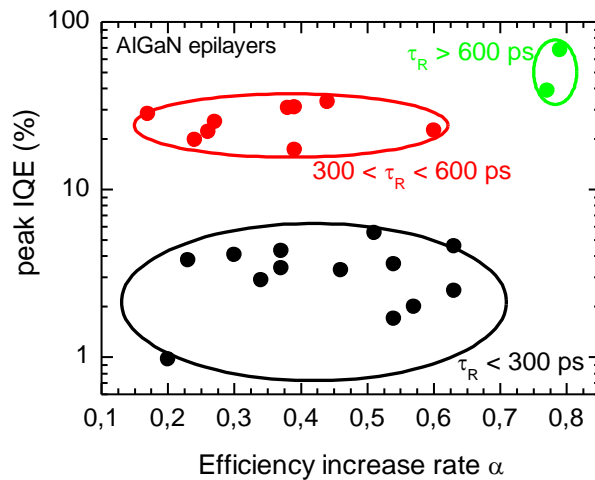

Fig. 3.1.4 The correlation between peak IQE, efficiency increase rate α, and carrier recombination time τ_R.[P7]

Fig. 3.1.4 reveals the correlation between the peak IQE, i.e. the IQE at droop onset (which occurs at different excitation power densities in different samples), efficiency increase rate α, and carrier lifetime τ_R. The peak IQE in the samples with similar carrier lifetimes exhibits no significant dependence on α, however, its value strongly increases with the carrier lifetime. This feature

indicates that strong localization is insufficient to ensure high IQE in AlGaN. The IQE increases as an increasing fraction of carriers becomes free and recombine via bimolecular recombination. At the droop onset, a substantial part of carriers becomes free enough to effectively reach the nonradiative recombination centers. Substantial population of the localized states or escape from regions with lower average potential[42] might be pointed out as feasible mechanisms for the enhanced probability to reach the NRC. The balance between the nonradiative recombination and the bimolecular radiative recombination depends on the density of NRC limiting the carrier lifetime and peak IQE.

Fig. 3.1.5 presents the temperature dependences of the PL intensity for the same AlGaN samples. All the samples exhibited similar dependences: the initial constant PL intensity at lowest temperatures followed by a slow decrease with temperature, and a fast decrease of the intensity at
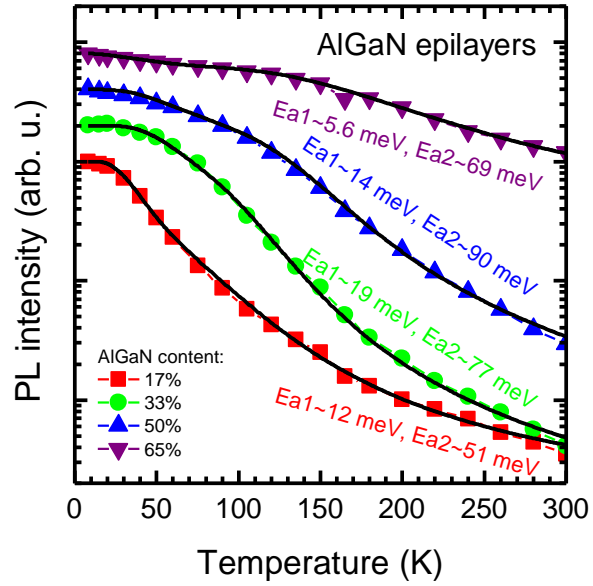

Fig. 3.1.5 Integrated PL intensity in AlGaN epilayers with different Al content (indicated). Solid lines show the best fits using Eq. (3.1.1). The extracted activation energy values (E_{a1} and E_{a2}) are indicated.

the elevated temperatures. The critical temperatures, at which the dependences change the character, differ for different samples. The temperature dependences of the PL intensity were approximated using the Arrhenius-type function with two activation energies[109–111]:

$$I(T) = \frac{I_0}{1 + c_1 \exp\left(-\dfrac{E_{a1}}{k_B T}\right) + c_2 \exp\left(-\dfrac{E_{a2}}{k_B T}\right)}.$$

(3.1.1)

Here, I_0 is the low-temperature PL intensity, E_{a1} and E_{a2} are the activation energies, and c_1 and c_2 are the weight coefficients of the corresponding recombination mechanisms. The estimated activation energies in different samples were in the ranges of 5-23 meV and 40-100 meV for E_{a1} and E_{a2}, respectively.

The two thermally activated recombination mechanisms can be attributed to the carrier redistribution and delocalization[110,111]. The first process, corresponding to the lower activation energy E_{a1}, dominates in the low temperature range. As the temperature is increased from 8 K, most carriers captured at the shallow localized states could be thermally activated and then relax down into deeper states, thus, redistributing within the localized states. Inevitably, some carriers may be captured by defects, resulting in a slow decrease in PL intensity. With the further temperature increase, the second mechanism, corresponding to the higher activation energy E_{a2}, starts to dominate. Carriers have sufficient energy not only to redistribute within the localized states, but also to completely delocalize. The delocalization leads to the rapid decrease of the integrated PL intensity.

Both activation energies as well as the localization parameter σ are estimated under the same excitation conditions and describe the same potential fluctuation profile in the sample. No correlation between the lower activation energy E_{a1} and the localization parameter σ was observed. On the other hand, the activation energy E_{a2} (attributed to the delocalization mechanism) should correlate with the localization parameter σ, since the energy required for the carrier to delocalize (hop to the mobility edge) should increase with the localization strength. Fig. 3.1.6 presents such correlation in the AlGaN samples under study.
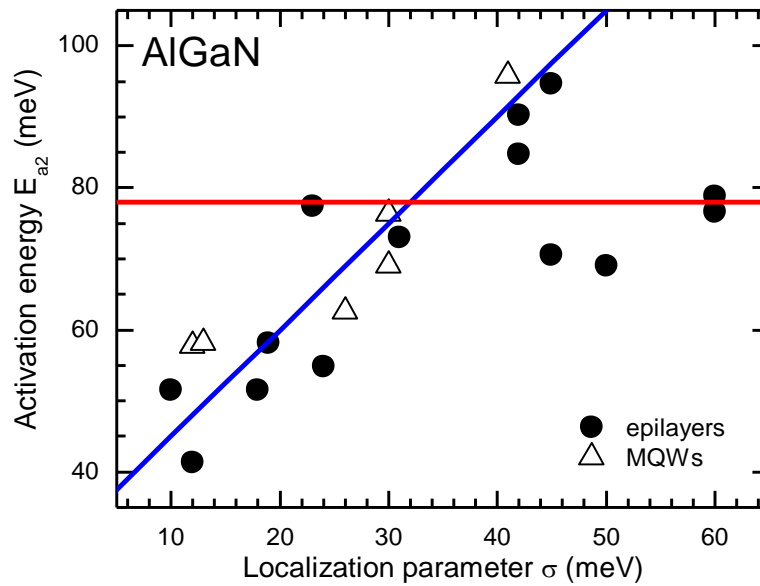
Fig. 3.1.6 Correlation between the activation energy Ea2 and localization parameter σ in AlGaN epilayers (closed circles) and MQWs (open triangles) under study. Solid lines are guides for the eye.[P3]

The results of both epilayers and MQWs are included in this figure, since no peculiarities specific to sample structure were detected. As can be observed, the activation energy E_{a2} correlates well with the localization parameter σ for the σ values up to ~45 meV. At even higher σ values, this correlation ceases, and the activation energy E_{a2} can be assumed to be constant or only weakly correlated with σ. This change of the correlation character is probably due to a change in the carrier transport mechanism: instead of the direct activation to mobility edge (similar to that described by the multiple trapping transport model[112]), the two-step activation process could become dominant. This two-step process is similar to the hopping transport model for disordered systems[113]: the localized carriers first hop up to the transport level, and then to the mobility edge. In this case, the activation energy corresponds to the first hop up to the transport level. Alternatively, the constant activation energy could be related to the direct transfer (tunneling) of carriers to the nonradiative centers[68].

To analyze the links between localization parameter, activation energies, and efficiency droop, we also measured the excitation power density dependences of the spectrally integrated PL efficiency at room
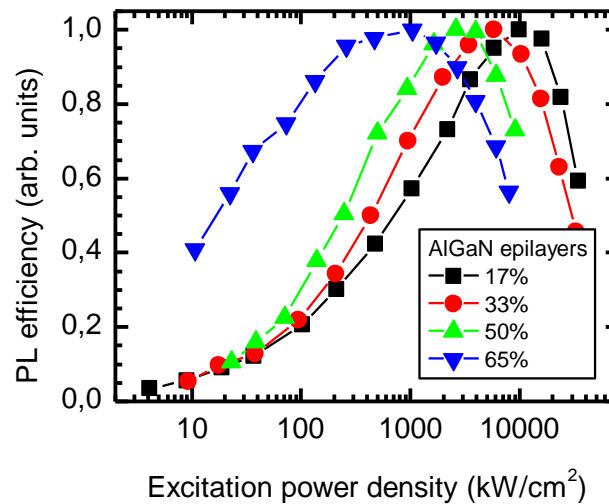

Fig. 3.1.7 Normalized PL efficiency dependences on excitation power density in AlGaN epilayers with different Al content (indicated), measured at room temperature.[P3]

temperature. Fig. 3.1.7 shows the typical dependences for several samples under study. Using the data presented in Fig. 3.1.7, the efficiency droop onset was estimated as the excitation power density corresponding to the highest PL efficiency and separating the initial increase in PL efficiency and its decrease (droop) above the onset.

Figure 3.1.8 illustrates the correlation between the droop onset and the parameters characterizing the potential fluctuation profile: the lower activation energy E_{a1} and the localization parameter σ. As previously, the results of both epilayers and MQWs are included. The higher activation energy E_{a2}, as discussed above, correlates with the localization parameter σ, and, thus, cannot serve as an independent parameter and does not provide any new insight. Several interesting features can be noticed: i) no correlation between droop onset and E_{a1} (see Fig. 3.1.8(a)); and ii) strong correlation between droop onset and σ (see Fig. 3.1.8(b)).

The lack of correlation (the Pierson's coefficient $R \sim 0$) between the lower activation energy E_{a1} and the efficiency droop indicates that the redistribution

of carriers within the localized states has no effect on room temperature efficiency droop.

The strong correlation ($R \sim -0.5$) between the localization parameter σ and the efficiency droop onset indicates a strong influence of the localization in determining the droop onset. As the excitation
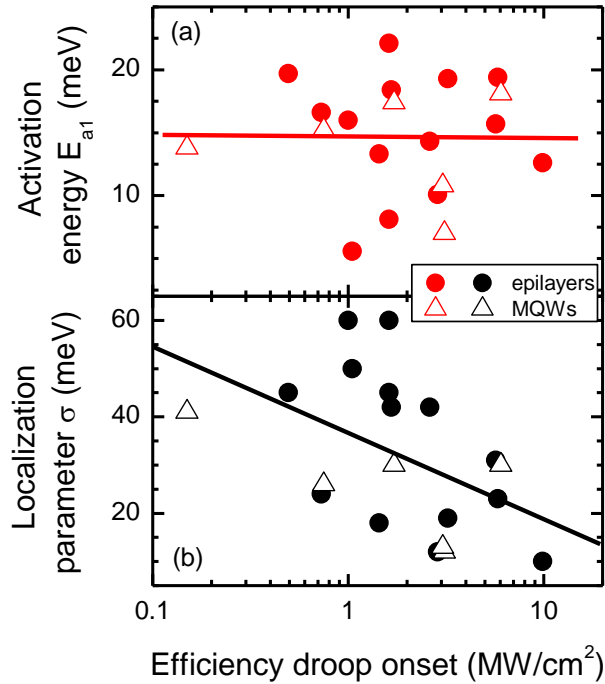

Fig. 3.1.8 Correlation between efficiency droop onset and activation energy Ea1 (a), and localization parameter σ (b) in AlGaN epilayers (closed circles) and MQWs (open triangles). Solid lines show the correlation trends.[P3]

power density is increased, the fraction of the delocalized carriers increases at the expense of the population of the lowest localized states. Additionally, the thermal delocalization also increases the fraction of free carriers. The delocalization affects the PL efficiency via the two mechanisms having the opposite effect: the bimolecular radiative recombination (increasing the PL efficiency) and the enhanced nonradiative recombination due to an increased probability to reach nonradiative recombination centers (decreasing the PL efficiency). In the samples with a stronger carrier localization, a higher fraction of the localized carriers causes the predominance of the nonradiative recombination and a lower threshold for the efficiency droop onset.

To summarize, we have studied the relations between nonradiative recombination, carrier localization conditions, thermally activated carrier transport and PL efficiency droop in a large set of AlGaN epilayers and MQWs with different carrier lifetime and localization strength. The dependence of the

peak IQE value on carrier lifetime and no significant dependence of the IQE on PL efficiency growth rate (see Fig. 3.1.4) shows that strong localization alone is not sufficient to ensure high internal quantum efficiency. The carriers in AlGaN are mobile enough at room temperature to reach the nonradiative recombination centers even in the localized state.

The observed thermal quenching of the PL intensity can be described by two activation energies (see Fig. 3.1.5). The smaller activation energy can be attributed to the carrier redistribution within the localized states and does not correlate with the room temperature efficiency droop onset. The larger activation energy describes the carrier delocalization to the mobility edge. This activation energy increases with the increasing localization parameter up to ~45 meV. However, when the localization parameter exceeds ~45 meV, the mechanism of reaching the nonradiative recombination centers changes from the direct activation to the mobility edge to a two-step activation process.

Delocalization of carriers affects the photoluminescence efficiency via the enhancement of the two mechanisms of opposite signs. Bimolecular recombination of the free carriers increases the IQE at elevated excitation intensities. However, the increasing filling of the localized states enhances the ability of free carriers to reach the nonradiative recombination centers, the nonradiative recombination becomes more efficient, and efficiency decreases.

3.2 Low-temperature redistribution of non-thermalized carriers

The efficiency droop has been mostly studied at room temperature, which is relevant to the operating devices, and relatively little attention has been paid to the droop temperature dependence. At lower temperatures, the droop is even more pronounced and the internal quantum efficiency (IQE) reaches its peak value at lower excitations[46,69,70] and at considerably lower carrier densities than those corresponding to the droop occurring at room temperature[70]. The excitation power densities corresponding to the droop onset at low and room temperatures differ considerably more than the carrier lifetimes determining the carrier densities[71]. Such temperature dependence cannot be explained by the Auger mechanism, both direct and indirect, since the Auger coefficient strongly depends on carrier density and is not expected to increase at low temperatures[59,60]. On the other hand, carrier delocalization and/or redistribution within localized states have been shown to correlate well with the droop onset[62,72]. In this section, we analyze the low-temperature efficiency droop in AlGaN epilayers to reveal the influence of carrier redistribution on the PL efficiency.
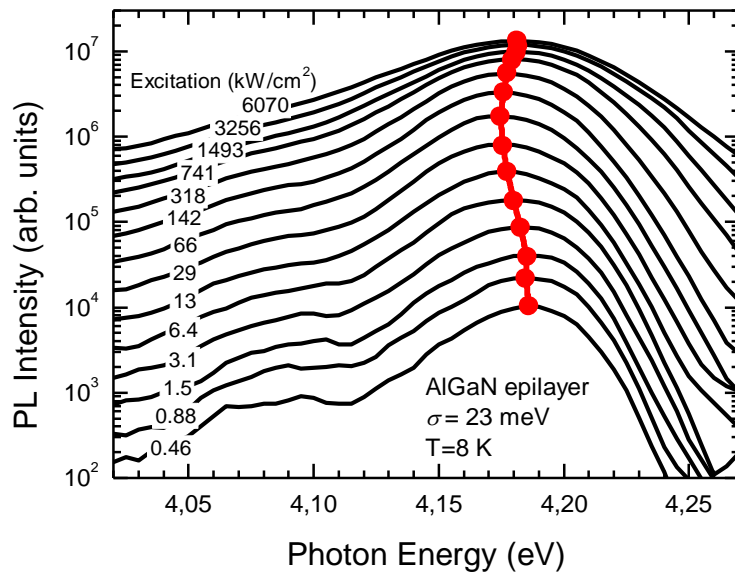

Fig. 3.2.1 PL spectra of an AlGaN epilayer (σ=23 meV) measured at 8 K temperature and different excitation power densities (indicated). Points indicate the peak positions.[P6]

Fig. 3.2.1 presents the PL spectra measured at the temperature of 8 K and different excitation power densities in sample S5. All the PL spectra consist of one broad

band. With increasing excitation power density, a nonmonotonous PL band peak position shift can be observed: the peak exhibits a redshift at low excitations gradually transformed to a blueshift at elevated excitations. Fig. 3.2.2 presents the PL band peak position shift dependence on excitation for several AlGaN epilayers under study.

The origin of the PL band redshift with excitation could be caused by two processes: band gap renormalization and carrier redistribution within localized states. Carrier heating effect can be excluded, since no significant increase of the
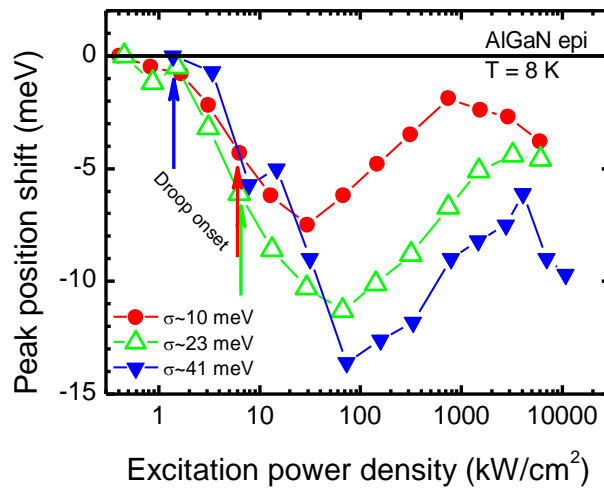

Fig. 3.2.2 Excitation power density dependences of peak position shift in AlGaN epilayers. Arrows indicate the onset of efficiency droop.[P6]

PL band width in the short-wavelength side of the band was observed.

The many-particle effects such as band gap renormalization are strongly reduced by carrier localization[114,115], which might be expected at low temperatures and excitations. The band redshift starts already at the excitation power density of ~1 kW/cm². For carrier lifetime of 1 ns, which is typical at low temperatures in the samples under study, such excitation corresponds to the carrier density of ~10^{17} cm^{-3}, i.e. is well below the density sufficient for significant band gap renormalization. Consequently, the carrier redistribution within localized states is the prevailing mechanism of the band redshift.

Fig. 3.2.3 shows the normalized PL efficiency at 8 K for several AlGaN epilayers with different carrier localization strength calculated as the ratio between the spectrally integrated PL intensity and the excitation power density. The PL efficiency increases at low excitation power densities and

decreases at elevated excitation intensities. As pointed out in Ref. [116], the efficiency decrease is more than an order of magnitude, contradicting a simple assumption that the nonradiative carrier recombination is negligible at temperatures as low as 8 K. The increasing part is less pronounced and
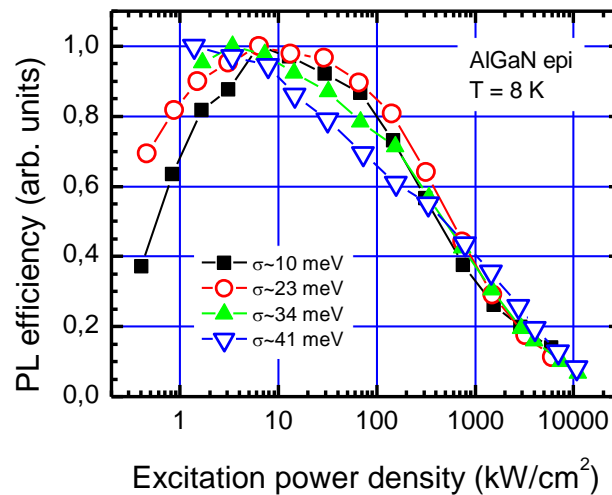

Fig. 3.2.3 Normalized PL efficiency dependences on excitation power density in AlGaN epilayers with different carrier localization strength (dispersion parameters are indicated).[P6]

ceases at lower excitation intensities in the epilayers with a stronger carrier localization. The efficiency droop at 8 K occurs at excitation power densities by more than three orders of magnitude lower than the droop at room temperature. The difference is substantially higher than a feasible difference in carrier densities, which should not exceed two orders of magnitude (estimated using the effective carrier lifetimes and the decay of PL intensity at 8 K and room temperature). This is an indication that the droop mechanisms at room and low temperatures are quite different.

The low temperature droop is probably related to carrier localization in consistence with the data on the dynamics of PL band presented above. The redshift of the PL band might be explained by carrier redistribution to lower localized states. As evidenced by the thermally-activated PL band shift observed at low temperatures as well as by the value of thermalization temperature T0, the carriers at low temperatures and low densities are not thermalized in AlGaN epilayers and quantum wells[77,99,102,103]. At low excitations, the carriers remain in the local potential minima where they are captured to.

As the excitation is increased, the local minima get filled in. Thus, the carriers have to move longer distances to find a free localized state (see Fig. 3.2.4). The deeper the localized state the lower is the probability of carrier delocalization from this state. Thus, this long
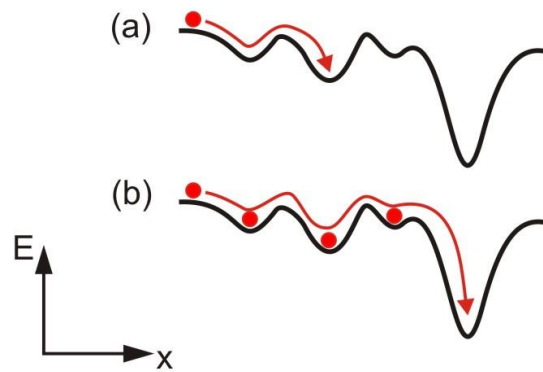

Fig. 3.2.4 Carrier localization at low (a) and high (b) carrier density. Population of localized states enhances the probability of reaching the lowest localized states.[P6]

range carrier redistribution populates various localized states but the population of the lowest localized states increases most significantly, since the carriers are not delocalized from these states. Thus, the PL band redshifts. Similar explanation has been previously used to interpret the PL band redshift in InAs/AlAs quantum dots[117], and semipolar InGaN/GaN quantum wells[118]. This carrier-density-induced red shift is similar to the effect caused by increasing temperature in the low-temperature region of the first red shift of PL band in the S-shaped temperature dependence of the band position.

At elevated excitations, as most of the lowest localized states become populated, the further increase in carrier generation rate results in the occupancy of less localized states, and the band blueshifts. Thus, the minimum of the PL peak position in the dependences presented in Fig. 3.2.2 approximately indicates the excitation power density corresponding to the complete exciton redistribution.

The occupation-enhanced carrier redistribution should also result in decreasing PL efficiency, since the more mobile excitons have a larger probability for reaching nonradiative recombination centers. Fig. 3.2.5 presents the excitation power densities corresponding to the droop onset and

the PL peak position minimum as functions of the localization parameter σ. The droop onset exhibits no strong dependence on the localization parameter. This is consistent with the assumption that the carrier-density-enhanced mobility is the main factor causing the droop at low temperatures. The
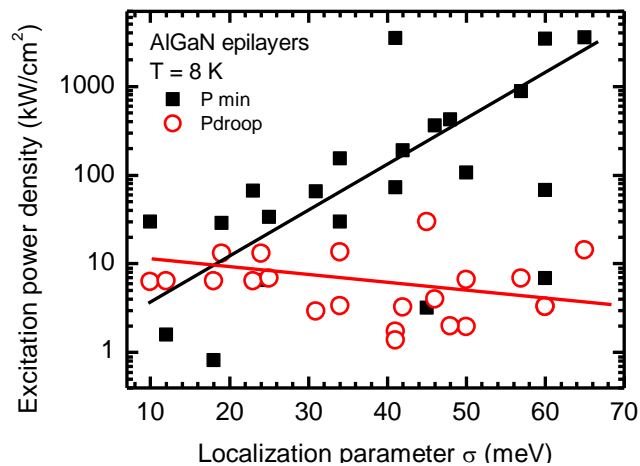

Fig. 3.2.5 Correlation between localization parameter σ and excitation power densities corresponding to droop onset and peak position minimum. Each point in both dependences corresponds to a different sample. The lines are guides for the eye[P6]

mobility might slightly decrease in the samples with a stronger localization. However, a higher density of the nonradiative recombination centers should be expected in such samples due to their lower structural quality.

Meanwhile, the minimum in the excitation dependence of the PL band position is reached at considerably higher excitation intensities in the samples with a longer tail of the density of localized states (and, correspondingly, with a larger σ). This behavior is consistent with the observation that higher temperatures are necessary to complete thermalization in the samples with larger values of σ (see chapter 1).

Thus, even small redistribution of nonequilibrium carriers in AlGaN epilayers at low temperatures substantially enhances the nonradiative recombination. This effect dominates over the increase in the rate of radiative recombination due to increasing contribution of free carriers. The latter effect is more pronounced at elevated temperatures, as is discussed in more detail in Ref. 103. The strong dependence of PL efficiency at low temperatures on the

carrier density should also be taken into account when estimating the IQE using the PL intensity dependence on temperature, as discussed in more details in[116].

The considerable decrease in PL efficiency at low temperature at comparatively low carrier densities seems to contradict to the generally accepted assumption that the nonradiative recombination at low temperatures is negligible due to low carrier thermal energy that is insufficient to overcome the potential barriers for the carriers to be captured to nonradiative recombination centers. However, many experimental data, though indirect, indicate that the electrons and holes in AlGaN are predominantly localized in the same locations in real space and move in pairs, like excitons[49,101]. Thus, to recombine nonradiatively, electrons and holes do not need to be captured one by one to the nonradiative recombination centers, but the nonradiative recombination centers serve as a channel to accept the energy from the recombining excitons.

To summarize, the nonmonotonous shift of PL band peak position with increasing excitation and low threshold for the onset of decrease in PL efficiency observed in many AlGaN epilayers with different strength of carrier (exciton) localization at low temperatures demonstrate that the nonradiative recombination is important even at low temperatures and at rather small carrier densities of ~10^{17} cm^{-3}. At increasing carrier densities, the nonradiative recombination is enhanced by increased mobility of carriers (excitons) moving to the nonradiative recombination centers due to the gradual filling-in of the localized states. The efficient nonradiative recombination at low temperatures is consistent with the excitonic (electron-hole pair) nonradiative recombination.

3.3 Mechanisms of the PL droop in AlGaN

In the first section we showed that delocalization of carriers can be both beneficial and detrimental to internal quantum efficiency. The bimolecular radiative recombination of the free carriers is more effective than the linear recombination of localized carriers and increases the internal quantum efficiency (IQE). On the other hand, the delocalized carriers are more likely to reach the nonradiative recombination centers and, therefore, the overall IQE is reduced. Aside from these competing mechanisms, a thermally activated PL intensity quenching effect was observed and found to be caused by carriers being delocalized to the mobility edge. However, as shown in previous section, nonradiative recombination can be enhanced even at low temperatures (8 K) and elevated excitations by filling in of the localized states and, consequently, increased carrier mobility. The competition of all of these processes influencing the PL efficiency depends on the conditions of carrier localization, temperature, and carrier density. In this section, we link the processes listed above with the PL efficiency droop in simultaneous study of the IQE, carrier delocalization, and stimulated emission (SE). This allows us to reveal different mechanisms of PL efficiency droop in AlGaN in a generalized case.

The temperature dependence of the PL intensity and efficiency have been measured for both AlGaN epilayers and MQWs. To analyze the links between carrier localization conditions and efficiency droop, we studied the excitation power density dependence of the spectrally integrated PL efficiency at several temperatures. The typical dependences are plotted in Fig. 3.3.1 for AlGaN samples with weak (a) and strong (b) localization. Using the data in Fig. 3.3.1, the efficiency droop onset was estimated as the excitation power density corresponding to the highest PL efficiency and separating the initial increase in PL efficiency and its decrease (droop) above the onset. The temperature dependence of the PL band peak position was exploited to estimate the carrier

localization parameters in the samples under study, as described in more detail in chapter 1. This approach enables us to estimate the standard deviation σ of the Gaussian distribution of the band gap fluctuations caused by the random fluctuations in aluminum content and/or QW width, and the parameter T_0 approximately corresponding to the temperature of the dip in the S – shaped dependence, i.e. the temperature above
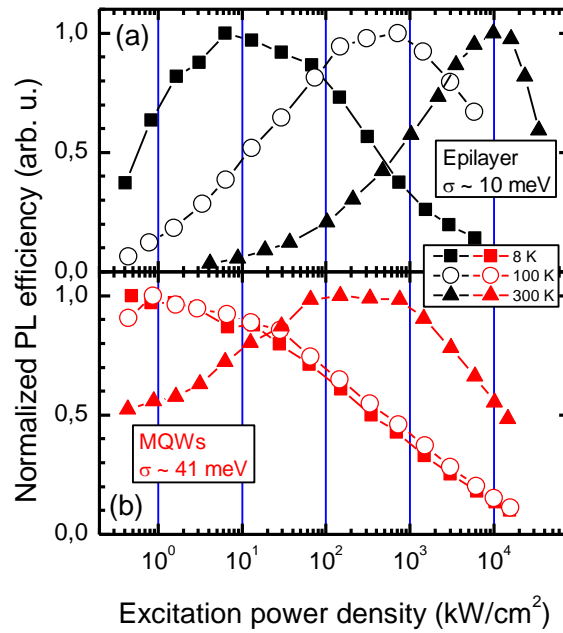

Fig. 3.3.1 Normalized PL efficiency dependences on excitation power density in AlGaN samples with weak (a) and strong (b) carrier localization at 8 K (closed squares), 100 K (open circles) and 300 K (closed triangles). [P1]

which the carrier thermalization becomes important. It is worth noting that, at any temperature, the droop onset is always higher in the samples with weaker carrier localization. Moreover, the droop onset increases with temperature more rapidly in the samples with weaker carrier localization.

The influence of localization conditions is most clearly pronounced in samples with strong localization – AlGaN MQWs with high aluminum content. In front – surface configuration, we observed efficiency droop, i.e. a decrease of photoluminescence efficiency as the excitation power density increases above a certain threshold (droop onset threshold). The droop is observed for all samples at all temperatures under study. In Fig. 3.3.2 a, the spectrally – integrated photoluminescence intensity recorded in front-surface configuration is presented as a function of excitation power density at different temperatures for sample with 5.0 nm-wide QWs. To better reveal the droop onset, the corresponding excitation power density dependences of

photoluminescence efficiency, which was calculated as the PL intensity divided by the excitation power density, are plotted in Fig. 3.3.2b.

It might be expected that the droop onset occurs at approximately the same carrier density at any temperature: at lower temperatures, the carriers localization is stronger, their lifetimes are longer, thus the excitation power density necessary to reach the same threshold carrier density becomes lower as the temperature is decreased.
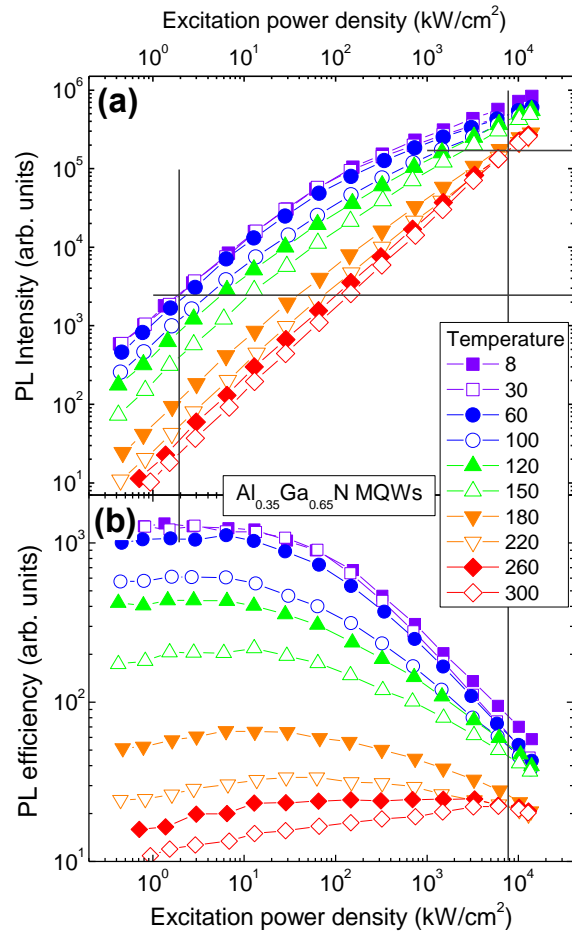

Fig. 3.3.2 Excitation power density dependence of photoluminescence intensity (a) and photoluminescence efficiency (b) at different temperatures (indicated) in $Al_{0.35}Ga_{0.65}N$ MQWs.[P9]

However, the data provided in Fig. 3.3.2 prove this expectation to be wrong. The vertical line in Fig. 3.3.2 indicates the droop onset at 8 K. The corresponding luminescence intensity is indicated in Fig. 3.3.2 a by a horizontal line. It is obvious that the droop threshold at room temperature corresponds to a considerably higher luminescence intensity. Since the increase in PL intensity at increasing excitation power density proceeds, at low excitation intensities up to the horizontal line at approximately the same rate at any temperature (see Fig. 3.3.2 a), the equal PL intensity observed at different temperatures indicates approximately the same carrier density. Therefore, the lower PL intensity corresponding to the droop onset threshold at lower

temperatures indicates also that a lower carrier density is sufficient for the droop effect to occur.

The interpretation of the droop onset should take into account the carriers occupying the localized states, which, as we show in chapter 2, are playing the dominant role even in such a high-carrier-density effect as stimulated emission. This section presents the results obtained by studying low-efficiency samples to exclude the saturation of nonradiative recombination as a possible origin of efficiency increase. Therefore, the enhancement due to increasing contribution of bimolecular recombination remains the only plausible explanation of the efficiency increase, which we observe in a wide range of excitation intensities at room temperature, and which is gradually overwhelmed by the droop as the temperature is decreased.
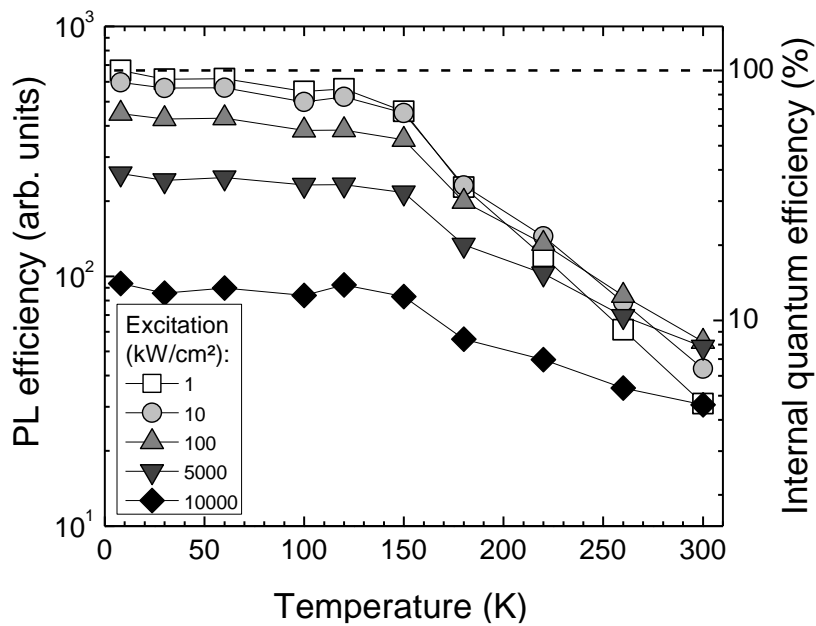
Fig. 3.3.3 Efficiency of photoluminescence in 2.5 nm-wide $Al_{0.35}Ga_{0.65}N$ MQWs in arbitrary units (left axis) and absolute units (right) as a function of temperature at different excitation power densities.[P9]

Both increasing carrier density and temperature facilitate the carrier delocalization. The strong influence of delocalization at increased excitation even at low temperatures is revealed in Fig. 3.3.3, where the luminescence

efficiency as a function of temperature is plotted for different excitation power densities. The coinciding upper two curves show that the dependence is insensitive of excitation, provided that the excitation is low enough. Meanwhile, at elevated excitation power densities the internal quantum efficiency (IQE) substantially decreases, according to the results presented in Fig. 3.3.3, from presumably 100 % down to 15 % even at the temperature of 8 K. The predominance of different effects caused by carrier delocalization at room and low temperatures can be interpreted by peculiarities of carrier localization at different temperatures. The delocalized carriers can either recombine radiatively or move to nonradiative recombination centers to recombine nonradiatively, or be trapped back to localized states with strongly restricted ability to move from one localized state to another. At low temperatures, most of the localized states at elevated carrier densities are occupied, thus the „excess" free carriers generated at increased excitation intensity have low probability to be trapped to localized states and high probability to reach nonradiative recombination centers. Thus, the delocalization predominantly results in enhancement of nonradiative recombination and, consequently, the efficiency droop. Meanwhile, at high temperatures, the occupation of the localized states is looser than that at low temperature: there are more states for the delocalized carrier to be trapped again to the localized state. This trapping-detrapping limits mobility of the carriers and is favorable for increasing contribution of the radiative bimolecular recombination in respect to nonradiative recombination. As a result, the emission enhancement at room temperature dominates over the droop for considerably wider range of excitation intensity than at low temperatures. Whatever the origin of the dominant droop effect at room temperature, the competition of the two opposite effects caused by carrier delocalization plays also a considerable role in the droop.

Stimulated emission was already demonstrated to cause PL droop in GaN (see chapter 2). When comparing the stimulated emission threshold and the droop onset dependences on localization parameter in AlGaN, several peculiarities were noticed. At low temperatures, the stimulated emission threshold is always at much higher excitations than the droop onset. Meanwhile, at 300 K, the values of droop onset and stimulated emission threshold are quite close, except for the strongest localization. Moreover, at low temperatures, the value of the ratio between the stimulated emission threshold and droop onset is above ~40 and steadily increases with localization parameter σ. The increase in temperature results in a decrease of the ratio for the MQWs with the weakest localization, while having no significant influence in the samples with the strongest localization.
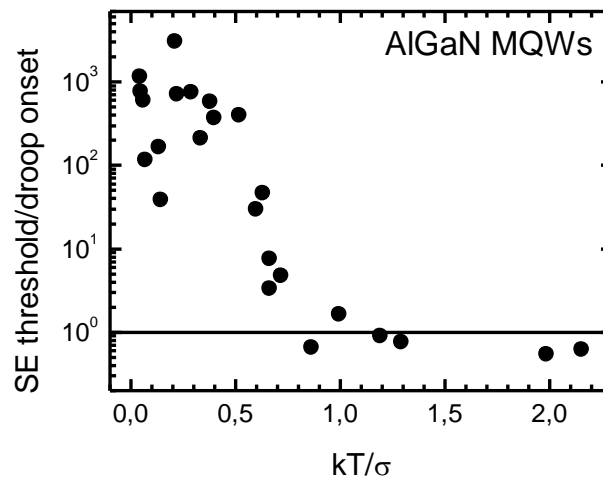

Fig. 3.3.4 Ratio of thresholds for stimulated emission and droop onset as a function of the ratio of thermal energy to dispersion of potential fluctuations for 6 different samples at various temperatures. The solid line indicates the ratio between stimulated emission threshold and droop onset equal to 1.[P8]

To summarize these trends, we plotted the ratio of the thresholds for stimulated emission and droop onset as a function of the ratio of the thermal energy to the dispersion of potential fluctuations (Fig. 3.3.4). Each point in Fig. 3.3.4 corresponds either to a different sample with a different σ value in the range from 12 to 41 meV or to a different temperature (20, 100, 180, or 300 K). Despite the strong scattering of the points in Fig. 3.3.4, which is expected, first of all, due to different carrier lifetimes in different samples, the plot reveals a clear trend: i) as the ratio kT/σ increases (either because of

smaller *σ* or larger *T*) up to 1, the ratio of the thresholds for stimulated emission and droop onset becomes smaller, and ii) the efficiency droop and stimulated emission occurs at the same excitation power density, when k*T* becomes larger than *σ*. This is an indication that the dominating droop origin in AlGaN with low band gap fluctuations at high temperatures might be caused by stimulated emission. It is worth noting that the light amplification by stimulated emission of radiation (i.e., the LASER effect) might be not observed in AlGaN MQWs and, especially, in epilayers, because the amplification due to stimulated emission is overcompensated by the light losses due to scattering and absorption by dislocations (abundant in AlGaN, especially in high-Al-content AlGaN). For LEDs, it is important that the stimulated emission, though being ineffective in the light amplification, effectively decreases the useful light output of an LED. As pointed out in our previous study on the droop in GaN[66], the total (spontaneous and stimulated) light emission efficiency might increase at increasing excitation intensity but the front-surface emission efficiency, which is actually important for LED operation in the current injection mode, decreases.

Since both temperature and localization parameter are important in determining the droop onset, we plotted the efficiency droop onset as a function of the dimensionless parameter k$_B$*T*/σ (see Fig. 3.3.5), similarly to what we did to reveal the influence of the SE on the droop mechanism in AlGaN (Fig. 3.3.4). Each point in Fig. 3.3.5 represents an AlGaN epilayer or MQW sample with specific *σ* value in the range from 10 to 65 meV and measured at a specific temperature in the range from 8 to 300 K. We indicate whether the temperature is above or below the thermalization temperature *T$_0$* by plotting red or black points, respectively. We include the results obtained for both the epilayers and MQWs (filled and open points, respectively). As seen, the epilayers and MQWs exhibit similar trends. This is an indication that the carrier dynamics mainly depends on the thermalization and the k$_B$T/σ ratio,

independently of the potential fluctuation origin (which might be different in the epilayers and MQWs).

Despite the considerable scattering of points, which might be expected due to the different densities of nonradiative recombination centers in different samples, the plot might be divided into three regions. The first region covers all points corresponding to the nonthermalized state of the nonequilibrium carriers ($T < T_0$). This region is observed for $k_B T/\sigma < 0.35$ (region I in Fig. 3.3.5). The droop onset in this region is low, in the range from 1 to 10 kW/cm^2, and does not depend on $k_B T/\sigma$. As the carrier distribution becomes thermalized, the droop onset rapidly increases with parameter $k_B T/\sigma$ increasing in the range from 0.35 to 1 (region II in Fig. 3.3.5). Finally, the increase tends to saturation for $k_B T/\sigma > 1$. The last feature is consistent with our observations of the droop caused by stimulated emission.
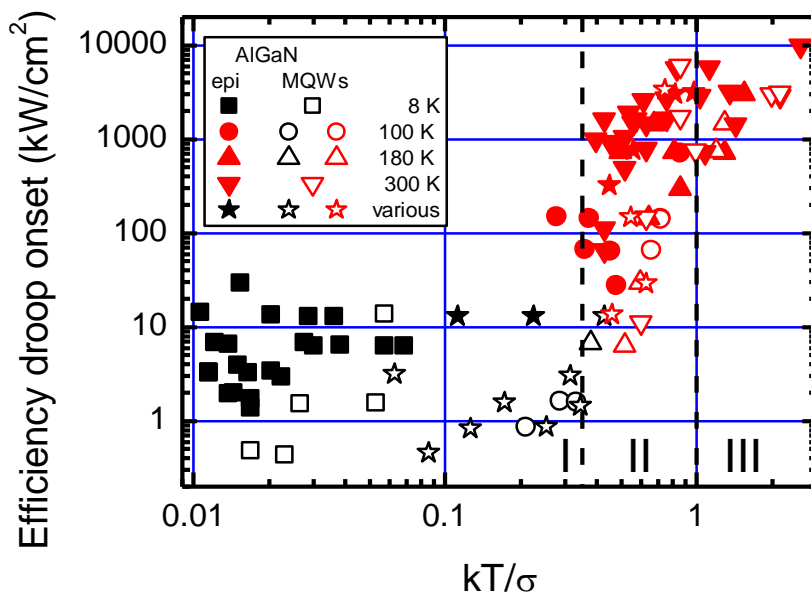
Fig. 3.3.5 Efficiency droop onset dependence on the ratio of thermal energy to localization parameter in AlGaN epilayers and MQWs at various temperatures. Filled and open points indicate epilayers and MQWs, respectively. Black and red points correspond to nonthermalized and thermalized distribution of carriers within localized states, respectively. Dashed lines separate regions corresponding to different efficiency droop mechanisms.[P1]

The three regions observed in the dependence of droop onset versus k_BT/σ are most likely related to the change in efficiency droop mechanism. The corresponding mechanisms are schematically shown in Fig. 3.3.6.

At temperatures below the thermalization temperature ($k_BT/\sigma < 0.35$, region I in Fig. 3.3.5), the carriers relax to the potential minima in the close vicinity of the carriers. Since the temperature is below the thermalization temperature T_0, the carrier redistribution is weak, and they are not able to leave the local potential minima where they are captured (Fig. 3.3.6 (a)). As the excitation is increased, the carriers (excitons) become more mobile, since most of the nearest local minima are already occupied. Such occupation-enhanced carrier redistribution (Fig. 3.3.6 (b)) results in decreasing PL efficiency due to a higher probability of reaching nonradiative recombination centers (see section 2 of this chapter).
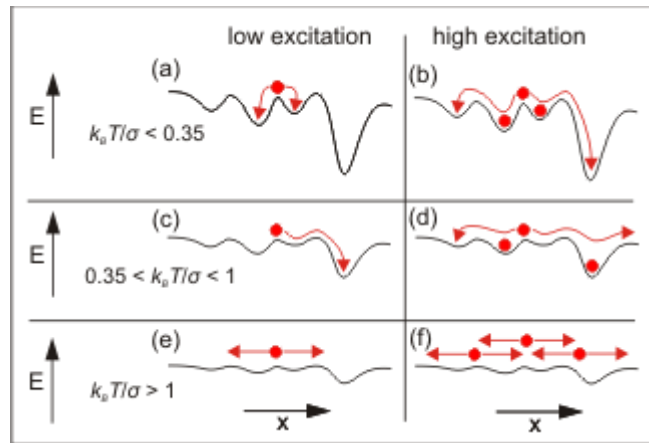

Fig. 3.3.6 Schematic diagrams of carrier transport at low (a), (c), (e) and high (b), (d), (f) excitations for the three regions represented in Fig. 3.3.5. [P1]

At elevated temperatures $T > T_0$ ($0.35 < k_BT/\sigma < 1$, region II in Fig. 3.3.5), the carriers are able to redistribute efficiently and become thermalized. As the excitation is increased, an increasing fraction of carriers becomes delocalized, while only the deeper localized states remain filled-in.[99,102] The delocalized carriers can decrease the PL efficiency by the enhancement of nonradiative recombination as well as increase it due to bimolecular recombination[102] (see section 1 of this chapter), with the competition between these two effects determined by the localization parameter σ. Due to the efficient thermal

redistribution, higher carrier densities and, hence, excitation power densities are required to saturate the localized states and result in the efficiency droop via increased probability to reach the nonradiative recombination centers [see Fig. 3.3.6 (d)].

At high temperatures and/or weak localization ($k_BT/\sigma > 1$, region III in Fig. 3.3.5), the carriers are predominantly free, since the thermal energy is higher than the localization parameter (Fig. 3.3.6 (e) and (f)). The efficiency droop onset in these samples is achieved at carrier densities in quite a wide range from 2×10^{19} to 2×10^{20} cm^{-3}. This renders the Auger mechanism less probable as the droop origin, since Auger recombination might be expected to emerge at similar carrier densities in any sample of the same material. Furthermore, at such high k_BT/σ ratio, the SE threshold coincides with the droop onset in AlGaN MQWs, as seen in Fig. 3.3.4. However, no stimulated emission has been observed at room temperature in the AlGaN epilayers under study. One more droop mechanism might be related to excitation-dependent carrier transport: at low carrier densities, the nonradiative processes caused by point defects limit the carrier mobility. As the carrier density is increased, the point defects are saturated. Thus, the distance a carrier can move in real space during its lifetime is increased, and the nonradiative recombination at extended defects starts to dominate.[74,119] Moreover, at high carrier densities, the carrier mobility is additionally enhanced due to carrier degeneracy.[120] The carrier-density-enhanced recombination at the extended defects with the distances between them larger than the average distance the carrier can travel during its lifetime at low temperature but comparable at room temperature is consistent with the supposed recombination at growth domains observed in AlGaN epilayers by scanning near-field optical microscopy.[118,121] During the growth, the adjacent islands coalesce into large grains. As a result of coalescence, the domain boundaries usually contain extended defects that form to accommodate the relative difference in crystal orientation among the

islands.[122] Thus, the onset of the droop caused by the fast nonradiative recombination at these boundaries does not strongly depend on $k_B T/\sigma$ but is rather determined by the grain size depending on lattice mismatch, buffer layer, and slightly on growth conditions.

In summary, it is observed that delocalization i) increases the PL efficiency by increasing the contribution of bimolecular recombination of free carriers, and ii) causes the PL droop by enhancement of nonradiative recombination. The study of the competition between these two opposite-sign effects revealed that the ratio $k_B T/\sigma$ between the carrier thermal energy $k_B T$ and the localization parameter σ might be treated as the parameter indicating the predominant origin of PL droop in AlGaN-based MQWs and epilayers.

For nonthermalized carriers ($k_B T/\sigma < 0.35$), the droop occurs due to occupation-enhanced redistribution of nonthermalized carriers. At elevated temperatures ($0.35 < k_B T/\sigma < 1$), the droop is caused by enhancement of the nonradiative recombination as the localized states are filled-in and an increasing fraction of carriers becomes delocalized. At high temperatures and/or weak localization ($k_B T/\sigma > 1$), the origin of the droop is stimulated emission in AlGaN MQWs and excitation-enhanced carrier transport to extended defects in AlGaN epilayers.

4. Investigation of Boron gallium nitride epilayers

A large technological effort is underway to improve the lattice matching at the interfaces of AlGaN heterostructures. One of the approaches to solve the problem is to alloy the nitride compounds with boron[18]. BGaN with boron content of up to ~12% could be lattice-matched to AlGaN in the entire range from GaN to AlN (see Fig. 4.1). Thus, the introduction of boron might improve the structural quality of AlGaN-based heterostructures.
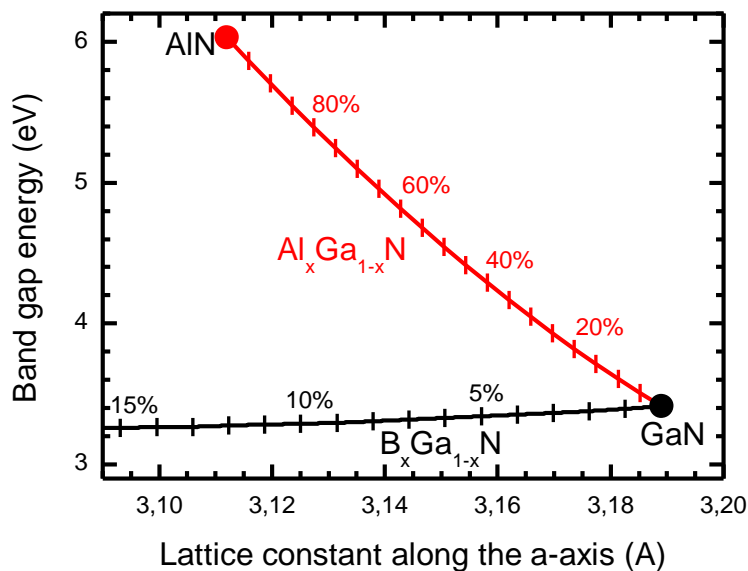

Fig. 4.1 Band gap energy of BGaN and AlGaN versus lattice parameter, calculated with data from Refs. 18, 19, and 23. [P2]

The incorporation of an increasing amount of boron is, however, accompanied by a substantial decrease in luminescence efficiency. This issue is targeted in the current study. BGaN is still a rather new material and its basic optical properties are not well known. The reports on optical properties are usually limited to comparison of BGaN photoluminescence (PL) spectrum with that of the reference GaN layer[15,20,21,27]. The extremely large band gap bowing parameter value of 9.2 eV was reported, based on BGaN layers with rather small boron content of up to ~1.8%[21]. Only a couple of papers by the same

group report the temperature dependence of PL in BGaN epilayer with boron content of 1%[20,27].

In this work, we report on the results of our efforts to optimize the growth conditions for growing BGaN epilayers with boron content of up to several percent. 23 different samples grown on SiC substrate and AlN and GaN templates on sapphire were under study. Structural and optical properties of BGaN epilayers grown using the same MOCVD reactor on different templates/substrates with boron content of up to 5.5% are analyzed.

The PL in BGaN epilayers with different boron content was studied under different excitation intensities at temperatures in the range from 8 to 300 K. By studying the photoluminescence (PL) peak position in many epilayers with different boron content, we determine the band gap bowing parameter. The PL properties of BGaN epilayers are compared to those of a purposely grown reference GaN epilayer.

The growth and structural characterization was carried out by Dr. A. Kadys, Dr. T. Malinauskas, S. Stanionytė, M. Kolenda and K. Badokas. Surface analysis was carried out by Dr. D. Dobrovolskas.

4.1 BGaN: Structural characterization

The boron content in BGaN layers was estimated from the X-Ray diffraction (XRD) scans along the (004) reflection shown in Fig. 4.2. The main
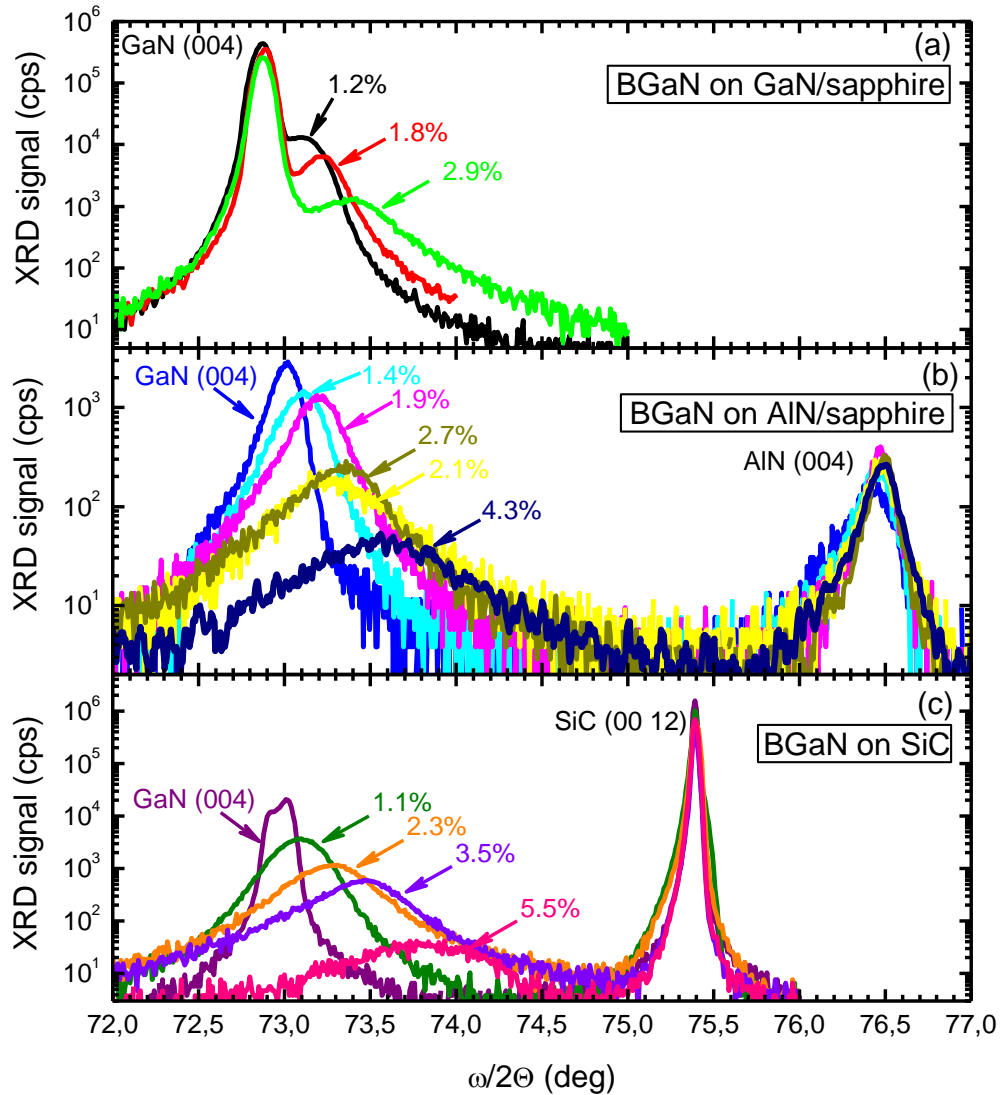
Fig. 4.2 XRD scans along (004) direction for BGaN layers grown on GaN/sapphire (a), AlN/sapphire (b), and SiC (c) substrates. The estimated boron content is indicated.[P5]

peak at 72.9° corresponds to the GaN buffer layer (or GaN reference sample in the case of samples grown directly on AlN or SiC, Fig. 4.2c). In samples grown on AlN/sapphire template and SiC substrate, the corresponding peaks for AlN and SiC are observed (76.45° for AlN buffer in Fig. 4.2b and 75.38° for SiC substrate in Fig. 4.2c, respectively). The smaller peaks at the angles larger than

those of GaN are assigned to the diffraction of BGaN layer. As expected, a higher TEB/III ratio, where III is the total number of moles of the group-III sources (TMGa + TEB), results in a higher angle value of the BGaN peak, indicating a higher boron content in the $B_xGa_{1-x}N$ layer. Henceforth, the structural analysis will be presented for each case (different template) separately.

Increasing the TEB/III ratio from 1.7% to 6.5% during layer growth on GaN/sapphire template resulted in an increase in the boron content from 1.2% to 2.9%, as deduced from ω-2θ scans by assuming complete relaxation of the BGaN layers. However, the decreasing intensity and the increasing width of the BGaN XRD peak indicate deterioration of the structural quality. The surface morphology was similar in all three samples grown on GaN/sapphire templates. A typical AFM image is shown in Fig. 4.3a. The surface roughness was in the range of 15-23 nm, with slightly higher roughness in the sample with the lowest boron content.

For the BGaN on AlN/sapphire template, the results are similar to those described above. As expected, the increase of TEB/III ratio results in a BGaN peak shift to higher angles, indicating an increase in boron content in the layers up to 4.3%. Again, the shift of the BGaN peak is accompanied by decreasing intensity and increasing width indicating the deteriorating structural quality of the BGaN layers. The deterioration was also confirmed by the rocking curves (ω-scans) measured at (004) reflection (not shown here): the rocking curve width increased from 2500 to 9400 arcsec, as the boron content in the layer increased from 1.9% to 4.3%. Nevertheless, the sample quality was comparable to that reported for the BGaN layers with the rocking curve width at 6000 arcsec for boron content of 1.83%[21].

The surface morphology of most of the BGaN layers grown on AlN/sapphire templates was similar to that of the samples grown on GaN/sapphire templates. The typical AFM image is shown in Fig. 4.3b. The

surface roughness was in the range from 40 nm to 8 nm, decreasing with the increase in boron content of up to 2.7%. Such behavior has previously been attributed to the filling of pits and V-defects present in the buffer layer[28]. On the other hand, two of the samples had a very rough surface with roughness in the range between 100 and 165 nm. Large crystallites with polygonal shape can be observed on their surfaces (see Fig. 4.3c). The presence of the crystallites on the surface has been attributed to the phase separation, which occurs when the layer thickness and/or TEB/III ratio exceed their optimal values[28].

In the case of BGaN epilayers grown on SiC substrate, we have achieved the highest increase of boron content (from 1.1% to 5.5%) by increasing the TEB/III ratio from 1.7% to 12.2%. For comparison, the XRD scan of the reference GaN sample is also shown in Fig. 4.2c. The GaN peak at 73° consists of two peaks, which, most probably, correspond to the relaxed and strained phases of the GaN grown directly on SiC substrate.

In addition to the peak shift with increasing boron content, the BGaN band also decreases in intensity and broadens, indicating the deteriorating structural quality of BGaN layers. The rocking curves revealed widths in the range from 2800 to 4000 arcsec for the BGaN layers with boron content of up to 2.3%, however, the rocking curve width increased up to 6500 and 9000 arcsec for the samples with the boron content of 3.5% and 5.5%, respectively.

The surfaces of BGaN layers grown on SiC substrate were rougher than the surfaces of the samples deposited on sapphire with GaN and AlN templates. Only a couple of samples had a rather smooth surface with the roughness in the range of 8-25 nm (see Fig. 4.3d). Meanwhile, large crystallites are evident on the surfaces of most of the samples grown on SiC, and the surface roughness varies in the range from 50 nm to 280 nm. The typical AFM image is shown in Fig. 3e. Again, the formation of the crystallites observed on the surface are, most probably, related to the phase separation occurring in the layers with

thickness above the optimal thickness[15,28,123]. This is especially evident in thick layers (~1.2 µm).
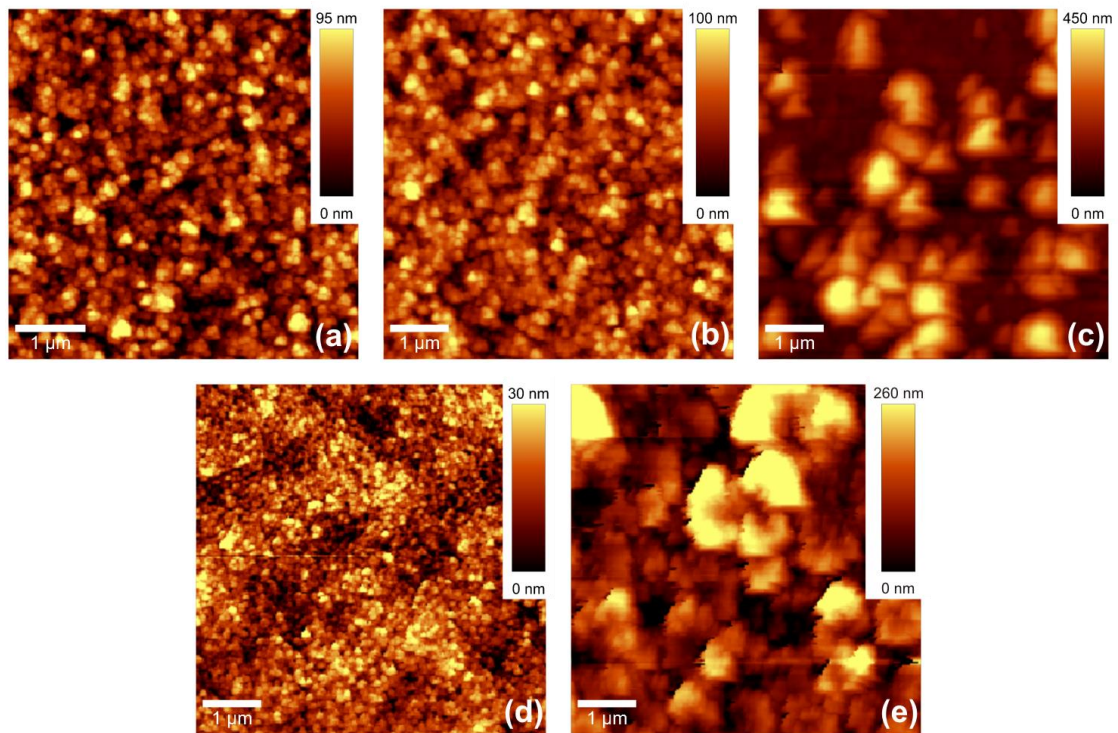

Fig. 4.3. Surface topography of BGaN layers grown on GaN/sapphire template (a), AlN/sapphire template (b), (c), and SiC substrate (d), (e).[P5]

4.2 Optical properties

The PL spectrum of BGaN epilayer (see a typical spectrum of BGaN with 2% of boron measured at 8 K temperature in Fig. 4.4) is similar to that of GaN. The spectrum consists of near-band-edge (NBE) luminescence and two broad bands well below the band gap, which should be attributed to the optical transitions involving deep defect levels. The first band, peaked at 2.1 – 2.2 eV, corresponds to the well-known yellow luminescence band in GaN[124], while the band peaked at ~2.7 eV corresponds to the blue luminescence band of GaN[124].

Both bands are slightly shifted to the lower energies in respect to their positions in GaN, similar to the shift of analogous PL bands in InGaN[125,126]. The main PL band peaked at ~3.4 eV is due to band-to-band transitions in BGaN layer.
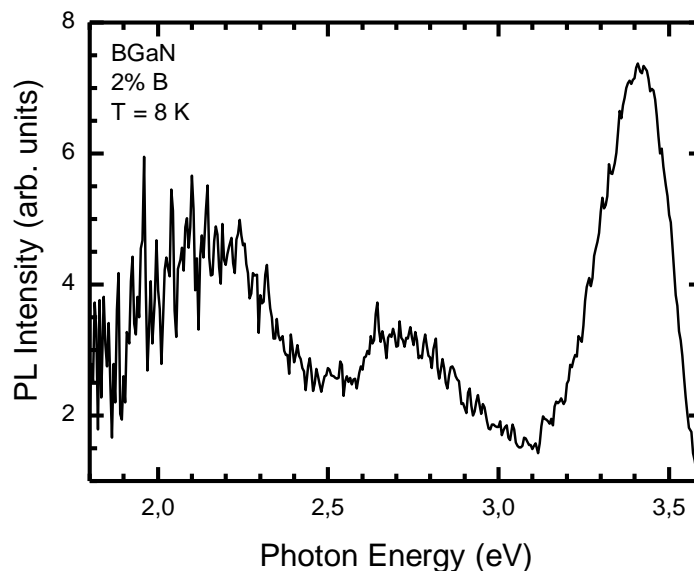
Fig. 4.4 The photoluminescence spectrum of the $B_{0.02}Ga_{0.98}N$ epilayer measured at 8 K temperature.[P2]

Meanwhile, the influence of lower-energy optical transitions are more substantial at room temperature (see Fig. 4.5). The PL spectra of BGaN epilayers strongly depend on excitation intensity. At low excitation intensities, the spectrum is dominated by a broad emission band at energies well below the band gap. This PL band might be attributed to the radiative carrier recombination via defect-related states. As the excitation power density is

95

increased above ~60 kW/cm², a narrower PL band peaked at ~360 nm emerges. The intensity of this narrower PL band grows with increasing excitation more rapidly than that of the defect-related band, and
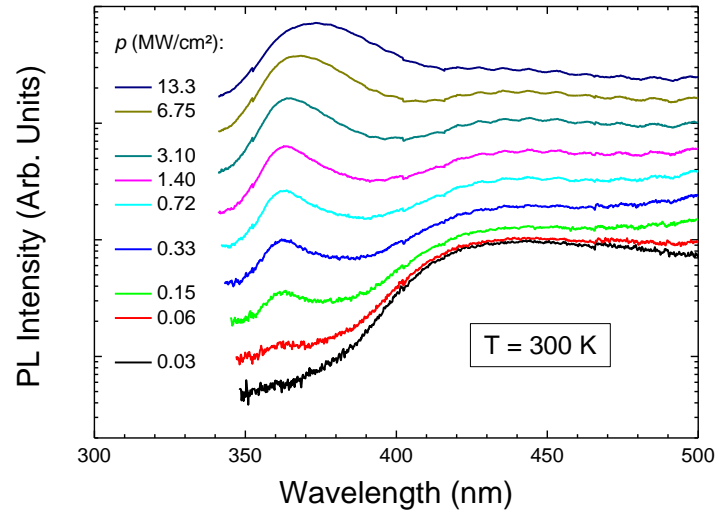

Fig. 4.5 Photoluminescence spectra of BGaN epilayers with 1.2 % boron content at different excitation power densities p (indicated).[P4]

the band becomes dominant above ~1.4 MW/cm². This higher energy band might be attributed to the band-to-band radiative transitions via radiative bimolecular recombination, the rate of which is proportional to the square of the density of photogenerated nonequilibrium carriers. At elevated excitation power densities (>1.4 MW/cm²) the PL band exhibits a red shift, most probably, caused by the band gap renormalization due to many-body interaction.

Hereinafter, we focus our study on the main PL band, caused by band-to-band transitions. Figure 4.6 presents the low-temperature PL spectra of several BGaN samples with different B content measured under the same excitation power density (1 MW/cm²). For comparison, the PL spectrum of the reference GaN sample grown under identical conditions is also shown. The PL band initially shifts to lower energies as the boron content is increased. However, at the boron content above ~3%, two PL bands can be clearly observed in the spectrum: a narrower low-energy band peaked at ~3.35 eV and a broader high-energy band with the peak at ~3.45 eV. The low-energy band is more pronounced in the NBE luminescence spectrum at low temperatures and low excitation power densities. Its intensity decreases with increasing temperature
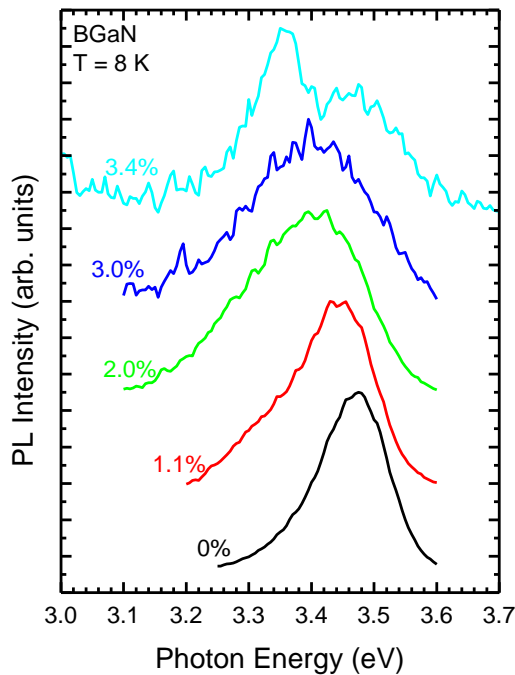
Fig. 4.6. PL spectra of BGaN epilayers with different boron content, measured at 8 K temperature. The spectra were normalized and shifted along the vertical axis for clarity. [P2]

considerably faster than the intensity of the high-energy band, and the latter band dominates the spectrum for temperatures above ~150 K. The intensity of the low-energy band saturates above ~0.5 MW/cm^2, and the band can be hardly traced on the background of the high-energy band at elevated excitation intensities.

The origin of the low-energy band can be interpreted in a few different ways. First of all, a comparatively narrow PL band at low temperatures and low excitation intensities might be attributed to the recombination of bound excitons. However, the separation between this band and the band due to band-to-band transitions (supposedly, the high-energy band in our spectra of BGaN) is too large for donor-bound exciton and too small for acceptor-bound exciton. The second possible origin of the low-energy band is optical transitions either from conduction band to shallow acceptor level or from a shallow donor level to the valence band. In GaN, typical shallow donors have activation energies of ~30 meV[124], or 140-180 meV for certain donors[127]. Meanwhile, the activation energies of acceptors are at least 200 meV and range up to 0.9 eV[124,128]. Thus, the expected energy separation does not fit again, unless BGaN contains donor or acceptor levels with activation energies considerably different from those in GaN.

The most feasible explanation would be the phase separation resulting in formation of regions with a higher boron content in the layer with a lower

boron content. The traces of the same high-boron-content PL band can be observed in most of the BGaN samples under study at low temperatures and low excitations (not shown here), indicating the presence of partial phase separation even for boron content as low as 1%. Meanwhile, the phase separation is much stronger in BGaN layers with boron content with 3.4%, and the high-boron-content PL band becomes more pronounced. Stronger phase separation at higher boron content is consistent with increasing unstable composition region as the growth temperature is decreased[17], which is required for incorporation of higher boron content[19,24,129].

The room temperature PL spectra of several BGaN samples are shown in Fig. 4.7. The PL spectrum of the reference GaN sample is also shown there. The PL band of the GaN sample is peaked at 3.415 eV, which is the usual position for GaN at room temperature. With the introduction of increasing amount of boron into GaN, the PL band shifts to lower energies. Unfortunately, the increasing boron
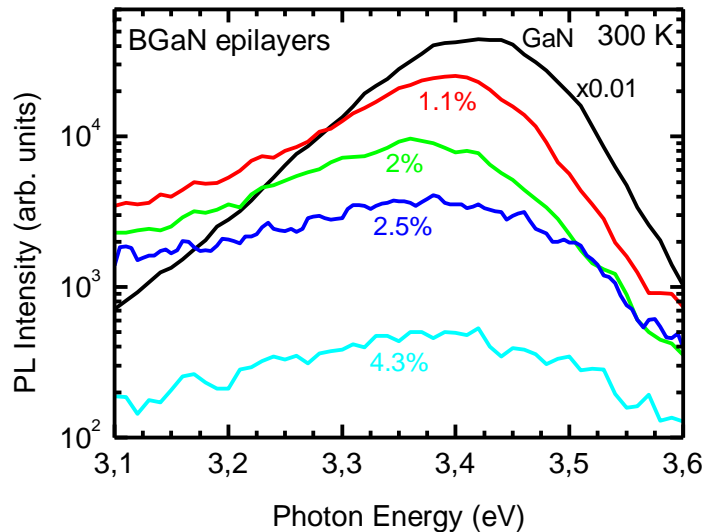
Fig. 4.7 Photoluminescence spectra of BGaN epilayers with different boron content (indicated) measured at room temperature under the excitation power density of 1 MW/cm^2. [P5]

content results also in a considerable decrease in PL intensity; probably, due to an increasing amount of defects. Even at a moderate boron content of 2%, the PL intensity is lower by at least 2 orders of magnitude compared to that in the reference GaN sample. Such behavior is observed in all the BGaN layers under study irrelevant of the substrate/template used for their deposition.

The PL band peak position dependence on boron content is shown in Fig. 4.8, where the points of different shape (color) correspond to the BGaN epilayers deposited on SiC substrate and sapphire with GaN and AlN templates. As far as the large dispersion of the points allows to estimate, the bandgaps of the BGaN epilayers deposited on different substrates or templates do not exhibit significantly different dependences of their band gaps on boron content. The band gap in this range decreases with increasing boron content. This behavior might be explained by a large value of bowing parameter due to high contrast between the average bond length for B-N

Fig. 4.8 Photoluminescence peak position variation with boron content (points) in BGaN epilayers grown on different substrates/templates (indicated). Lines show the bandgap variation calculated with bowing parameter b = 4 eV (solid line) and b = 9.2 eV (dashed line).[P5]

and Ga-N[21]. The common band gap dependence on boron content for all BGaN epilayers irrelevant to their substrates/templates is depicted by solid line in Fig. 4.8 in the form $E_g(x) = xE_g^{BN} + (1-x)E_g^{GaN} - bx(1-x)$. Here, E_g^{BN} = 5.8 eV (Ref. [130]) and E_g^{GaN} = 3.415 eV (Ref. [81]), are the band gaps of BN and GaN, respectively. The depicted best fit curve corresponds to the bowing parameter b = 4 eV. Moreover, the points in Fig. 4.8 for the epilayers with the boron content exceeding 2% indicate that the band gap decrease with increasing boron content probably slows down even faster than the dependence depicted by the solid line. Thus, the b value might be even smaller than 4 eV. The
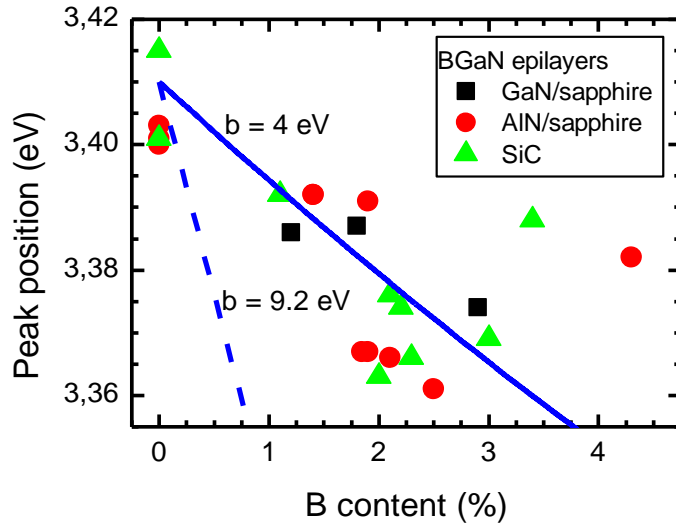
corresponding curve with b = 9.2 eV, which is reported as the b value in Ref. [21], is depicted in Fig. 4 by a dashed curve. It is obvious that b = 9.2 eV does not fit our experimental data. Thus, the best estimate of the bowing coefficient of BGaN compound is ~4.0 eV.

Estimating the value of boron content in the boron-rich regions, causing the low – energy band observed at low temperatures (see Fig. 4.6) requires taking into account the band – gap bowing parameter. The value of the bowing parameter determined above, which is estimated using the PL band positions at room temperature, is 4 eV. However, the PL band peak positions obtained for BGaN with different boron content at 8 K are better fitted with the value of 5 eV. The corresponding contents of boron in the boron – rich regions are 8.7% and 4.7%, respectively. Despite the differences in estimated boron content, it can be concluded that the inclusions of boron-rich phases with a stable boron content of 5 – 9% are formed in BGaN epilayers with lower boron content.

The observed vanishing of the low-energy PL band at elevated temperatures can hardly be explained by escape of the carriers from the boron-rich regions, since the separation between the emission peaks of the two PL bands (~100 meV) is by an order of magnitude larger than the thermal energy (~10 meV) corresponding to the vanishing of the low-energy band. Meanwhile, it is feasible that the boron-rich regions contain considerably higher density of nonradiative recombination centers (in the bulk or boundaries of the region). Therefore, the increasing temperature facilitates the carrier capture to these centers, and the intensity of the emission from these regions decreases at elevated temperature faster than that from the rest of the epilayer with a lower content of boron and a lower density of nonradiative recombination centers.

The saturation of the intensity of emission from the boron-rich regions with increasing excitation power density, which is observed in all the samples

under current study, is an indication that the relative volume of the boron-rich phase is small even in the high-boron-content samples we studied.

A common feature of the BGaN PL observed in our study is significant

Fig. 4.9. Temperature dependences of the PL efficiency i BGaN epilayers with different boron content (indicated).[P2]

deterioration of the PL efficiency by introduction of even a small amount of boron. The PL efficiency at certain temperature is usually estimated as a ratio between the PL intensity at the temperature under consideration and the intensity at the temperatures low enough to assume that the efficiency is 100%. The temperature dependence of PL intensity is plotted for BGaN epilayers with boron content of 0, 1.1, 2, and 3% in Fig. 4.9. All the samples were measured under nominally identical excitation and signal detection conditions, thus, the arbitrary units of the PL intensity in the plot are the same for all the samples under study. Two unusual features are obvious in the figure: i) a relatively weak change of PL intensity with temperature for all the epilayers and ii) a drastic difference in PL intensity of the epilayers with different boron content even at low temperatures. A straightforward application of the conventional estimation of the PL efficiency by taking the ratio of PL intensities at room and low temperatures provides BGaN efficiency between 40 and 60%, which is definitely far from the real values. This huge discrepancy might be caused by the high excitation power densities we maintained during our PL experiments to obtain the dependences in Fig. 4.9. As demonstrated for AlGaN epilayers in
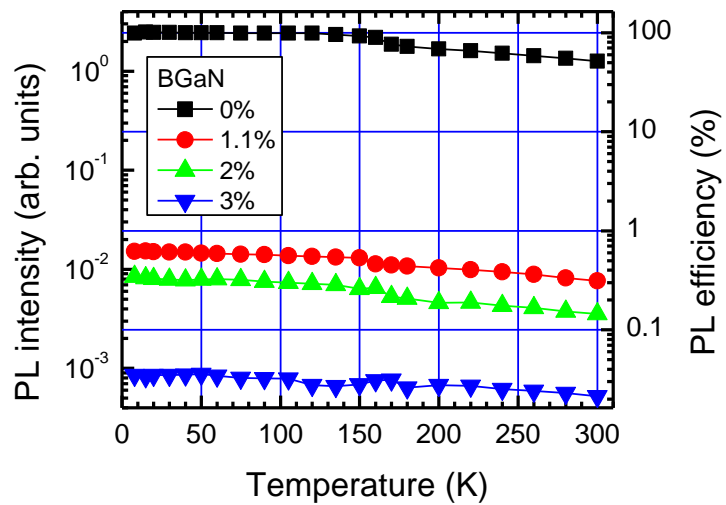
our earlier work[116], the PL efficiency ceases to depend on excitation intensity only at relatively low excitation power densities. Thus, the excitation intensity selected for the measurements of
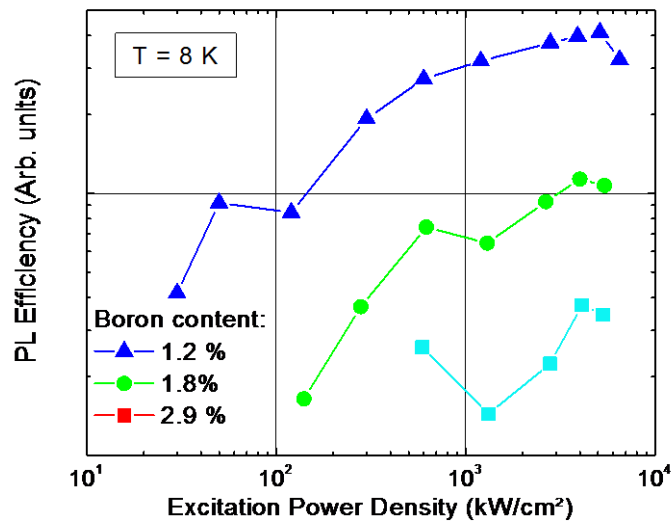

Fig. 4.10. Low temperature excitation power density dependence of PL efficiency of BGaN epilayers with different boron content.[P4]

PL intensity temperature dependence should be low enough to assume the 100-percent efficiency at low temperatures. Since the PL intensities of the BGaN epilayers under study are quite weak, it is difficult to perform accurate measurements of the temperature dependence of the PL intensity at the excitation intensities low enough to satisfy the requirement pointed out above. Instead, we combined our measurements at elevated excitation intensity for BGaN and at sufficiently low excitation in the reference sample of GaN to obtain the estimated efficiency at room temperature in absolute values. Under assumption that the efficiency of GaN epilayer is 100% at 8 K temperature, the obtained efficiency values are 0.3%, 0.15%, and 0.02% for BGaN epilayers with boron content of 1.1%, 2%, and 3%, respectively.

For BGaN samples with sufficiently strong PL intensity, we have measured the PL efficiency dependences on excitation power density at low temperature (8 K) (see Fig. 4.10). A nearly linear growth tending to saturation at elevated excitation power densities was observed for the PL efficiency in the epilayer with 1.2 % boron content. An increase in boron content results in a

considerable decrease in the PL efficiency, but the function of the PL efficiency dependence on excitation power density remains similar. The efficiency saturation could hardly be interpreted by the usual efficiency droop effect observed in ternary nitride InGaN due to high density of nonequilibrium carriers. The carrier density expected in BGaN under study is considerably lower than that in InGaN under similar excitation intensity. It is obvious that the emission efficiency of BGaN is by far not 100 % even at the temperatures as low as 8 K. The excitation power density dependence of photoluminescence efficiency presented in Fig. 4.10 can be explained by assuming that a part of nonequilibrium carriers are localized in potential fluctuations probably occurring due to fluctuations in boron content. In such conditions, the carrier dynamics is governed by two effects resulting from the enhanced carrier delocalization as the excitation intensity increases: the bimolecular recombination of free carriers enhances the photoluminescence, while the
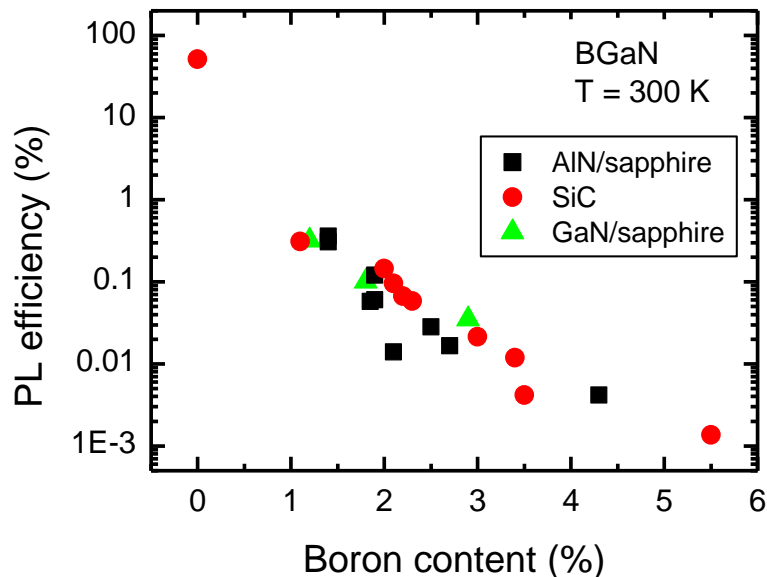

Fig. 4.11. PL efficiency dependence on boron content in BGaN epilayers grown on different substrates (indicated) [P2].

increased ability of the delocalized carriers to reach the nonradiative recombination centers reduces the photoluminescence efficiency, as discussed

in more detail in the previous chapter. The increase of PL efficiency could also be due to saturation of defect recombination.

A plot of the dependence of room-temperature PL efficiency on boron content in BGaN epitaxial layers is shown in Fig. 4.11. Each point here corresponds to the efficiency of a different BGaN epilayer under study. The different types of points are used to indicate the samples grown on different substrates/templates. Within the error reflected by scattering of the points in Fig. 4.11, the dependences for the epilayers grown on GaN/sapphire, AlN/sapphire, and SiC are similar. The BGaN efficiency decreases nearly exponentially with introduction of boron in the range from 1 to 4%, and the decrease slightly slows down at elevated boron content.

The very low PL intensity of BGaN even at low temperatures might be partially attributed to significant heating under relatively intense photoexcitation used in our experiments. The elevated thermal energy enhances capturing of the carriers into nonradiative recombination centers. The temperature of the system of nonequilibrium electrons and holes can often be estimated from the nearly exponential high-energy slope of the PL band. However, the slope of the low-temperature PL band in the BGaN samples under study shows no significant dependence on excitation intensity at low temperatures and corresponds approximately to the temperatures of ~475 K and ~1130 K for boron content of 1.1% and 3%, respectively. This is an indication that the PL band exhibits a strong inhomogeneous broadening, and the band slope does not reflect the carrier temperature. Thus, a considerable carrier or lattice heating is feasible, though not proven. Moreover, the capture of the nonthermalized photoexcited carriers directly to the nonradiative recombination centers at their density presumably high in BGaN might also have a strong influence on the strong nonradiative recombination at low lattice temperatures.

In conclusion, the double band structure observed at low temperatures in the photoluminescence spectra evidence a partial phase separation, which is observed at any boron content but becomes significant in the BGaN epilayers containing more than 3% of boron. The boron-rich phase contains approximately 5-9% of boron independently of the average boron content, technological growth conditions and templates used to deposit the BGaN epilayers. The volume of the boron-rich regions encompasses only a small fraction of the entire epilayer. Nonradiative recombination in these regions (or their boundaries) decrease luminescence efficiency at elevated temperatures. However, due to high excitation levels, delocalized carriers reach the nonradiative recombination centers even at low temperatures and overall luminescence efficiency is lower by orders of magnitude than that of pure GaN even at 8 K.

The room temperature PL efficiency is approximately 0.3% in BGaN with 1% of boron and decreases down to ~0.02% for the boron content of 3%. The efficiency is determined predominantly by boron content and does not show significant correlation with either the type of substrate/template used for BGaN deposition or the combination of growth temperature and precursor fluxes to obtain an epilayer of good crystal quality or surface morphology.

At optimized growth conditions, similar layer quality and photoluminescence intensity at the same boron content were observed in the layers deposited on 6H-SiC substrate and on sapphire substrate with AlN templates. SiC substrate is slightly more favorable for boron incorporation. GaN templates on sapphire are less appropriate for growth of BGaN than those of AlN. The photoluminescence band peak positions estimated under the same conditions at room temperature in 23 BGaN epilayers with different boron content show that the bowing parameter in this material approximately equals 4 eV, substantially lower than that reported before (9.2 eV).

Concluding summary

1. The efficiency droop observed in photoluminescence of GaN epilayers is caused by stimulated emission propagating parallel to the sample surface and limiting the growth of carrier density at elevated excitation intensities.

2. Stimulated emission occurs via extended states in AlGaN MQWs with lower Al content (up to approximately 20%) and via localized states in MQWs with elevated aluminum content.

3. The main factor determining the SE threshold is the density of nonradiative recombination centers. High aluminum content is favorable for the formation of dislocations and point defects in AlGaN epilayers and MQWs on sapphire substrate and, consequently, reduces carrier density and increases the threshold for stimulated emission.

4. The dependence of the peak IQE value on carrier lifetime and no significant dependence of the IQE on PL efficiency growth rate show that strong localization alone is not sufficient to ensure high internal quantum efficiency. Even the carriers in localized states in AlGaN are mobile enough at room temperature to reach the nonradiative recombination centers.

5. Delocalization of carriers affects the photoluminescence efficiency via the enhancement of the two mechanisms of opposite signs. Bimolecular recombination of the free carriers increases the IQE at elevated excitation intensities, while the increasing filling of the localized states enhances the ability of free carriers to reach the nonradiative recombination centers, decreasing the photoluminescence efficiency.

6. The nonmonotonous shift of PL band peak position with increasing excitation and low threshold for the onset of decrease in PL efficiency observed in AlGaN epilayers at low temperatures demonstrate that the nonradiative recombination is important even at low temperatures and

at carrier densities of $\sim10^{17}$ cm^{-3}. At increasing carrier densities, the nonradiative recombination is enhanced by increased mobility of carriers moving to the nonradiative recombination centers due to the gradual filling-in of the localized states. The efficient nonradiative recombination at low temperatures is consistent with the excitonic nonradiative recombination.

7. The ratio $k_B T/\sigma$ between the carrier thermal energy $k_B T$ and the localization parameter σ might be treated as the parameter indicating the predominant origin of PL droop in AlGaN-based MQWs and epilayers. For nonthermalized carriers ($k_B T/\sigma$ < 0.35), the droop occurs due to occupation-enhanced redistribution of nonthermalized carriers. At elevated temperatures (0.35 < $k_B T/\sigma$ < 1), the droop is caused by enhancement of the nonradiative recombination as the localized states are filled-in and an increasing fraction of carriers becomes delocalized. At high temperatures and/or weak localization ($k_B T/\sigma$ > 1), the origin of the droop is stimulated emission in AlGaN MQWs and excitation-enhanced carrier transport to extended defects in AlGaN epilayers

8. The double band structure observed in the PL spectra of BGaN epilayers at low temperatures evidences a partial phase separation, resulting with regions of boron-rich phase (approximately 5-9% independently of the average boron content, technological growth conditions and templates used to deposit the BGaN epilayers). Nonradiative recombination in these regions (or their boundaries) decreases luminescence efficiency at elevated temperatures.

9. The room temperature PL efficiency is approximately 0.3% in BGaN with 1% of boron and decreases down to ~0.02% for the boron content of 3%. The efficiency is determined predominantly by boron content and does not show significant correlation with either the type of substrate/template used for BGaN deposition or the combination of

growth temperature and precursor fluxes to obtain an epilayer of good crystal quality and surface morphology.

10. At optimized growth conditions, similar layer quality and photoluminescence intensity at the same boron content were observed in the layers deposited on 6H-SiC substrate and on sapphire substrate with AlN templates. SiC substrate is slightly more favorable for boron incorporation. GaN templates on sapphire are less appropriate for growth of BGaN than those of AlN.

11. The photoluminescence band peak positions estimated under the same conditions at room temperature in 23 BGaN epilayers with different boron content show that the bowing parameter in this material approximately equals 4 eV, substantially lower than that reported before (9.2 eV).

List of References

1.   Pankove, J. I., Miller, E. A. & Berkeyheiser, J. E. GaN electroluminescent diodes. in *1971 International Electron Devices Meeting* **17,** 78–78 (IRE, 1971).

2.   *III-Nitride Semiconductors: Electrical, Structural and Defects Properties*. (Elsevier, 2000).

3.   Amano, H. *et al.* P-Type Conduction in Mg-Doped GaN Treated with Low-Energy Electron Beam Irradiation (LEEBI). *Jpn. J. Appl. Phys.* **28,** L2112–L2114 (1989).

4.   Nakamura, S. *et al.* Room-temperature continuous-wave operation of InGaN multi-quantum-well structure laser diodes with a lifetime of 27 hours. *Appl. Phys. Lett.* **70,** 1417 (1997).

5.   Singh, J. *Electronic and Optoelectronic Properties of Semiconductor Structures*. (Cambridge University Press, 2003). doi:10.1017/CBO9780511805745

6.   Neumann, H. J. H. Edgar (ed.). Properties of Group III Nitrides. (EMIS Datareviews Series No. 11). INSPEC, The Institution of Electrical Engineers, London 1994. 302 Seiten, 121 Abbildungen, 77 Tabellen. ISBN 0–85296–818–3. *Cryst. Res. Technol.* **30,** 910–910 (1995).

7.   Gil, B. (Bernard). *Group III nitride semiconductor compounds : physics and applications*. (Clarendon Press, 1998).

8.   Kuokštis, E. & Tamulaitis, G. *Plačiatarpių puslaidininkių technologija ir prietaisai*. (2008).

9.   Levinshteĭn, M. E. (Mikhail E., Rumyantsev, S. L. & Shur, M. *Properties of advanced semiconductor materials : GaN, AlN, InN, BN, SiC, SiGe*. (Wiley, 2001).

10.   Watanabe, K., Taniguchi, T. & Kanda, H. Direct-bandgap properties and evidence for ultraviolet lasing of hexagonal boron nitride single crystal. *Nat. Mater.* **3,** 404–9 (2004).

11.   Madelung, O. *Semiconductors: Data Handbook*. (Springer Berlin Heidelberg, 2004). doi:10.1007/978-3-642-18865-7

12.   Ponce, F. A., Bour, D. P., Young, W. T., Saunders, M. & Steeds, J. W. Determination of lattice polarity for growth of GaN bulk single crystals and epitaxial layers. *Appl. Phys. Lett.* **69,** 337 (1996).

13.   Ponce, F. A., Bour, D. P., Götz, W. & Wright, P. J. Spatial distribution of

the luminescence in GaN thin films. *Appl. Phys. Lett.* **68,** 57 (1996).

14. Gassmann, A. *et al.* Homoepitaxial growth of GaN using molecular beam epitaxy. *J. Appl. Phys.* **80,** 2195 (1996).

15. Wei, C. H. *et al.* MOCVD growth of GaBN on 6H-SiC (0001) substrates. *J. Electron. Mater.* **29,** 452 (2000).

16. Wei, C. . & Edgar, J. . Thermodynamic analysis of GaxB1–xN grown by MOVPE. *J. Cryst. Growth* **217,** 109–114 (2000).

17. Wei, C. H. & Edgar, J. H. Unstable composition region in the wurtzite B1-x-yGaxAlyN system. *J. Cryst. Growth* **208,** 179–182 (2000).

18. Ougazzaden, A. *et al.* BGaN materials on GaN/sapphire substrate by MOVPE using N2 carrier gas. *J. Cryst. Growth* **298,** 316–319 (2007).

19. Wei, C. H. & Edgar, J. H. Thermodynamic analysis of GaxB1-xN grown by MOVPE. *J. Cryst. Growth* **217,** 109–114 (2000).

20. Honda, T., Kurimoto, M., Shibata, M. & Kawanishi, H. Excitonic emission of BGaN grown on (0001) 6H-SiC by metal-organic vapor-phase epitaxy. *J. Lumin.* **87,** 1274–1276 (2000).

21. Ougazzaden, A. *et al.* Bandgap bowing in BGaN thin films. *Appl. Phys. Lett.* **93,** 3–6 (2008).

22. Baghdadli, T. *et al.* Electrical and structural characterizations of BGaN thin films grown by metal-organic vapor-phase epitaxy. *Phys. Status Solidi* **6,** S1029–S1032 (2009).

23. Kadys, A. *et al.* Optical and structural properties of BGaN layers grown on different substrates. *J. Phys. D. Appl. Phys.* **48,** 465307 (2015).

24. Polyakov, a. Y. *et al.* Growth of GaBN ternary solutions by organometallic vapor phase epitaxy. *J. Electron. Mater.* **26,** 237–242 (1997).

25. Gautier, S. *et al.* Application of dilute boron B(Al,In,Ga)N alloys for UV light sources. **7940,** 79400X–79400X–7 (2011).

26. Malinauskas, T. *et al.* Growth of BGaN epitaxial layers using close-coupled showerhead MOCVD. *Phys. Status Solidi Basic Res.* **252,** 1138–1141 (2015).

27. Honda, T. *et al.* Band-Gap Energy and Effective Mass of BGaN. *Jpn. J. Appl. Phys.* **39,** 2389–2393 (2000).

28. Orsal, G. *et al.* Effect of boron incorporation on growth behavior of BGaN/GaN by MOVPE. *J. Cryst. Growth* **310,** 5058–5062 (2008).

29. Gautier, S. *et al.* Deep structural analysis of novel BGaN material layers grown by MOVPE. *J. Cryst. Growth* **315,** 288–291 (2011).

30. Polyakov, a. Y. *et al.* Growth of AlBN solid solutions by organometallic vapor-phase epitaxy. *J. Appl. Phys.* **81,** 1715 (1997).

31. Ilyasov, V. V., Zhadanova, T. P. & Nikiforov, I. Y. Electronic energy structure and X-ray spectra of GaN and BxGa1-x N crystals. *Phys. Solid State* **48,** 654–662 (2006).

32. Riane, R., Boussahl, Z., Zaoui, A., Hammerelaine, L. & Matar, S. F. Structural and electronic properties of zinc blende BxGa1–xN nitrides. *Solid State Sci.* **11,** 200–206 (2009).

33. Shatalov, M. *et al.* AlGaN Deep-Ultraviolet Light-Emitting Diodes with External Quantum Efficiency above 10%. *Appl. Phys. Express* **5,** 082101 (2012).

34. Li, S. *et al.* Polarization induced pn-junction without dopant in graded AlGaN coherently strained on GaN. *Appl. Phys. Lett.* **101,** 122103 (2012).

35. Li, S. *et al.* Polarization induced hole doping in graded AlxGa1−xN (x = 0.7 ∼ 1) layer grown by molecular beam epitaxy. *Appl. Phys. Lett.* **102,** 062108 (2013).

36. Shatalov, M. *et al.* High power AlGaN ultraviolet light emitters. *Semicond. Sci. Technol.* **29,** 084007 (2014).

37. Chichibu, S., Azuhata, T., Sota, T. & Nakamura, S. Spontaneous emission of localized excitons in InGaN single and multiquantum well structures. *Appl. Phys. Lett.* **69,** 4188 (1996).

38. Collins, C. J. *et al.* Enhanced room-temperature luminescence efficiency through carrier localization in Alx Ga1-x N alloys. *Appl. Phys. Lett.* **86,** 1– 3 (2005).

39. Kim, H. S., Mair, R. A., Li, J., Lin, J. Y. & Jiang, H. X. Time-resolved photoluminescence studies of Al[sub x]Ga[sub 1–x]N alloys. *Appl. Phys. Lett.* **76,** 1252 (2000).

40. Cho, Y.-H. *et al.* Dynamics of anomalous optical transitions in Al x Ga 1 − x N alloys. *Phys. Rev. B* **61,** 7203–7206 (2000).

41. Chen, C. H., Huang, L. Y., Chen, Y. F., Jiang, H. X. & Lin, J. Y. Mechanism of enhanced luminescence in In[sub x]Al[sub y]Ga[sub 1–x–y]N quaternary alloys. *Appl. Phys. Lett.* **80,** 1397 (2002).

42. Kazlauskas, K. *et al.* Double-scaled potential profile in a group-III nitride alloy revealed by Monte Carlo simulation of exciton hopping. *Appl. Phys. Lett.* **83,** 3722–3724 (2003).

43. Francesco Pecora, E. *et al.* Sub-250 nm room-temperature optical gain from AlGaN/AlN multiple quantum wells with strong band-structure potential fluctuations. *Appl. Phys. Lett.* **100,** 061111 (2012).

44. Francesco Pecora, E. *et al.* Sub-250 nm light emission and optical gain in AlGaN materials. *J. Appl. Phys.* **113,** 013106 (2013).

45. Shen, Y. C. *et al.* Auger recombination in InGaN measured by photoluminescence. *Appl. Phys. Lett.* **91,** 141101 (2007).

46. Wang, J., Wang, L., Zhao, W., Hao, Z. & Luo, Y. Understanding efficiency droop effect in InGaN/GaN multiple-quantum-well blue light-emitting diodes with different degree of carrier localization. *Appl. Phys. Lett.* **97,** 201112 (2010).

47. Ryu, H.-Y., Kim, H.-S. & Shim, J.-I. Rate equation analysis of efficiency droop in InGaN light-emitting diodes. *Appl. Phys. Lett.* **95,** 081114 (2009).

48. Bochkareva, N. I., Rebane, Y. T. & Shreter, Y. G. Efficiency droop and incomplete carrier localization in InGaN/GaN quantum well light-emitting diodes. *Appl. Phys. Lett.* **103,** 191101 (2013).

49. Shatalov, M. *et al.* Efficiency of light emission in high aluminum content AlGaN quantum wells. *J. Appl. Phys.* **105,** 073103 (2009).

50. Ozgur, U., Huiyong Liu, H., Xing Li, X., Xianfeng Ni, X. & Morkoç, H. GaN-Based Light-Emitting Diodes: Efficiency at High Injection Levels. *Proc. IEEE* **98,** 1180–1196 (2010).

51. Ahn, B.-J. *et al.* Experimental determination of current spill-over and its effect on the efficiency droop in InGaN/GaN blue-light-emitting-diodes. *Appl. Phys. Lett.* **100,** 031905 (2012).

52. Verzellesi, G. *et al.* Efficiency droop in InGaN/GaN blue light-emitting diodes: Physical mechanisms and remedies. *J. Appl. Phys.* **114,** 071101 (2013).

53. Rozhansky, I. V. & Zakheim, D. A. Analysis of dependence of electroluminescence efficiency of AlInGaN LED heterostructures on pumping. *Phys. status solidi* **3,** 2160–2164 (2006).

54. Schubert, M. F. *et al.* Effect of dislocation density on efficiency droop in GaInN∕GaN light-emitting diodes. *Appl. Phys. Lett.* **91,** 231114 (2007).

55. Delaney, K. T., Rinke, P. & Van de Walle, C. G. Auger recombination rates in nitrides from first principles. *Appl. Phys. Lett.* **94,** 191109 (2009).

56. Iveland, J., Martinelli, L., Peretti, J., Speck, J. S. & Weisbuch, C. Direct Measurement of Auger Electrons Emitted from a Semiconductor Light-

Emitting Diode under Electrical Injection: Identification of the Dominant Mechanism for Efficiency Droop. *Phys. Rev. Lett.* **110,** 177406 (2013).

57. Sadi, T., Kivisaari, P., Oksanen, J. & Tulkki, J. On the correlation of the Auger generated hot electron emission and efficiency droop in III-N light-emitting diodes. *Appl. Phys. Lett.* **105,** 091106 (2014).

58. Binder, M. *et al.* Identification of nnp and npp Auger recombination as significant contributor to the efficiency droop in (GaIn)N quantum wells by visualization of hot carriers in photoluminescence. *Appl. Phys. Lett.* **103,** 071108 (2013).

59. Hader, J., Moloney, J. V. & Koch, S. W. Temperature-dependence of the internal efficiency droop in GaN-based diodes. *Appl. Phys. Lett.* **99,** 181127 (2011).

60. Kioupakis, E., Rinke, P., Delaney, K. T. & Van de Walle, C. G. Indirect Auger recombination as a cause of efficiency droop in nitride light-emitting diodes. *Appl. Phys. Lett.* **98,** 161107 (2011).

61. Wang, Z., He, P., Wang, R., Zhao, J. & Gong, M. New red phosphor for near-ultraviolet light-emitting diodes with high color-purity. *Mater. Res. Bull.* **45,** 240–242 (2010).

62. Hammersley, S. *et al.* The consequences of high injected carrier densities on carrier localization and efficiency droop in InGaN/GaN quantum well structures. *J. Appl. Phys.* **111,** 083512 (2012).

63. Hader, J., Moloney, J. V. & Koch, S. W. Density-activated defect recombination as a possible explanation for the efficiency droop in GaN-based diodes. *Appl. Phys. Lett.* **96,** 221106 (2010).

64. Bourdon, G., Robert, I., Sagnes, I. & Abram, I. Spontaneous emission in highly excited semiconductors: Saturation of the radiative recombination rate. *J. Appl. Phys.* **92,** 6595 (2002).

65. Shim, J.-I., Kim, H., Shin, D.-S. & Yoo, H.-Y. An Explanation of Efficiency Droop in InGaN-based Light Emitting Diodes: Saturated Radiative Recombination Rate at Randomly Distributed In-Rich Active Areas. *J. Korean Phys. Soc.* **58,** 503 (2011).

66. Mickevičius, J. *et al.* Photoluminescence efficiency droop and stimulated recombination in GaN epilayers. *Opt. Express* **20,** 25195 (2012).

67. Efremov, A. A. *et al.* Effect of the joule heating on the quantum efficiency and choice of thermal conditions for high-power blue InGaN/GaN LEDs. *Semiconductors* **40,** 605–610 (2006).

68. Monemar, B. & Sernelius, B. E. Defect related issues in the 'current roll-

off' in InGaN based light emitting diodes. *Appl. Phys. Lett.* **91,** 181103 (2007).

69. Watanabe, S. *et al.* Internal quantum efficiency of highly-efficient In[sub x]Ga[sub 1–x]N-based near-ultraviolet light-emitting diodes. *Appl. Phys. Lett.* **83,** 4906 (2003).

70. Fujiwara, K., Jimi, H. & Kaneda, K. Temperature-dependent droop of electroluminescence efficiency in blue (In,Ga)N quantum-well diodes. *Phys. status solidi* **6,** S814–S817 (2009).

71. Kohno, T. *et al.* Internal Quantum Efficiency and Nonradiative Recombination Rate in InGaN-Based Near-Ultraviolet Light-Emitting Diodes. *Jpn. J. Appl. Phys.* **51,** 072102 (2012).

72. Badcock, T. J. *et al.* Low temperature carrier redistribution dynamics in InGaN/GaN quantum wells. *J. Appl. Phys.* **115,** 113505 (2014).

73. Lin, Y. *et al.* Spatially resolved study of quantum efficiency droop in InGaN light-emitting diodes. *Appl. Phys. Lett.* **101,** 252103 (2012).

74. Lin, Y. *et al.* Interplay of point defects, extended defects, and carrier localization in the efficiency droop of InGaN quantum wells light-emitting diodes investigated using spatially resolved electroluminescence and photoluminescence. *J. Appl. Phys.* **115,** 023103 (2014).

75. Varshni, Y. P. Temperature dependence of the energy gap in semiconductors. *Physica* **34,** 149–154 (1967).

76. Eliseev, P. G., Perlin, P., Lee, J. & Osiński, M. 'Blue' temperature-induced shift and band-tail emission in InGaN-based light sources. *Appl. Phys. Lett.* **71,** 569 (1997).

77. Bell, A. *et al.* Exciton freeze-out and thermally activated relaxation at local potential fluctuations in thick Al xGa 1-xN layers. *J. Appl. Phys.* **95,** 4670–4674 (2004).

78. Kazlauskas, K. *et al.* Exciton hopping and nonradiative decay in AlGaN epilayers. *Appl. Phys. Lett.* **87,** 1–3 (2005).

79. Kazlauskas, K. *et al.* Exciton hopping in InxGa1–xN multiple quantum wells. *Phys. Rev. B* **71,** 085306 (2005).

80. Mickevičius, J. *et al.* Well-width-dependent carrier lifetime in AlGaN/AlGaN quantum wells. *Appl. Phys. Lett.* **90,** 131907 (2007).

81. Nepal, N., Li, J., Nakarmi, M. L., Lin, J. Y. & Jiang, H. X. Exciton localization in AlGaN alloys. *Appl. Phys. Lett.* **88,** (2006).

82. Zhao, C.-Z. *et al.* Investigation of localization effect in GaN-rich InGaN alloys and modified band-tail model. *Bull. Mater. Sci.* **36,** 619–622 (2013).

83. Wang, Q. *et al.* Stimulated emission at 340 nm from AlGaN multiple quantum well grown using high temperature AlN buffer technologies on sapphire. *Appl. Phys. Lett.* **95,** 161904 (2009).

84. Jmerik, V. N. *et al.* Low-threshold 303 nm lasing in AlGaN-based multiple-quantum well structures with an asymmetric waveguide grown by plasma-assisted molecular beam epitaxy on c-sapphire. *Appl. Phys. Lett.* **96,** (2010).

85. Jmerik, V. N. *et al.* Optically pumped lasing at 300.4 nm in AlGaN MQW structures grown by plasma-assisted molecular beam epitaxy on c-Al2O3. *Phys. Status Solidi Appl. Res.* **207,** 1313–1317 (2010).

86. Lachab, M. *et al.* Ultraviolet Stimulated Emission From Optically Pumped AlGaN/AlGaN Multiple Quantum Wells on Pulsed Laterally Overgrown a-Plane GaN. *Appl. Phys. Express* **4,** 082103 (2011).

87. Wunderer, T. *et al.* Pseudomorphically Grown Ultraviolet C Photopumped Lasers on Bulk AlN Substrates. *Appl. Phys. Express* **4,** 092101 (2011).

88. Mickevičius, J. *et al.* Stimulated emission in AlGaN/AlGaN quantum wells with different Al content. *Appl. Phys. Lett.* **100,** (2012).

89. Satake, A., Masumoto, Y., Miyajima, T., Asatsuma, T. & Ikeda, M. Two-dimensional exciton dynamics and gain formation processes in In x Ga 1 − x N multiple quantum wells. *Phys. Rev. B* **60,** 16660–16666 (1999).

90. Žukauskas, A. *et al.* Role of band potential roughness on the luminescence properties of InGaN quantum wells grown by MBE on bulk GaN substrates. in *Physica Status Solidi (B) Basic Research* **243,** 1614–1618 (2006).

91. Holst, J., Kaschner, A. & Gfug, U. No Comparison of the Mechanism of Optical Amplification in InGaN/GaN Heterostructures Grown by Molecular Beam Epitaxy and MOCVD. *Phys. Status Solidi A* **180,** 327–332 (2000).

92. Strassburg, M. *et al.* The origin of the PL photoluminescence Stokes shift in ternary group-III nitrides: Field effects and localization. in *Physica Status Solidi C: Conferences* **0,** 1835–1845 (2003).

93. Kawakami, Y. *et al.* Dynamics of spontaneous and stimulated emissions in GaN-based semiconductors. *Proc. SPIE* **4280,** 45–57 (2001).

94.   Lermer, T. *et al.* Gain of blue and cyan InGaN laser diodes. *Appl. Phys. Lett.* **98,** 021115 (2011).

95.   Kojima, K., Funato, M., Kawakami, Y., Narukawa, Y. & Mukai, T. Suppression mechanism of optical gain formation in InxGa1-xN quantum well structures due to localized carriers. *Solid State Commun.* **140,** 182–184 (2006).

96.   Ishibashi, A. *et al.* Systematic studies on optical gain spectra in GaInN/GaN-MQWs. *J. Lumin.* **87,** 1271–1273 (2000).

97.   Chow, W. W. & Kneissl, M. Laser gain properties of AlGaN quantum wells. *J. Appl. Phys.* **98,** 114502 (2005).

98.   Chichibu, S., Onuma, T., Hazu, K. & Uedono, A. Time-resolved luminescence studies on AlN and high AlN mole fraction AlGaN alloys. *Phys. Status Solidi Curr. Top. Solid State Phys.* **10,** 501–506 (2013).

99.   Mickevičius, J. *et al.* Correlation between carrier localization and efficiency droop in AlGaN epilayers. *Appl. Phys. Lett.* **103,** 011906 (2013).

100.   Mickevičius, J. *et al.* Stimulated emission due to localized and delocalized carriers in Al 0.35Ga 0.65N/Al 0.49Ga 0.51N quantum wells. *Appl. Phys. Lett.* **101,** (2012).

101.   Tamulaitis, G. *et al.* Photoluminescence efficiency in AlGaN quantum wells. *Phys. B Condens. Matter* **453,** 40–42 (2014).

102.   Mickevičius, J. *et al.* Influence of carrier localization on high-carrier-density effects in AlGaN quantum wells. *Opt. Express* **22,** A491 (2014).

103.   Mickevičius, J. *et al.* Nonradiative Recombination, Carrier Localization, and Emission Efficiency of AlGaN Epilayers with Different Al Content. *J. Electron. Mater.* **44,** 4706–4709 (2015).

104.   Mickevičius, J. *et al.* Efficiency droop and carrier transport in AlGaN epilayers and heterostructures. *Phys. Status Solidi Basic Res.* **252,** 961–964 (2015).

105.   Sun, Q. *et al.* Lateral phase separation in AlGaN grown on GaN with a high-temperature AlN interlayer. *Appl. Phys. Lett.* **87,** 121914 (2005).

106.   Gao, M. *et al.* Compositional modulation and optical emission in AlGaN epitaxial films. *J. Appl. Phys.* **100,** 103512 (2006).

107.   Chichibu, S. F., Hazu, K., Onuma, T. & Uedono, A. Collateral evidence for an excellent radiative performance of AlxGa1−xN alloy films of high AlN mole fractions. *Appl. Phys. Lett.* **99,** 051902 (2011).

108. Fan, S. *et al.* Optical investigation of strong exciton localization in high Al composition AlxGa1-xN alloys. *Opt. Express* **21,** 24497 (2013).

109. Leroux, M. *et al.* Temperature quenching of photoluminescence intensities in undoped and doped GaN. *J. Appl. Phys.* **86,** 3721 (1999).

110. Abell, J. & Moustakas, T. D. The role of dislocations as nonradiative recombination centers in InGaN quantum wells. *Appl. Phys. Lett.* **92,** 091901 (2008).

111. Liang, M.-M. *et al.* Influence of barrier thickness on the structural and optical properties of InGaN/GaN multiple quantum wells. *Chinese Phys. B* **23,** 054211 (2014).

112. Orenstein, J. & Kastner, M. Photocurrent Transient Spectroscopy: Measurement of the Density of Localized States in a - As 2 Se 3. *Phys. Rev. Lett.* **46,** 1421–1424 (1981).

113. Monroe, D. Hopping exponential band tails. *Phys. Rev. Lett.* **54,** 146–149 (1985).

114. Majumder, F. A., Shevel, S., Lyssenko, V. G., Swoboda, H. E. & Klingshirn, C. Luminescence and gain spectroscopy of disordered CdS1?x Se x under high excitation. *Zeitschrift fur Phys. B Condens. Matter* **66,** 409–418 (1987).

115. Hirano, D., Tayagaki, T. & Kanemitsu, Y. Disorder-induced rapid localization of electron-hole plasmas in highly excited In x Ga 1 − x N mixed crystals. *Phys. Rev. B* **77,** 073201 (2008).

116. Mickevičius, J. *et al.* Internal quantum efficiency in AlGaN with strong carrier localization. *Appl. Phys. Lett.* **101,** 211902 (2012).

117. Ma, Z. & Pierz, K. Carrier thermalization and activation within self-assembled InAs/AlAs quantum dot states. *Surf. Sci.* **511,** 57–64 (2002).

118. Marcinkevičius, S. *et al.* Carrier redistribution between different potential sites in semipolar (202̄1) InGaN quantum wells studied by near-field photoluminescence. *Appl. Phys. Lett.* **105,** 111108 (2014).

119. Gfroerer, T. H., Zhang, Y. & Wanlass, M. W. An extended defect as a sensor for free carrier diffusion in a semiconductor. *Appl. Phys. Lett.* **102,** 012114 (2013).

120. Malinauskas, T., Jarasiunas, K., Heuken, M., Scholz, F. & Brückner, P. Diffusion and recombination of degenerate carrier plasma in GaN. *Phys. status solidi* **6,** S743–S746 (2009).

121. Pinos, A. *et al.* Localization potentials in AlGaN epitaxial films studied by scanning near-field optical spectroscopy. *J. Appl. Phys.* **109,** 113516

(2011).

122. Kim, S. *et al.* Two-step growth of high quality GaN using V/III ratio variation in the initial growth stage. *J. Cryst. Growth* **262,** 7–13 (2004).

123. Akasaka, T., Kobayashi, Y. & Makimoto, T. BGaN micro-islands as novel buffers for growth of high-quality GaN on sapphire. *J. Cryst. Growth* **298,** 320–324 (2007).

124. Reshchikov, M. A. & Morkoç, H. Luminescence properties of defects in GaN. *J. Appl. Phys.* **97,** 061301 (2005).

125. Grandjean, N., Massies, J., Leroux, M. & De Mierry, P. Band edge versus deep luminescence of In[sub x]Ga[sub 1−x]N layers grown by molecular beam epitaxy. *Appl. Phys. Lett.* **72,** 3190 (1998).

126. Manz, C., Kunzer, M., Obloh, H., Ramakrishnan, A. & Kaufmann, U. In[sub x]Ga[sub 1−x]N/GaN band offsets as inferred from the deep, yellow-red emission band in In[sub x]Ga[sub 1−x]N. *Appl. Phys. Lett.* **74,** 3993 (1999).

127. Demchenko, D. O., Diallo, I. C. & Reshchikov, M. A. Yellow Luminescence of Gallium Nitride Generated by Carbon Defect Complexes. *Phys. Rev. Lett.* **110,** 087404 (2013).

128. Lyons, J. L., Alkauskas, A., Janotti, A. & Van de Walle, C. G. First-principles theory of acceptors in nitride semiconductors. *Phys. status solidi* **252,** 900–908 (2015).

129. Kadys, A. *et al.* Optical and structural properties of BGaN layers grown on different substrates. *J. Phys. D. Appl. Phys.* **48,** 465307 (2015).

130. Edgar, J. H. *et al.* Characterization of bulk hexagonal boron nitride single crystals grown by the metal flux technique. *J. Cryst. Growth* **403,** 110–113 (2014).